NOVEL TECHNIQUES FOR FAULT LOCATION,

VOLTAGE PROFILE CALCULATION AND VISUALIZATION OF TRANSIENTS

A Dissertation

by

CANSIN YAMAN EVRENOSOGLU

Submitted to the Office of Graduate Studies of
Texas A&M University
in partial fulfillment of the requirements for the degree of

DOCTOR OF PHILOSOPHY

December 2006

Major Subject: Electrical Engineering

NOVEL TECHNIQUES FOR FAULT LOCATION,

VOLTAGE PROFILE CALCULATION AND VISUALIZATION OF TRANSIENTS

A Dissertation

by

CANSIN YAMAN EVRENOSOGLU

Submitted to the Office of Graduate Studies of
Texas A&M University
in partial fulfillment of the requirements for the degree of

DOCTOR OF PHILOSOPHY

Approved by:

Chair of Committee,   Ali Abur
Committee Members,   Chanan Singh
   Aniruddha Datta
   Ergun Akleman
Head of Department,   Costas N. Georghiades

December 2006

Major Subject: Electrical Engineering

ABSTRACT

Novel Techniques for Fault Location, Voltage Profile Calculation and

Visualization of Transients. (December 2006)

Cansın Yaman Evrenosoğlu, B.S.; M.S., Istanbul Technical University

Chair of Advisory Committee: Dr. Ali Abur

This dissertation addresses three different problems in power systems. The first problem is related to the fault location in complex topologies such as three terminal circuits with series compensation and mutually coupled line sections and distribution networks with distributed generation. Novel methods are presented by using traveling wave approach and wavelet transformation technique to overcome the difficulties introduced by the discontinuities and integrated components such as Metal Oxide Varistor (MOV) protected series capacitors and distributed generation in complex topologies. Simulation results show good correlation between the actual and estimated fault locations for all the studied cases. The second problem concerns the calculation techniques of voltage profiles along transmission lines. A simple yet effective approach to accurately and rapidly obtain the voltage profile along a transmission line during fault transients is presented. The objective of the presented method is to eliminate the need to use wave equations and line parameters provided that an electromagnetic Transients Program (EMTP) type transients simulator is available for generating bus voltage transients for a given fault. This is accomplished by developing a time series model to estimate the voltage at an intermediate point along the transmission line. The model is formed for each intermediate point separately. Once the model is obtained it can be used to predict the transient voltage at that point along the line during any fault in the system. The approach can potentially be useful

as a post processor to a transient simulator and can be used by developers of transient animations and movies for illustrating fault-initiated propagation of traveling waves in power systems. The third problem is the lack of powerful visualization and animation methods, which can help understanding the complex behavior of power systems during transients. The goal of this part of the dissertation is to develop new animation and visualization methods for power system electromagnetic transients for both educational and research purposes. Proposed approaches are implemented in different environments such as MATLAB and Microsoft Visual Studio to show the effectiveness of two and three-dimensional visualization of power system transients. The implementations of the proposed methods provide better understanding of the power systems during transient phenomena due to the faults or switchings.

To my grandfathers Burhan Ali Evrenosoğlu and İzzet Öğün and to my grandaunt Selçuk Uraz

ACKNOWLEDGMENTS

that putting up with the life in small places is indescribable. Surviving in such small cities requires extra effort, infinite patience, strong commitment and on top of all, a real love for life. At those times, one of the important components of life is friendship. I thank all of my close friends in College Station for being around. Thanks Feyza Berber for providing invaluable support and encouragement anytime I needed. Thanks Dilhan İlk, Taner Özdil, Elif Aygen, Slavko Vasilic, Ahmet Uğursal, Ozan Ö. Özener, Ceki Halmen and Celile Itır Göğüş for accompanying me to dining, cooking, drinking and hanging around. Thank y'all ;)...

'İlim cehaleti alır, eşeklik baki kalır.' (Education can only eliminate ignorance, but a donkey is still a donkey.) - A famous Turkish proverb which I learned from my grandfather İzzet Öğün when I was around 12. He was also an electrical engineer, a Yıldız Technical University graduate of 1949.

TABLE OF CONTENTS

LIST OF TABLES

LIST OF FIGURES

FIGURE Page

FIGURE Page

CHAPTER I

INTRODUCTION

A.   Motivations of the Dissertation

Electrical power is one of the most needed resources of the industrialized world. The population of the world is increasing tremendously creating an ever-increasing shortage of electrical power not only for the well-developed countries but also for developing and under developed countries. Thus, using the existing world resources requires careful planning and optimal operation of the power grids.

Usually, the AC generation units are far away from the consumption areas due to the location of the resources, which brings the problem of transmitting the generated power through transmission lines over long distances. Generation of power is done at tens of kilovolts due to the construction limits, however voltage is increased to high voltage levels of hundreds of kilovolts by using step up transformers. High voltage levels are used for transmission in part due to the need to limit line currents and reduce transmission losses for a given amount of transmitted power. Nevertheless, the distribution is done at the levels of tens of kilovolts requiring step down transformers. In addition to the generators, generator step-up transformers, transmission lines, and distribution step-down transformers, power systems contain various other devices and systems for increasing the efficiency and preventing failures. Parallel capacitor/reactor banks and series capacitors equipped with FACTS devices in this new deregulated environment are some of those devices used for reducing the losses, increasing the transmission efficiency, increasing the transient stability margins and etc.

The journal model is *IEEE Transactions on Power Delivery.*

Since electrical power systems are built as interconnected grids, as the size of these systems grow, operating them becomes more complicated and the systems become more vulnerable to disturbances especially to cascading events. The main goal of Energy Management Systems (EMS) is to keep the system intact and to secure the reliable operation of power systems. Supervisory Control and Data Acquisition (SCADA) systems in EMS facilities provide not only monitoring the large power systems by gathering real time data from the measurement devices but also controlling the system and displaying information in an organized fashion for power engineers.

The primary concern of a transmission system operator is the security of the system. Hence, the system is expected to ride through different types of possible disturbances. These disturbances may occur due to permanent or temporary faults, and will result in over voltages, over currents, voltage sags, etc. The frequency and the severeness of these disturbances alongside with their permanent or temporary impacts on the power system constitute the *quality* of the power transmitted.

The main focus of this dissertation is fault or switching initiated electromagnetic transients along power transmission lines. Once a fault occurs along a transmission line protective devices (relays, circuit breakers and etc.) respond to save the system from the transient impacts of the fault by taking the faulted transmission line out of service. If the fault is permanent, once the relays operate and take the transmission line out of the service, the system will operate at another operating point, which is typically desirable. Thus, an action is required to clear the fault. For instance if a transmission line is disconnected or a transmission tower is damaged, repairs will be needed. Accurate and timely location of the source of the disturbance greatly facilitates the job of the repair crew. In the competitive power markets, utilities are concerned with minimizing service interruptions and down times by fast and accurate location of system faults.

The analysis of fault initiated system transients has so far been based on analytical techniques and simulations. Understanding the mechanism of propagation of waves caused by system faults can benefit from visualization of voltage profiles along transmission lines. Voltage profile of a transmission line especially during transient phenomena provides critical information about the behavior of the traveling waves, which disperse into the power system. Visualization of the power system transients is very important for educational and research purposes to better understand the traveling wave phenomenon and the response of the power system. This dissertation mainly focuses on these challenging topics and the contributions dealing with these problems are introduced in the following section.

B.   Contributions

The main contributions of this dissertation are itemized and briefly summarized below under three different topics. Detailed explanations of the proposed techniques are provided within the dissertation.

1.   Fault location using wavelets

There are two contributions under this topic:

- A new fault location method is proposed for three terminal circuits with Metal Oxide Varistor (MOV) protected series capacitors and mutually coupled line sections.

- A novel fault location technique is proposed for distribution systems with distributed generators.

Both techniques are based on traveling wave theory and they utilize discrete wavelet transformation (DWT). Once the terminal voltage/voltages is/are obtained,

the modal transformation is applied in order to decouple the system into independent three circuits (Two aerial mode circuits and one ground mode circuit). Aerial and ground mode voltages are used to determine the fault type and fault location. Discrete wavelet transformation is applied to the modal voltages to extract the fault transient information and the exact fault location is found by using traveling wave knowledge via Bewley [1] diagrams.

2. Voltage profile calculation

A novel transmission line voltage profile calculation method in modal domain is proposed. There are currently two types of voltage profile calculation techniques. The first and widely known method is obtaining the intermediate point voltages through the series connection of short sections to simulate the transmission line. The second and recently proposed method calculates the intermediate point voltages of a transmission line in modal domain using the traveling wave equations. Frequency dependent line model is used for more accurate results. In this dissertation a novel and simple method is proposed based on estimation of the intermediate point voltages in modal domain. For each intermediate point a separate model is developed by using history terms of terminal voltages and the intermediate point voltage itself. In order to develop a time series model for an intermediate point, a study case, involving a fault, is created and the simulations are carried out in ATP/EMTP program. Once the model is developed it is used to predict the intermediate point voltage for different cases, involving different types of faults at different locations along the neighboring transmission lines.

3. Visualization and animation of transients

Various number of software programs with powerful visualization tools are developed in the literature so far, however all of them concentrate on power system steady state operation. Visualization and animation of traveling waves help to understand and examine the behavior of the power systems during transient operation. Visualization and animation are not only beneficial tools for researchers but also they are crucial for educational purposes. The first and the only attempt for animation of electromagnetic transients is presented in Woodruff's paper [2] in 1938. In this dissertation new visualization and animation techniques are developed and implemented for power system transients. A new software tool is also developed in order to implement one of the proposed animation techniques. Application of one of the visualization methods to the fault location problem along transmission lines is also discussed.

C. Chapter Organization

Chapter II gives an introduction to fault location in power systems. Transmission line models are reviewed alongside with traveling wave theory. A general review of fault location methods are given and existing traveling wave based fault location methods are briefly explained in this chapter.

Chapter III gives an overview of wavelet theory and its power system applications. Fault location using discrete wavelet transform is also introduced in this chapter.

Chapter IV describes a novel fault location method for three terminal transmission line circuits involving MOV protected series capacitors and mutually coupled line sections.

Chapter V presents a new fault location technique for distribution systems with distributed generation.

Chapter VI presents a new voltage profile calculation technique in modal domain for power system transmission lines.

Chapter VII describes novel methods for visualization and animation of power system electromagnetic transients.

Chapter VIII suggests the use of one of the proposed visualization techniques for fault location purpose in transmission lines.

Finally, Chapter IX summarizes the contributions of this dissertation and draws conclusions.

CHAPTER II

FAULT LOCATION IN POWER SYSTEMS

A. Introduction

Accurate fault location in power transmission and distribution systems saves time and resources for the electric utilities. Since the visual search of faulted lines are costly and sometimes inconclusive, accurate information needs to be obtained in a form most useful to the system operator who is in charge of guiding the field personnel. A sophisticated system of fault location technology, software, hardware and communications systems is designed to acquire accurate information. Technology is available which can provide a fault location determination in a transmission span of 300 m [3].

Communications systems can gather and quickly provide fault location information from substations to the system operators. Other communications systems, such as Supervisory Control and Data Acquisition (SCADA) collect information regarding status of the circuit breakers, switches, the sequence of events, relays and oscillographs, which can also be used for fault location selection. However, concise information is required and a central computer collects the bulk data and filters the information sufficient for field personnel communications. Fault location systems usually provide *distance to fault* from a transmission line end. Field personnel can utilize these data to figure out the fault locations from transmission line maps and drawings.

Fast and precise fault location is also very important for speedy restoration of power, particularly on transmission lines with distributed loads. Power system operators can identify and isolate faulted sections on tap-loaded lines by opening circuit breakers or switches. Subsequently the power is restored to the tap loads serviced by

the healthy transmission sections.

Locating the faults on important bulk transmission lines accurately and timely can be more expensive. Due to their length and size, search efforts may take longer to complete. Consequently load becomes less economic to supply since large distances separate the power generation and the load. The remaining power system may be operating inefficiently from a system security standpoint in order to meet power delivery requirements.

The fault location methods in the literature can be classified under three main titles [4]:

1. Power frequency based approaches

2. Differential equation based approaches

3. High frequency based approaches

Once a general review of transmission line models is given in the next section, existing fault location methods are briefly reviewed followed by a detailed description of traveling wave theory and traveling wave based fault location techniques.

B.   A General Review of Transmission Line Models

A transmission line is a crucial link between power generation units and distribution units in consumption areas. A fault or switching transient originated in the line or in the substation propagates along the transmission line from one point to another. Correct behavior of the power systems during the transients can only be understood by accurate modeling of transmission lines. Although the transmission lines have a simple geometry with simple parameters; series resistance, R, series inductance, L,

shunt capacitance, C, and shunt resistance, $1/G$ (conductance, G), line modeling can be complicated due to the following matters:

- Line parameters (R, L, $1/G$ and C) are not lumped but distributed along the transmission line,

- Series parameters, R and L, are not constant but frequency dependent [5, 6],

- The ground behaves like a return wire, constituting an asymmetrical structure of coupled conductors with the ground.

Fault or switching initiated travelling waves propagating along the transmission line conductors may have multiple velocities with different magnitudes due to this multi-conductor, asymmetrical, lossy, distributed and frequency dependent nature of the transmission line. However, since steady state operation consists of one power frequency, 60 Hz, the frequency dependence and coupling matters are not of concern. Under these circumstances transmission line models can be reviewed under two main topics: *steady state models* and *transient state models*.

A very detailed reference concerning transmission line models is [7]. Travelling wave theory and transmission line discrete time models are extensively described in [8] - [10]. These references are used to compile the information in this chapter.

1.   Transmission line models for steady state

Three models for steady state operation are explained briefly in the following sections. Models are developed by using a single phase transmission line however they are easily generalized to multi-conductor systems by replacing the scalars with matrices.

a. Short line model

Short line model in frequency domain is generally used for transmission lines less than 50 mi length. Model uses lumped line parameters and shunt admittance, $y = G + j\omega C$ is neglected.
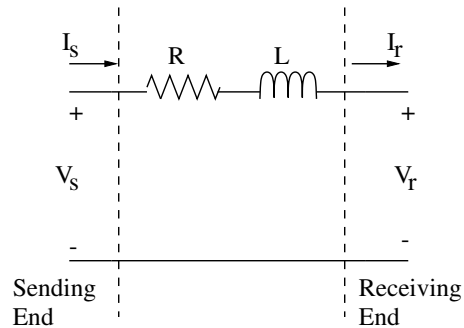
Fig. 1. Short line model

In Figure 1, line series impedance is $z = R + j2\pi f L$ [Ω/mi] where f is power frequency, 60 Hz. Total series impedance is $Z = z \cdot \ell$ [Ω] where ℓ is total line length. $V_s = V_r + I_s Z$ and sending end current is equal to receiving end current.

b. Medium line model

This model is also known as *nominal π model*. Medium line model is generally preferred for transmission lines whose lengths vary between 50 mi and 150 mi. This model also uses lumped line parameters, however, unlike in short line model shunt susceptance, $B = j\omega C$, is taken into account while shunt conductance, G, is neglected as seen in Figure 2.

Line series impedance is $z = R + j2\pi f L$ and total series impedance is $Z = z \cdot \ell$ where ℓ is total line length. Line shunt admittance is $y = j2\pi f C$ [S/mi] and total shunt admittance is $Y = y \cdot \ell$ [S]. The current through the series impedance is
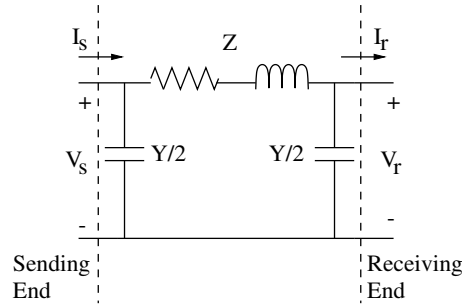
Fig. 2. Medium line model

$I_r + V_r \cdot Y/2$ and sending end voltage $V_s = V_r + Z \cdot (I_r + V_r \cdot Y/2)$. Using KCL sending end current, I_s is obtained as $I_s = I_r + V_r \cdot Y/2 + V_s \cdot Y/2$. If the expressions are rearranged the following structure in frequency domain is obtained:

$$\begin{bmatrix} V_s \\ I_s \end{bmatrix} = \begin{bmatrix} A & B \\ C & D \end{bmatrix} \cdot \begin{bmatrix} V_r \\ I_r \end{bmatrix} \tag{2.1}$$

where $A = D = 1 + ZY/2$, $B = Z$ and $C = Y(1 + ZY/4)$.

c. Long line model

This model is also known *exact π model (equivalent π model)*. For simplicity, model is developed for a single-phase transmission line in Figure 3.
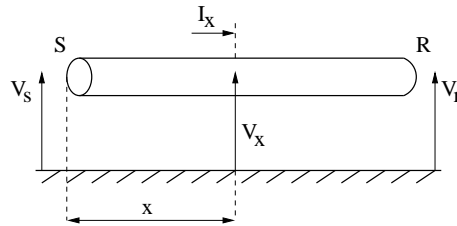
Fig. 3. A single-phase transmission line

An infinitesimal dx element of the transmission line is also given in Figure 4 where $dx \rightarrow 0$.
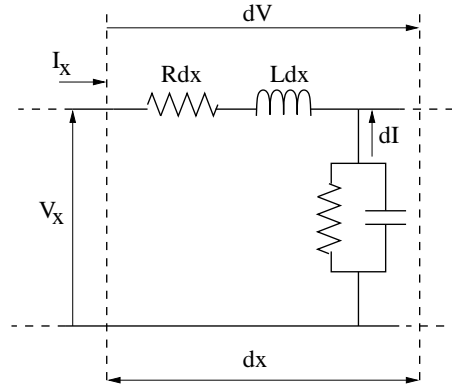
Fig. 4. A dx element of the transmission line in Figure 3

Line equations can be written in frequency domain as follows based on the voltage drop, dV and the current drop, dI:

$$-\frac{dV(x,\omega)}{dx} = (R + j\omega L)I = zI \tag{2.2}$$

$$-\frac{dI(x,\omega)}{dx} = (G + j\omega C)V = yV \tag{2.3}$$

where all line parameters are given in per unit length. Line series parameters R and L are in general frequency dependent while shunt admittance $y = G + jwC$ is assumed to be constant in practice. Following propagation equations can be obtained in frequency domain by combining Equations (2.2) and (2.3):

$$-\frac{d^2V(x,\omega)}{dx^2} = (zy)I \tag{2.4}$$

$$-\frac{d^2I(x,\omega)}{dx^2} = (yz)V \tag{2.5}$$

Once the Equations (2.4) and (2.5) are solved, the voltages and currents along the transmission line are related as follows:

$$V_x + Z_c I_x = (V_s + Z_c I_s) \cdot e^{-\gamma x} \qquad (2.6)$$

where x is any point along the transmission line,

$$Z_c = \sqrt{\frac{(R + jwL)}{(G + jwC)}} \quad and \quad \gamma = \sqrt{(R + jwL)(G + jwC)}$$

In Equation (2.6) Z_c is called *characteristic impedance (surge impedance)* and γ is called *propagation constant.* It can be interpreted from Equation (2.6) that the sending end quantity, $V_s + Z_c I_s$, is transmitted to any point, x, along transmission line according to propagation function, $e^{-\gamma x}$. Sending end and receiving end voltage and currents can be related by using Equation (2.6) as:

$$V_r + Z_c I_r = (V_s + Z_c I_s) \cdot e^{-\gamma \ell} \qquad (2.7)$$

where V_r and Ir are receiving end voltage and current respectively. If $V + Z_c I$ is called forward line function, F, then Equation (2.7) is expressed in a compact way as:

$$F_r = F_s \cdot e^{-\gamma \ell} \qquad (2.8)$$

Equation (2.7) can be used derive transmission line models both for steady state and transient analyses.

By using Equation (2.7) the relation between sending end and receiving end voltages can be expressed in the form of Equation (2.1) for steady state analysis where $A = D = \cosh(\gamma \ell)$, $B = Z_c \sinh(\gamma \ell)$ and $C = \sinh(\gamma \ell)/Z_c$. π-circuit can also be derived using the ABCD form as shown in Figure 5:
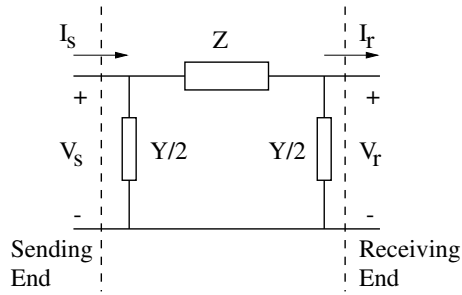
Fig. 5. Exact line model

where

$$Z \;=\; z \cdot \ell \cdot \frac{\sinh(\gamma\ell)}{(\gamma\ell)} \qquad (2.9)$$

$$Y \;=\; y \cdot \ell \cdot \frac{\tanh(\gamma\ell/2)}{(\gamma\ell/2)} \qquad (2.10)$$

Here z and y are the line series impedance and shunt admittance in per unit length as in Equations (2.2) and (2.3). Note that the π-circuit components Z and Y are both frequency dependent. For medium line models hyperbolic correction factors in Equations (2.2) and (2.3), $\frac{\sinh(\gamma\ell)}{(\gamma\ell)}$ and $\frac{\tanh(\gamma\ell/2)}{(\gamma\ell/2)}$ approach *1* approximating the *exact π model* to *nominal π model* where $Z = z \cdot \ell$ and $Y = y \cdot \ell$.

2. Travelling wave theory and transmission line models for transient state

As indicated before, for single frequency solutions such as for steady state operation exact *pi*-circuit parameters, Z and Y, are calculated in frequency domain using Equations (2.9) and (2.10). However, since these parameters are functions of frequency, it is difficult to approximate these for time-domain transients analyses. A simple circuit structure of transmission lines for time-domain transient studies is derived by considering the decoupling effect between sending and receiving ends of a transmission line which is due to the travelling time, τ, of the waves along the line. That means;

sending and receiving ends of a transmission line are disconnected from each other at a time t, if the simulation step size, Δt, is smaller enough than wave travelling time, τ.

a. Transmission line wave equations and ideal line model

Transmission line equations introduced in Equations (2.2) to (2.5) in frequency domain, is studied for time domain analysis considering a lossless transmission line with distributed parameters. The infinitesimal dx element in Figure 4 is assumed to be lossless where series resistance, R, and shunt conductance, G, are ignored. Transmission line equations in time domain is then given as:

$$\frac{dV}{dx} = -L\frac{dI}{dt} \tag{2.11}$$
$$\frac{dI}{dx} = -C\frac{dV}{dt} \tag{2.12}$$

Once differentiated with respect to x, following equations are obtained from Equations (2.11) and (2.12):

$$\frac{d^2V}{dx^2} = LC\frac{d^2V}{dt^2} \tag{2.13}$$
$$\frac{d^2I}{dx^2} = LC\frac{d^2I}{dt^2} \tag{2.14}$$

Equations (2.13) and (2.14) constitute the well-known transmission line *wave equations*. D'Alembert showed that these equations are satisfied with:

$$v(x,t) = F(t - \frac{x}{\nu}) + B(t + \frac{x}{\nu}) \tag{2.15}$$

$$i(x,t) \quad = \quad \frac{1}{Z_c}[F(t - \frac{x}{\nu}) - B(t + \frac{x}{\nu})] \tag{2.16}$$

where $\nu = 1/\sqrt{LC}$ is the travelling wave velocity of the lossless line, $Z_c = \sqrt{\frac{L}{C}}$ is the characteristic impedance and F and B are the forward and backward travelling wave functions respectively which are arbitrary and determined by boundary conditions. If we multiply Equation (2.16) by Z_c and add it to or subtract it from Equation (2.15) following expressions are obtained:

$$v(x,t) + Z_c i(x,t) = 2Z_c \cdot F(t - \frac{x}{\nu}) \tag{2.17}$$

$$v(x,t) - Z_c i(x,t) = 2Z_c \cdot B(t + \frac{x}{\nu}) \tag{2.18}$$

The left side of Equation (2.17), $v + Z_c i$ remains constant when the argument $t - \frac{x}{\nu}$ is constant. Thus, $v + Z_c i$ remains constant to a fictitious observer traveling at velocity ν in the positive x direction along the transmission line. If travelling time $\tau = \ell/\nu$ is the transit time from sending end to receiving end of the line, the value of $(v + Z_c i)$ at time t at sending end must be the value at time $t + \tau$ at receiving end. Similarly, $(v - Z_c i)$ in Equation (2.18) remains constant when $t + \frac{x}{\nu}$ is constant. $v - Z_c i$ remains constant to a fictitious observer travelling at a velocity, ν, in the negative x direction. Consequently, the value of $(v - Z_c i)$ at time t at receiving end must be the value at time $t + \tau$ at sending end. These can be expressed respectively as follows [8]:

$$v_s(t) + Z_c i_s(t) \quad = \quad v_r(t + \tau) + Z_c i_r(t + \tau) \tag{2.19}$$

$$v_r(t) - Z_c i_r(t) \quad = \quad v_s(t + \tau) - Z_c i_s(t + \tau) \tag{2.20}$$

Note that for a lossless transmission line where $\gamma = j\omega\sqrt{LC}$ Equation (2.19) is

inverse laplace transformation of (2.7) given that $\tau = \ell/\nu = \ell\sqrt{LC}$ and $\gamma\ell = j\omega\tau$. Following these manipulations, an ideal (lossless) transmission line in time-domain is represented as:
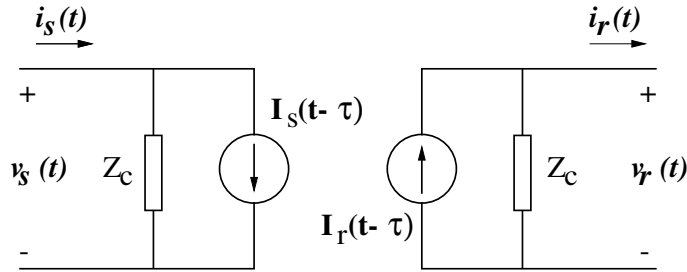
Fig. 6. Discrete-time model for a lossless transmission line

Necessary manipulations lead to the explicit formulas of terminal currents in terms of the equivalent current sources, I_s and I_r as follows:

$$i_s(t) = I_s(t-\tau) + \frac{v_s(t)}{Z_c} \tag{2.21}$$

$$i_r(t) = I_r(t-\tau) - \frac{v_r(t)}{Z_c} \tag{2.22}$$

History updates of the current sources are given as:

$$I_s(t) = I_r(t-\tau) - \frac{2}{Z_c}v_r(t) \tag{2.23}$$

$$I_r(t) = I_s(t-\tau) + \frac{2}{Z_c}v_s(t) \tag{2.24}$$

In time-domain transient simulations continuous time circuit parameters such as L and C are transformed to discrete time parameters. A lumped inductance, L is expressed by parallel connection of a resistance $R_L = 2L/\Delta t$ (Δt is simulation step

size) and a history term of a current source. The current flowing through a lumped inductance is explicitly given as:

$$i(t) = \frac{v(t)}{2L/\Delta t} + I_L(t - \Delta t)$$

$$I_L(t - \Delta t) = i(t - \Delta t) + \frac{v(t - \Delta t)}{2L/\Delta t}$$

Similarly discrete model for a lumped capacitance C is expressed by parallel connection of a resistance $R_C = \Delta t/2C$ and a history term of a current source. The current flowing through a lumped capacitance is given as:

$$i(t) = \frac{v(t)}{\Delta t/2C} - I_C(t - \Delta t)$$

$$I_C(t - \Delta t) = i(t - \Delta t) + \frac{v(t - \Delta t)}{\Delta t/2C}$$

Discrete-time model for an ideal transmission line is given. Now the losses will be taken into account under two categories. The lumped resistance model is given first followed by the more accurate frequency dependent line model.

b.   Lumped resistance line model

The original line model in ATP/EMTP is based on the ideal (lossless) line model as shown in Figure 6 adding the lumped resistances at two ends and the middle of the transmission line as given in Figure 7. Thus, in practice when a lossy transmission line with line length ℓ is created in ATP/EMTP, inside the program the line is simulated as if there are two ideal transmission lines of equal lengths, $\ell/2$ and the losses are simulated with constant resistances.

This approach gives accurate results as long as total line series resistance is con-
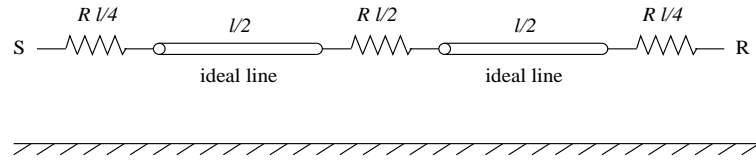
Fig. 7. Constant parameter (CP) line model in EMTP

siderably smaller than the characteristic impedance: $R\ell \ll Z_c$. Frequency dependent line model introduced by J.R. Marti [11] is discussed next which considers all line parameters, R, L, G and C as functions of frequency and distributed along the transmission line.

c.   Frequency dependent line model

In order to obtain a frequency dependent line model, Z_c is approximated by using RC network as shown in Figure 8. J.R. Marti shows that it is better to approximate frequency dependent quantities; propagation function $A(w) = e^{-\gamma\ell}$ and characteristic impedance $Z_c(w)$ in frequency domain. The weighting function $a(t)$ can then be written as a sum of exponentials, avoiding the inverse fourier transformation of $A(w)$. Similarly the rational function approximation of $Z_c(w)$ produces directly the values of R and C in the RC network in Figure 8 [6, 11].
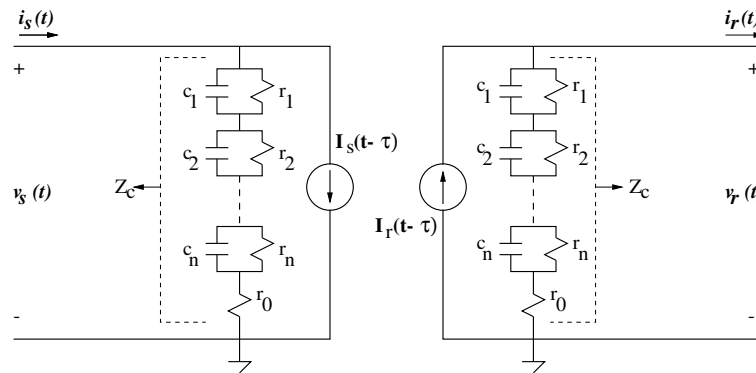
Fig. 8. Frequency dependent (FD - J. Marti) line model in EMTP

The characteristic impedance $Z_c(w)$ is approximated by a rational function as follows [11]:

$$Z_c(j\omega) = k\frac{(s + z_1)(s + z_2)...(s + z_n)}{(s + p_1)(s + p_2)...(s + p_n)} \tag{2.25}$$

which is also expressed as:

$$Z_c(j\omega) = k_0 + \frac{k_1}{s + p_1} + \frac{k_2}{s + p_2} + ... + \frac{k_n}{s + p_n} \tag{2.26}$$

corresponding to RC network in Figure 8:

$$
\begin{aligned}
r_0 &= k_0 \\
r_i &= \frac{k_i}{p_i} \quad and \quad c_i = \frac{1}{k_i}, \quad i = 1...n
\end{aligned}
$$

The rational approximation for propagation function $A(w)$ is also similar however the number of zeros is smaller than the number of poles. Details of the procedure can be found in [11].

Since approximated Z_c is now composed of only resistances and capacitances, the solution of the transmission line is straight forward as in CP model because as explained in the previous section capacitances are expressed in terms of resistances and current sources in discrete time domain.

d. Lattice diagram

Fault or switching initiated transients are composed of travelling waves. The details of forward and backward travelling waves are given in the previous sections. While these waves are travelling along the lines reflections occur due to the discontinuities such as the fault point, receiving or sending end terminals of a line. These transients

continue to bounce back and forth between the fault point and the terminals until a post-fault steady state is reached. The change in terminal bus transients can only be understood by using the famous *Lattice Diagram* method [1]. Figure 9 shows an example where a single-phase lossless line is considered with a fault near bus B. The Lattice diagram shows multiple reflections and refractions initiated by the fault.
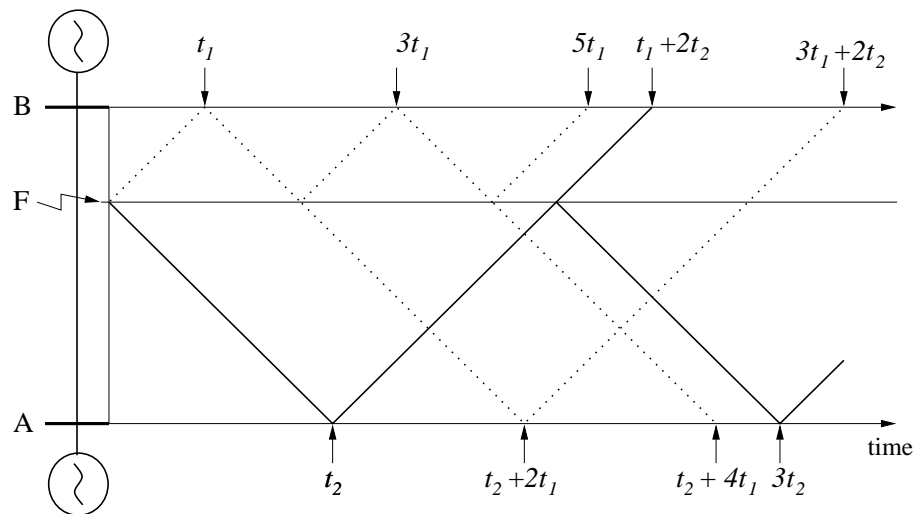
Fig. 9. Lattice diagram for a fault near bus B

The arrival times of the backward and forward travelling waves are indicated. Assume that the fault is x miles away from bus A. Then the arrival time of the forward travelling wave at bus B, $t_1 = \frac{\ell - x}{\nu}$, and the arrival time of the backward travelling wave at bus A, $t_2 = x/\nu$ where ℓ is the total line length and ν is the travelling wave velocity. This information is utilized to locate the fault.

In multi-phase lossy systems there are three modes of propagation as described in the previous section, therefore the travelling wave calculations have to be done in the modal domain.

e.   Time-domain models for multi conductors and modal transformation

Travelling wave propagation in multi-phase systems are complicated due to the coupling effects of inductances and capacitances. The power systems are composed of three phases. Due to the induced voltages there are mutually coupled impedances between conductors. By using linear algebra modal decomposition theory initially introduced by Wedepohl [12] three-phase problem is reduced to three single-phase problems. Coupled three phases are decoupled to three single circuits each having its own characteristic impedance Z_c and time delay τ. Since each mode has its own time delay, travelling waves propagate through each mode have different velocities. One of the commonly used modal transformations is Clarke's transformation [13] for fully transposed transmission lines. Main advantage of Clarke's transformation is that, the transformation matrix is real unlike the symmetrical component transformations. Once decoupled the three-phase system can be represented by using the constant parameter line model or frequency dependent line model for each separate mode. Clarke's transformation matrix is given as:

$$
\begin{bmatrix} V_1 \\ V_2 \\ V_3 \end{bmatrix} = \frac{1}{\sqrt{3}} \begin{bmatrix} 1 & 1 & 1 \\ \sqrt{2} & -\frac{1}{\sqrt{2}} & -\frac{1}{\sqrt{2}} \\ 0 & \frac{\sqrt{3}}{\sqrt{2}} & -\frac{\sqrt{3}}{\sqrt{2}} \end{bmatrix} \cdot \begin{bmatrix} V_a \\ V_b \\ V_c \end{bmatrix} \tag{2.27}
$$

where V_a, V_b and V_c are the phase voltages, V_1 is ground mode voltage and V_2, V_3 are aerial mode voltages. A more convenient representation is:

$$
\begin{aligned}
V_{phase} &= T \cdot V_{mode} \\
I_{phase} &= T \cdot I_{mode}
\end{aligned}
$$

where T is the transformation matrix.

The series impedance matrix Z is given as:

$$Z = \begin{bmatrix} Z_{aa} & Z_{ab} & Z_{ac} \\ Z_{ba} & Z_{bb} & Z_{bc} \\ Z_{ca} & Z_{cb} & Z_{cc} \end{bmatrix} \tag{2.28}$$

where Z_{ii} is self impedance of the phase i and Z_{ij} is the mutual impedance between the phases i and j. $Z_{ij} = Z_{ji}$ for transposed lines. The phase voltages and phase currents are related to each other as:

$$V_{phase} = Z \cdot I_{phase} \tag{2.29}$$

Phase quantities in Equation (2.29) are transformed into modal domain using the transformation matrix T:

$$\begin{aligned} T \cdot V_{mode} &= Z \cdot T \cdot I_{mode} \\ V_{mode} &= T^{-1} \cdot Z \cdot T \cdot I_{mode} \\ Z_{mode} &= T^{-1} \cdot Z \cdot T \end{aligned}$$

Subsequently Z_{mode} has the following form:

$$Z_{mode} = \begin{bmatrix} Z_s + 2Z_m & 0 & 0 \\ 0 & Z_s - Z_m & 0 \\ 0 & 0 & Z_s - Z_m \end{bmatrix} \tag{2.30}$$

where Z_s is self impedance of the transmission line (assuming that $Z_{aa} = Z_{bb} = Z_{cc}$) and Z_m is the mutual impedance (assuming that $Z_{ab} = Z_{bc} = Z_{ac}$).

If the transmission line is untransposed, an eigenvalue/eigenvector analysis yields

a frequency dependent transformation matrix. Usually the matrix is calculated at a certain frequency close to the frequency of the fault transients and the imaginary part is ignored [6].

C.   A General Review of Fault Location Techniques

All fault location methods require either single end or double end voltage and current information for each phase. Many of the signal processing techniques required for line protection are also necessary for fault location techniques. Following, most common fault location techniques are briefly reviewed.

1.   Power frequency based methods

The power frequency based methods are also known as *impedance-based* methods. They are the most common methods used in protection schemes. The main idea of these methods is to calculate the apparent impedance by looking into the line from one end [14]. These methods can be developed using either one-end or two-end voltage and current information. The advantage of two-end fault location techniques is to be able to locate the ground faults without knowing the zero-sequence impedance of the transmission line [15]. Accurate fault location using impedance-based methods first requires successful extraction of the phasor quantities. This filtering process guarantees that transients do not affect the measurement of phasors. The procedure is generally as follows:

- Voltage and current phasors are measured,

- Fundamental components are extracted,

- Phasors and fault type are determined,

- Impedance algorithm is applied.

If the fault resistance is assumed to be negligible, the following impedance equations in Table I can be used for fault location:

Table I. Simple impedance equations

Fault Type	Positive Sequence Impedance Equation (mZ_1)
A-ground	$V_a/(I_a + \beta \cdot 3 \cdot I_0)$
A-B or A-B-g	V_{ab}/I_{ab}
A-B-C	V_{ab}/I_{ab}, V_{bc}/I_{bc} or V_{ca}/I_{ca}

where

$$k = \frac{Z_0 - Z_1}{3Z_1}$$

Z_0 = *is the zero sequence line impedance*

Z_1 = *is the positive sequence line impedance*

m = *Per − unit distance to fault from sending end*

    (i.e. distance to fault divided by the total line length)

I_0 = *is the zero sequence current*

These simple formulas have been developed in the literature so far taking the fault resistance into account, yielding more complex and accurate fault location techniques. These techniques and the challenges for fault location accuracy are well reviewed and described in [16] and [17], with new techniques in [18] and [19]. The well-known method for fault location with a fault resistance is the simple reactance method.

During a fault, the voltage drop from the sending end is given as:

$$V_s = m \cdot Z_1 * I_s + R_f \cdot I_f \tag{2.31}$$

where for and phase A to ground fault $V_s = V_{ag}$ and $I_s = Ia + \beta \cdot 3 \cdot I_0$. The goal here is to minimize the effect of $R_f \cdot I_f$ term. Once all terms are divided by I_s, $R_f \cdot I_f / I_s$ term is ignored in simple reactance method and the imaginary part is solved for m:

$$m = \frac{Im(\frac{V_s}{I_s})}{Im(Z_1)} \tag{2.32}$$

Takagi et al. further developed simple reactance technique by using the prefault and fault data in [20].

The challenges of the commonly used impedance-based algorithms can be summarized as follows [21]:

- Combined effect of fault resistance and load

- System infeeds

- Zero-sequence mutual coupling

2. Differential equation based methods

The main advantage of the fault location methods using differential equation solutions is that they don't need to estimate the voltage and current phasors. The basic idea is to solve the transmission line differential equations and consequently estimate the fault impedance. Once the fault impedance is calculated the distance to fault is easily determined. [22] and [23] use the short line model where the line differential equation is given as:

$$v_{x1}(t) - v_{x2}(t) = (x_2 - x_1[Ri(t) + L\frac{di(t)}{d(t)}] \tag{2.33}$$

where x_1 and x_2 are two different locations along the line.

[24], [25] and [26] utilize long line model (exact π model) solving the well-known *Telegrapher's Equations*:

$$\frac{dv}{dx} + L\frac{di}{dt} = -Ri$$
$$C\frac{dv}{dt} + \frac{di}{dx} = 0$$

where v is the phase voltage, i is the phase current, R is the line series resistance, L is the line series inductance, C is the line capacitance.

As explained under the section of transmission line models, short line model is simple but it is useful for very short lines. Neglecting the line capacitance causes inaccurate fault location results. Fault location methods using exact line model are more accurate, however, they are sensitive to transposition, line coupling, fault inception angle, parameter changes in different frequency ranges and in some cases to line compensation.

3. High frequency based methods

High frequency based methods utilize the very fast transients initiated by a fault. Fast transients are composed of very high frequencies varying from kHz to MHz comparing to steady state frequency, 60 Hz. These transients are evolved according to the forward and backward travelling waves propagating along the transmission lines with a velocity near the speed of light. Travelling wave based fault location for transmission lines is initially formulated in [27] by defining a discriminator identifying the fault

whether it is located in front or behind the relay. [28] proposed another technique calculating the variation of the voltage and current signals and using a $\Delta V - R\Delta I$ trajectory to locate the fault. [29] and [30] proposed correlation based methods calculating the time delay between forward travelling wave and its reflection from fault location by a cross-correlation function. [31] proposes a new method using maximum likelihood estimation technique to estimate the arrival times of the travelling waves.

A brief overview of travelling wave based fault location methods can be found in [32] and [33] gives an extensive overview of the all travelling wave based fault location algorithms in the literature.

Recently, sophisticated signal processing techniques are also introduced to overcome the complexities of correlation based travelling wave methods. One such technique is initially introduced by Magnago and Abur in [34] and extended to more complex power system topologies in [35] and [36]. Magnago and Abur proposed the use of wavelet transformation technique to extract the transients' information from voltage signals. This technique is briefly reviewed in Chapter III. [35] extends the results of [34] to the three terminal circuits with Metal Oxide Varistor (MOV) protected series capacitors and mutually coupled line sections. The proposed method is given in Chapter IV. [36] presents a similar approach for fault location in distribution systems with distributed generators. The proposed method is described in Chapter V.

The travelling-wave approach is the fastest approach among the fault location techniques; however, the travelling wave based fault location techniques are sensitive to close-up faults where the fault is located very close to terminals. Another disadvantage of these methods is that existences of discontinuities along the transmission lines increase the travelling wave realization.

D. Summary

A detailed background of power system transmission lines for fault location is given. Transmission line models for steady state and transient state analyses are briefly explained. Travelling wave theory is reviewed followed by a general summary of the common fault location techniques. Next chapter reviews the limitations of Fourier based transforms, gives background information about wavelet transform followed by a summary of its applications in power system analysis. A review of a travelling wave based fault location technique using wavelet analysis is also given at the end of the chapter.

CHAPTER III

FUNDAMENTALS OF WAVELET TRANSFORM BASED

FAULT LOCATION

A.   Introduction

The wavelet theory is initially developed in the early 20th century, however, it became widely popular in various areas from acoustics to earthquake prediction in 1980s to study the analysis and synthesis of non-stationary signals. Like Fourier analysis, wavelet analysis is based on the expansion of functions in terms of a set of basis functions. Unlike the Fourier analysis, wavelet analysis expands the functions not in terms of trigonometric polynomials but in terms of small waves, wavelets, by applying translations and dilations. Unlike the Fourier analysis, which gives a representation of a signal in frequency, wavelet analysis provides a representation in both time and frequency. Thus, wavelet analysis specifies the occurrence time and the frequency of a transient disturbance on a signal. Following sections give a brief overview of the limitations of Fourier based transforms followed by the description of wavelet transform fundamentals. Then, applications of wavelet transform to power system analysis are summarized followed by a review of a traveling wave based fault location technique using wavelet analysis.

[37]-[45] are only a few of the references in the literature covering the fundamentals of the wavelet transformation. These references are extensively used to compile the following sections including the review of Fourier techniques' limitations and the wavelet fundamentals.

B.   Brief Review of Fourier Techniques' Limitations

Understanding the limitations of Fourier based techniques (i.e. Fourier Transform and Windowed Fourier Transform) leads to a motivation for the use of wavelet analysis. The Windowed Fourier Transform (WFT) is able to overcome some of the problems that Fourier Transform presents, however to a certain degree. Eventually it is proved that the Wavelet Transform is the only signal analysis method, which can represent a signal in time domain with a perfect frequency resolution.

In general, signals can be classified in two groups with respect to their frequency spectrum: stationary and non-stationary. A stationary signal contains the same frequency components throughout its duration resulting in a constant spectrum in time. Perfect square waves and triangular waves are examples of such stationary signals. However, a non-stationary signal, unlike a stationary one, has frequency components varying with time. A music piece is a good example of a non-stationary signal, which is made up of different notes (frequencies) at different moments.

The conventional Fourier Transform provides a frequency spectrum for an entire signal, which is very convenient for analyzing a stationary signal. However, analyzing a music piece with Fourier Transform brings in the spectrum of entire piece, giving the information of the presence of different frequencies but contains no information regarding the time location of a given frequency. Nevertheless, time-frequency information is of great importance in the analysis of electromagnetic transients in power systems, machine vibrations, and traces on a seismogram or electrical pulses on a heart monitor.

Historically, when time and frequency information of a signal were simultaneously needed, the signal would be cut into several pieces with the length of each piece corresponding to the preferred time resolution. This procedure is called *windowing*

and each signal could then be investigated by using Fourier Transform. Without completely avoiding the Fourier Transform, the problem is overcome to a certain degree by using the *Windowed Fourier Transform* (WFT, a.k.a. Short Term Fourier Transform or Gabor Transform). Thanks to *windowing* technique that WFT allows real time processing unlike Fourier Transform which requires the entire signal.

During WFT procedure the first step requires to chop the signal in to smaller parts. In order to break a signal, $f(t)$, into pieces, a window function, $g(u)$, which is square-integrable, continuous, smooth and always positive, is defined. Once a parameter t is chosen to be the center of interest in the signal, the windowing function, $g(u)$, is translated in time to that position, i.e. $g(u - t)$. Multiplying the translated window function $g(u-t)$ with the signal $f(u)$ helps to *window-out* the desired interval of the signal by dampening everything outside of it resulting in a new function $f_w(u)$. Finally, the Fourier analysis is used to analyze the new signal $f_w(u)$.

A square window is usually considered to be a good window, however, it is neither smooth nor continuous and truncation of the main signal happens near the window edges causing artificial high frequencies in the spectrum. Instead of defining the translation parameter t as a constant, it can be defined as a variable through the Fourier Transform. Consequently, a complex function of two variables, frequency, w and time translation, t, is defined constituting the fundamentals of WFT. Gaussian functions are generally preferred as window functions. They are smooth and continuous and their compactly supported (narrow) and broadly supported (broad) forms for desired frequencies are very suitable for windowing.

WFT does also have disadvantages despite its supremacy over Fourier Transform with respect to time-frequency resolution. The most important drawback of WFT is the natural need of cutting the signal. This procedure is carried out by convolving the signal with the cutting window in the time domain. Since the convolution in the time

domain corresponds to multiplication in the frequency domain, it is very important how one cuts the signal to prevent unnatural frequencies in the Fourier Transform. The other drawback of the WFT is the fixed window size. If there are few oscillations in the window, WFT gives a good time (space) and frequency (scale) resolution. However, if there are many oscillations in the window, then, like in Fourier Transform the time resolution is bad. A compactly supported (short wavelength) window results in a bad frequency resolution if the signal has a longer wavelength than the window. Similarly, a broadly supported window (long wavelength) causes a bad time resolution if the duration of a transient feature is much less than the wavelength (support) of the window. The phenomenon can be summarized as follows: By using fixed window functions, high frequencies sacrifice the accuracy of their time location to achieve a precise frequency while low frequencies become smeared out in the frequency domain, but are located well in the time domain [37].

Wavelet Transformation replaces the complex exponential function with a function more localized in time and overcomes the shortcomings of Fourier-based techniques. Perfect time-frequency resolution is achieved by Wavelet Transformation technique, which will be described briefly in the following section.

C.   Fundamentals of Wavelet Transform

Signal-cutting problem in WFT is overcome in wavelet analysis by using a fully scalable modulated window. The window is shifted along the signal and for every location the spectrum is calculated. This process then repeated several times with a shorter or longer window for every cycle. Eventually a collection of time-frequency representations of the signal is obtained with different resolutions. Due to the nature of this collection this analysis is often called multi-resolution analysis [38].

The window is composed of *wavelets* which are functions that satisfy certain mathematical requirements. These wavelets are used to represent signals or other functions. Representing signals or functions by using other functions was first proposed in 1822 by Joseph Fourier who used the superposition of the sines and the cosines in order to represent other functions. Since the sines and the cosines, which comprise the bases of Fourier analysis, are global (not local) stretching out to infinity, they give unsatisfying results when used to approximate sharp spikes or transients [39]. However, functions can be approximated in finite domains by using wavelet analysis since the individual wavelet functions are localized in space unlike the sinusoidal functions. Wavelet analysis uses different *scales* (resolutions) to process the data in wavelet algorithms.

A *scale* is the fundamental idea behind the wavelet analysis and it corresponds to a concept opposite to the frequency since the frequency term is reserved for the Fourier Transform. A scale is actually a frequency interval (frequency range) and the large scales show the low frequency resolution of the signals while the small scales reveals the high frequency details. In other words, if one looks at the signal through a *large window* - large scale -, gross features will be noticed, if a *small window* - small scale - is used, small features will be noticed. Due to this opportunity wavelet analysis presents, wavelets are very suitable for approximating signals with sharp discontinuities [38] such as electromagnetic power system transients.

The wavelet analysis procedure starts with adopting a wavelet prototype function which is called an *analyzing wavelet* or *mother wavelet*. The wavelets are basically *little waves* that start and stop, and they all are derived from one *mother wavelet* by translation in space and dilation (change of the scale and space simultaneously). A mother wavelet has to satisfy the *admissibility* and *regularity* conditions. These are the properties, which gave wavelets their name [38]. Basically, admissibility condition

implies that the average value of a wavelet has to be zero in time domain. Consequently a wavelet has to be oscillatory. In other words the mother wavelet function must be a *wave*. According to the regularity condition wavelet transform must decrease quickly with decreasing scales indicating that the wavelet function must have smoothness and concentration in both time and frequency domains [38]. Temporal analysis is conducted by using a contracted, high-frequency version of the mother wavelet, and the frequency analysis is carried out by using a dilated, low-frequency version of the same mother wavelet.

One important detail is that there isn't a single set of basis functions in wavelet analysis like sines and cosines in Fourier Transform. In wavelet analysis there is an infinite set of possible basis functions comprised of wavelets. Accordingly, the wavelet analysis provides immediate access to information that can be obscured by Fourier analysis.

An advantage of wavelet transforms is that unlike in Fourier transforms the windows change. Long basis functions (wavelets) are used to obtain detailed frequency analysis and short basis functions are used to extract signal discontinuities [39].

There are two forms of wavelet analysis; continuous and discrete, which will be briefly reviewed in the following sections.

1. Continuous Wavelet Transformation (CWT)

Dilations (scaling or speed-up) and translations (time delay or time shift) of the mother wavelet *W(t)* given in Equation (3.1) define a basis (i.e. wavelet basis) [39].

$$W_{d,\tau}(t) = \frac{1}{\sqrt{d}} \cdot W(\frac{t - \tau}{d}) \tag{3.1}$$

where d stands for the dilation (scaling) parameter and τ is the translation parameter of the mother function $W_{d,\tau}(\text{t})$ to generate wavelets. The scale index d indicates the wavelet's width, and the location index τ gives its position. The $\frac{1}{\sqrt{d}}$ factor is for energy normalization at different scales. Once the mother wavelet function is known, a CWT of a function, f(t), is given in Equation (3.2):

$$CWT(f, d, \tau) = \int_{-\infty}^{\infty} f(t) \cdot W_{d,\tau}^{*}(t) dt \qquad (3.2)$$

where * stands for complex conjugation. Equation (3.2) shows how to decompose a function into a set of basis functions, wavelets as represented by $W_{d,\tau}(t)$, which are derived from one mother wavelet $W(t)$.

As presented in Equation (3.2), the CWT of a function, f(t), is obtained by continuously shifting a continuously scalable function, W(t) over f(t) and calculating the correlation between the two. However, continuously translating and scaling a wavelet function results in an infinite number of wavelets and eventually leads to a redundant number of wavelet coefficients and an enormous computational burden. In order to overcome this redundancy Discrete Wavelet Transform is introduced.

2. Discrete Wavelet Transformation (DWT)

Discrete wavelets are not continuously scalable and translatable but they are dilated and translated in discrete time steps. In DWT, filters of different cutoff frequencies are utilized in order to decompose the signal at different scales. A series of high-pass filters are repeatedly applied to a signal to extract the high frequencies and another series of low-pass filters are applied to the signal to analyze the low frequencies [40].

The amount of the detail information in the signal constitutes the resolution (scale) of the signal, which is varied by the filtering operations. Up-sampling and

down-sampling operations are used to change the scale. Up-sampling a signal increases the sampling rate of the signal by introducing new samples to the signal while down-sampling corresponds to decreasing the sampling rate by deleting some samples of the signal. As an example, down-sampling a signal by two implies to drop every other sample while up-sampling by two refers to adding new samples, generally zero or an interpolated value, between every two samples [40].

The DWT decomposes the signal into approximation and detail information in order to analyze the signal at different scales. Two sets of functions, scaling and wavelet functions are employed for this purpose. Scaling functions are associated with low-pass filters while wavelet functions are associated with high-pass filters. The decomposition of the signal into different scales is achieved by low-pass and high-pass filtering of the signal in time domain [40].

A general form of the discrete mother wavelet function used in DWT is given in Equation (3.3) [38]:

$$W_{j,k}(t) = \frac{1}{\sqrt{d_0^j}} \cdot W(\frac{t - k\tau_0 d_0^j}{d_0^j}) \tag{3.3}$$

where j and k are integers and $d_0 > 1$ is a fixed dilation step. τ_0 is the translation factor and depends on the dilation step, d_0. Usually the discrete mother wavelets are dilated by powers of two and translated by integers. The translation factor, τ_0 is chosen as *1* so that the sampling of both the frequency (since $d_0 = 2$) and time axes are *dyadic*.

The scaling function is obtained in Equation (3.4) by using the mother wavelet function, $W_{j,k}(t)$, in order to span the data domain at different scales [39].

$$\omega(t) = \sum_{k=-1}^{N-2} (-1)^k c_{k+1} W(2t + k) \tag{3.4}$$

where ω is the scaling function for the mother wavelet W; and c_k are the wavelet coefficients. The wavelet coefficients are composed of two dominant patterns corresponding to low-pass and high-pass filters. The main idea behind the DWT analysis is to reapply this set of filters, the filter bank, to the signal. The low-pass output (averages or approximation) becomes the input to a second filter bank while the high-pass output corresponds to the details having the high-frequency information of the signal. Typical applications of a DWT have four to five levels each level corresponding to a scale [41].

Haar, Morlet, Meyer, Mexican Hat wavelets as well as Coiflets, Biorthogonal wavelet pairs and Daubechies' wavelet family are among the most popular in the literature, however, one can create her/his own mother wavelet satisfying the necessary mathematical requirements briefly reviewed in the previous sections. More detailed information regarding different mother wavelets can be found in [42]. MATLAB Wavelet Analysis Toolbox also provides extensive information about continuous and discrete wavelet transforms presenting sophisticated tools to utilize the transforms via graphical user interface or command line.

Daubechies' wavelet family provides the most suitable mother wavelets for power system electromagnetic transients' studies. Following section briefly reviews the use of wavelet analysis in power systems and finally a travelling-wave fault location technique along power system transmission lines using DWT is explained. This fault location technique is initially proposed in [34, 4] and it constitutes the basis of the fault location methods presented in the following chapters.

D.   Power System Analysis Applications of Wavelet Transform

The uses of wavelet analysis in power engineering applications emerge in early 90s. Several publications have been presented in the literature applying the wavelet analysis to different areas in power engineering, which can be categorized as:

- Transient signal analysis and identification

- Non-stationary voltage distortions analysis

- Waveform signature recognition

- System transient data compression and storage

- Characterization of voltage transients or harmonics

- Network analysis

[46] gives an extensive study by comparing the applications of wavelet, Fourier and short Fourier methods to power system transients. The benefits of wavelet analysis for power quality, detection of incipient failures of transformer windings and transient disturbance studies are emphasized. Analysis of arc furnace current and turbine vibrations are presented by using discrete wavelet analysis in [47]. An application of wavelets to non-stationary power system disturbances is given in [48]. Detection and classification of power quality disturbances using wavelet transform are given along with the fundamentals with wavelet theory in [49]. [50] introduces the wavelet domain equivalents of the network elements to analyze the power system disturbances. [51] proposes the use of Morlet wavelets to detect and localize power system disturbances such as voltage sag, voltage swell, momentary interruption and oscillatory transients. It is also showed that the proposed method is successfully applied to investigate the harmonic distortion of an arc furnace. In [52], based on the

discrete time domain approximation the system components are modelled in discrete wavelet domain for transient and harmonic studies.

E. Fault Location Using Wavelet Transform

In this section a fault location algorithm introduced in [34, 4] is reviewed. The method calls for a three stage procedure. In the first stage, the Clarke's modal transformation is applied to the sampled voltage signals at the line terminals. In the second stage, DWT is applied to the modal voltages and the squares of the wavelet transform coefficients (WTC^2) are used in order to determine the instant when the energy of the signal reaches its maximum value. Daubechies-4 [42] mother wavelet is used for wavelet transformation. In the third and the final stage, the fault type (grounded or ungrounded) is determined based on the squared coefficients for the ground mode voltage (WTC^2) in scale-1. This is followed by a fault location procedure that is derived from the Bewley's lattice diagrams of the fault initiated traveling waves. Squared coefficients for the aerial mode voltage (WTC^2) in scale-1 are used in this stage. Fault location procedure of this final stage for the transmission line in Figure 9 initially proposed in [34] is briefly reviewed below.

For two-end synchronized measurements: It is assumed that voltage measurements at bus A and bus B are fully synchronized using Global Positioning System (GPS)-[34]:

$$x = \frac{\ell - \nu \cdot (t_2 - t_1)}{2} \qquad (3.5)$$

where x is the distance to the fault from bus A, t_2 is the initial arrival time of the backward traveling wave at bus A corresponding to occurrence time of the first peak of WTC^2s of aerial mode voltages at bus A in scale-1, t_1 is the initial arrival time

of the forward traveling wave at bus B corresponding to occurrence time of the first peak of WTC^2s of aerial mode voltages at bus B in scale-1, ν is aerial mode traveling velocity and ℓ represents the total line length.

For single-end measurements: In the case of ungrounded faults there are no remote end reflections. Thus, the fault location is determined by using [34]:

$$x = \frac{\nu \cdot \Delta t}{2} \tag{3.6}$$

where Δt is the arrival time difference between two consecutive peaks of aerial mode voltage WTC^2 the first corresponding to the backward traveling wave initiated from fault point and arriving at bus A and the second corresponding to the backward traveling wave traveling from bus A, reaching at fault point and arriving back at bus A once reflected from the fault point.

If the fault is grounded a discrimination criterion is used to identify whether the fault is located at the first half or at the second half of the transmission line. The criterion is based on the time delay between the arrival times of the traveling waves in ground and aerial modes. At high frequencies due to the zero coupling the characteristic impedance of the ground mode is higher than the characteristic impedance of the aerial mode. Thus, waves travel faster in aerial mode than they travel in ground mode. This knowledge is utilized such as for a fault at the middle of the line the time delay between the arrival times of ground mode and aerial mode traveling waves is calculated. Then, during a fault once the time delay is computed, it is compared with the one of the mid-point fault to determine the faulted half of the line. Once the faulted section is figured out then the following equation is used to locate the fault precisely:

$$x = \frac{\nu}{2}(2\tau - \Delta t) \qquad (3.7)$$

where $\tau = \ell/\nu$ is travel time for the entire line and Δt is the arrival time difference between two consecutive peaks of aerial mode voltage WTC^2.

F. Summary

This chapter reviews the fundamentals of the wavelet transformation followed by the application of wavelet technique to the power system analysis. Finally, a traveling wave based fault location method using wavelet analysis proposed in [34] is briefly reviewed. A new fault location technique for three terminal circuits with MOV protected series capacitors and mutually coupled line sections is presented in Chapter IV extending the initial results of [34].

CHAPTER IV

DWT BASED FAULT LOCATION IN THREE TERMINAL CIRCUITS *

A. Introduction

Due to the superimposed reflections of the fault signal from the T-node and the
fault point, fault location in teed circuits (Figure 10) presents unique challenges. In
addition to the impedance based fault location techniques, there are various types
of fault location methods proposed for teed circuits using either phasor-based or
traveling wave-based models.

The post fault differential currents from each terminal is used in [53] in order to
locate the fault in multi terminal transmission lines. A fault location technique using
the pre-fault load flow for phase alignment is described in [54] by utilizing the multi
end phasor measurements in order to determine the fault location. The post fault
synchronized phasor measurements are used to solve the system differential equations
for fault location in multi terminal lines in [55]. The use of negative sequence multi-
ended measurements for fault location in three terminal lines is proposed in [56].
Recently a new fault locator for three terminal lines is described in [57] using phasor
measurement units in order to solve the traveling wave differential equations.

Travelling wave-based fault location techniques for two terminal transmission
lines are briefly explained in Chapter II. A traveling wave technique for teed circuits is
introduced in [58] considering the cross correlation between the forward and backward
traveling waves and a polarity change criterion in order to determine the faulted region
prior to fault location estimation. More recently, in [34], the use of the discrete wavelet

transform (DWT) of the modal components of the fault initiated traveling waves is proposed in order to estimate the location of the fault. The general procedure of the fault location method in [34] is reviewed in Chapter III.
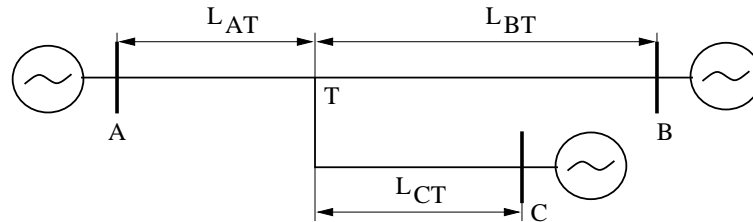
Fig. 10. Three-terminal power transmission system

The presence of parallel transmission lines with mutually coupled line sections makes the fault location problem more difficult in transmission lines. Two different algorithms for different types of faults are developed in [59] and [60] by applying the Z-transform to the loop equations and using Newton Raphson method to solve the nonlinear equation. One ended data with the simplified line model is used by neglecting the shunt capacitance. Another phasor based single ended fault location technique is proposed in [61] where post and pre fault data are used with zero sequence current from a healthy line in order to solve the algebraic equation. A similar approach to [57] is used in [62] by introducing the synchronized measurements. A complex and nonlinear equation is derived from the nodal equations and solved by Newton Raphson iterative scheme in [63]. The technique is validated for a parallel transmission line with a teed circuit, using a lumped line model and for single-phase to ground faults only.

Another source of difficulty in fault location problem is the presence of series capacitors, which are widely used in power systems in order to improve the transfer capability and increase the stability margins. Metal Oxide Varistor (MOV) is the

most popular protection device, which is connected across the capacitor. The existing fault location techniques have to be adapted in order to cope with the complexity introduced by the nonlinear V-I characteristics of the MOV. Different solutions including the use of Artificial Neural Networks [64], single ended [65] and multi-ended [66] measurements have been proposed.

In this chapter, a traveling wave-based fault location technique which is developed earlier in [34] will be extended to the three terminal circuits with mutually coupled line segments and MOV protected series capacitors. Preliminary results in [67] and [68] indicate that this approach can overcome the challenges presented by such topologies. The performance of the proposed fault location algorithm is tested by introducing random errors representing the quantization error introduced by A/D converters, to the simulated signals and using various fault resistances.

B.   Fault Location Procedure

The following assumptions are made in developing the fault location procedure:

- Three terminal measurements are available

- The measurements need not be synchronized

- An open communication channel is available between the terminals

- There is no injection or load at the tee point.

As introduced in Chapter III, the procedure consists of three stages. The modal transformation is applied to the measured voltage signals and the DWT is applied to the modal voltages and the squares of the WTC^2s are obtained in order to determine the instant when the energy of the signal reaches its maximum value. In the following

sections the last stage of the fault location procedure is described in detail for various possible cases.

1. Fault location in teed circuit

Fault location in teed circuits involves two basic steps. In the first step the faulted line segment is identified and in the second stage the fault location along the faulted line segment is determined. The aerial mode WTC^2s are compared at each bus in order to identify the faulted line segment. The magnitude of the first peak of the aerial mode WTC^2s obtained at the sending end of the faulted line segment will be significantly higher than those obtained at the sending ends of the other non-faulted line segments. Once the faulted line segment is known, the location of the fault is determined by using a modified version of the single ended algorithm proposed in [34] as described below.
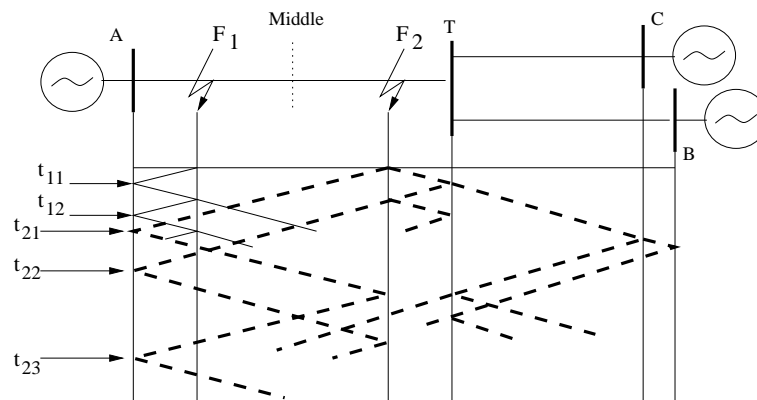
Fig. 11. Lattice diagram [1] for faults at line segment A-T

A grounded fault is assumed to occur at the first half of the line segment $A - T$, at point F_1 in Figure 11. The first peak of the aerial mode WTC^2 is due to the backward traveling wave arriving at bus A at time t_{11}. The second peak is due to the

reflected backward traveling wave arriving at bus A at time t_{12}. The fault location is given by [34]:

$$x = \frac{v \times \Delta t}{2} \qquad (4.1)$$
$$\Delta t = t_{12} - t_{11}$$

where v is the aerial mode propagation velocity in scale-1.

Now consider a fault close to the T-node, shown as F_2 in Figure 11. The backward traveling wave arrives at bus A at time t_{21} while the forward traveling wave arrives at bus A at time t_{22}. The fault location can then be determined as in [34]:

$$x = \frac{\Delta t' \times v}{2} \qquad (4.2)$$
$$\Delta t' = \frac{2 \times L}{v} - \Delta t$$
$$\Delta t = t_{22} - t_{21}$$

where L is the total length of the line segment $A - T$ and v is the aerial mode propagation velocity in scale-1. Fault location can also be determined by using the third peak of the aerial mode WTC^2 which arrives at bus A at time t_{23}. The following equation is used for the calculations [67]:

$$x = \frac{v \times \Delta t}{2} \qquad (4.3)$$
$$\Delta t = t_{23} - t_{21}$$

Nevertheless, as the fault location moves closer to the T-node, the second peak gradually decreases, coming very close to the first peak and eventually the two becom-

ing indistinguishable. The difficulty of identifying the second peak when the fault is in the second half, can be overcome by using Equation (4.3) instead of using Equation (4.2) to calculate the fault location.

The faulted half of the line is determined by comparing the time difference Δt_0, between the arrival time instants of the aerial mode and the ground mode WTC^2s with the time difference, Δt_m, obtained for a fault located right at the middle of the line.

Since the ungrounded and symmetric faults do not produce remote end reflections, Equation (4.1) will be used in order to locate the fault independent of the half in which the fault occurs.

2. Fault location in a teed circuit with MOV protected series capacitor

The most popular and widely used device for protecting a series capacitor against high voltage during faults is the Metal Oxide Varistor (MOV), which is installed directly across the series capacitor as shown in Figure 12, and has a nonlinear I-V characteristics:

$$i = I \cdot \left(\frac{V}{V_{ref}} \right)^q \tag{4.4}$$

The nonlinear characteristics given in Equation (4.4) allows no current to flow through the MOV under normal operating conditions. In case of fault, when the voltage across the capacitor reaches the threshold V_{ref}, MOV clamps the voltage and starts to conduct. The voltage recorded at the sending end will have a different waveform because of this clamping action compared with the waveform obtained without using the MOV.

Assume that a single-phase to ground fault occurs on the line segment $A - T$
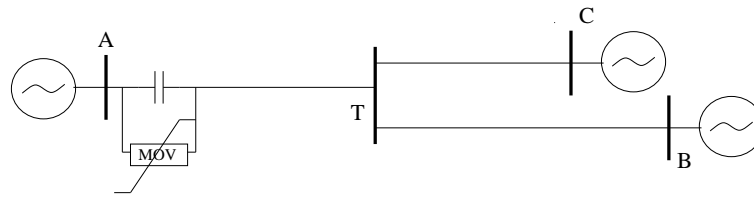
Fig. 12. Teed circuit with MOV protected series capacitor

and voltage transients are recorded at the sending end of the line segments A-T, B-T and C-T in Figure 12. These signals are **not** synchronized. The voltage signals of the faulted phase are presented in Figures 13 and 14 for the cases with or without the MOV in order to show the effect of the varistor. Note that in Figure 14, after the fault occurs the phase voltage is clamped between ∓ 200 kV thanks to the MOV protection.
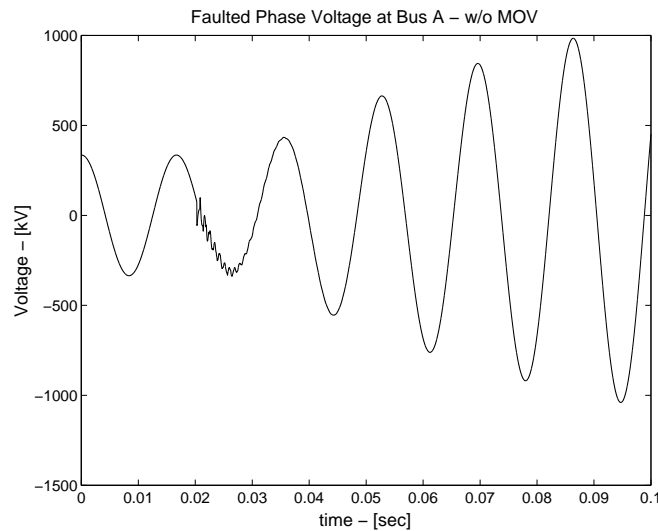
Fig. 13. Faulted phase voltage, without MOV

The simulated voltage signals at each bus are subsequently transformed into the modal domain. Discrete wavelet transform coefficients (WTC) of different scales for the aerial and ground mode signals are then calculated using the wavelet transform. The WTC^2s of the aerial mode voltages in scale-1 for both cases with and without
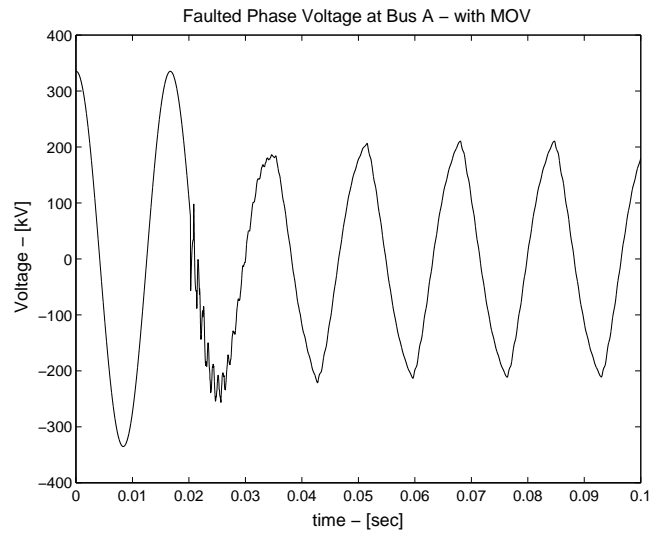
Fig. 14. Faulted phase voltage, with MOV

the MOV are given in Figures 15 and 16. It is observed that both the shape and the peak arrival instants of the wavelet transform coefficients of the aerial mode voltages for each case are identical for a certain period after the fault. This period extends well beyond the needed duration for the successful application of the fault location procedure described in the previous section.
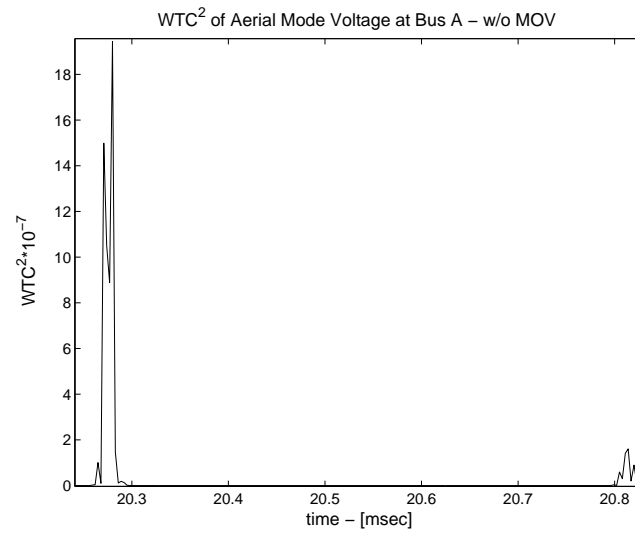
Fig. 15. WTC^2 of the aerial mode voltage, without MOV
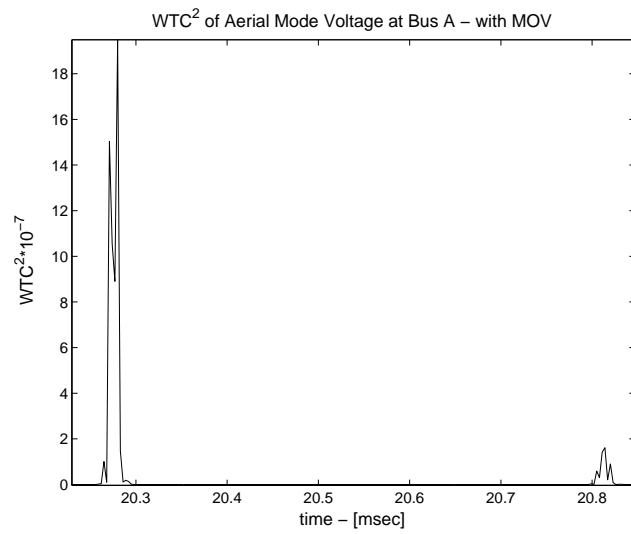
Fig. 16. WTC^2 of the aerial mode voltage, with MOV

3.   Fault location in a teed circuit with mutually coupled line section

A partially coupled teed circuit is studied as shown in Figure 17. The detailed interpretation of the lattice diagram in [68] shows that the end point of the mutually coupled section, M, behaves like a discontinuity where multiple reflections occur during a fault. Because of this complexity introduced by the coupled section the following situations must be studied depending on where the fault occurs:

- Fault is in the coupled section, $A - M$

    – In the first half of the coupled section

    – In the second half of the coupled section

- Fault is beyond the coupled section, $M - T$
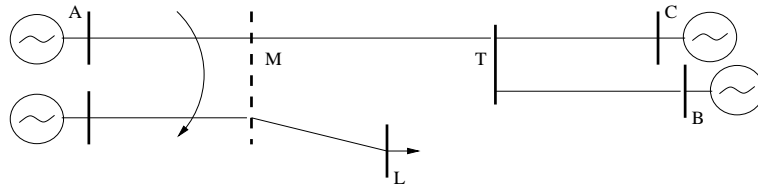
Fig. 17. Teed circuit with mutually coupled line section

In order to specify the faulted section (coupled or uncoupled), the difference between the arrival time instants of the WTC^2s peaks of the aerial mode and the ground mode voltages are calculated. Then the calculated value is compared with the time difference obtained for a fault right at the end of the coupled section.

In case a grounded fault occurs in the coupled line section, the algorithm described in the previous section will be valid, and the equations (4.1) and (4.3) will be used in order to locate the fault.
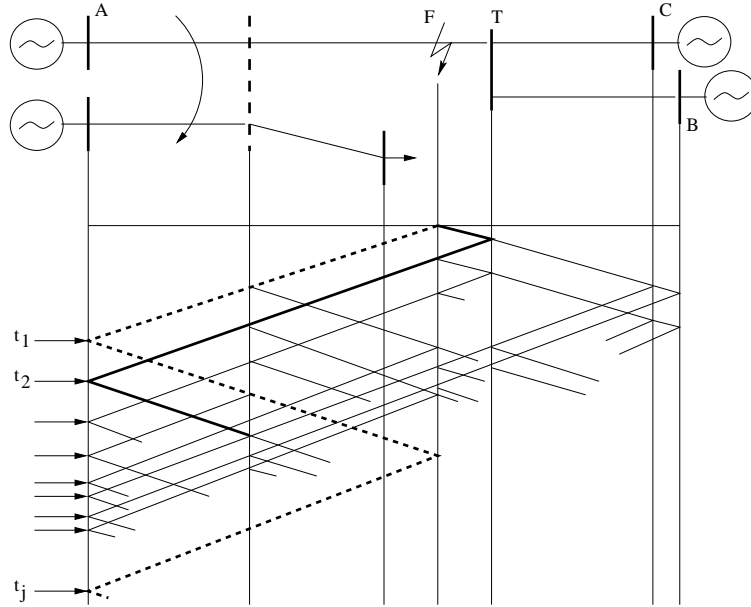
Fig. 18. Lattice diagram for a fault in the uncoupled section

When the fault is in the uncoupled section as shown in Figure 18, the first peak of the aerial mode WTC^2 which is due to the backward traveling wave, arrives at bus A at time t_1 and the jth peak which is due to the backward traveling wave that is first reflected from bus A, will arrive back at bus A at time t_j. It is observed that, the WTC^2 peak (jth) which has the largest magnitude after the first two WTC^2 peaks is due to the backward traveling wave which is reflected from the fault point. As can be seen from the Figures 19 to 21, the arrival time of the WTC^2 peak due to the reflected backward traveling wave increases (from fifth to tenth) as the fault location approaches the T node. The fault location can be calculated by the following equation:

$$x = \frac{v \times \Delta t}{2}, \Delta t = t_j - t_1 \tag{4.5}$$

Provided that the fault location is not too close to the T-node, an alternative and simpler procedure can be used as follows [34]:
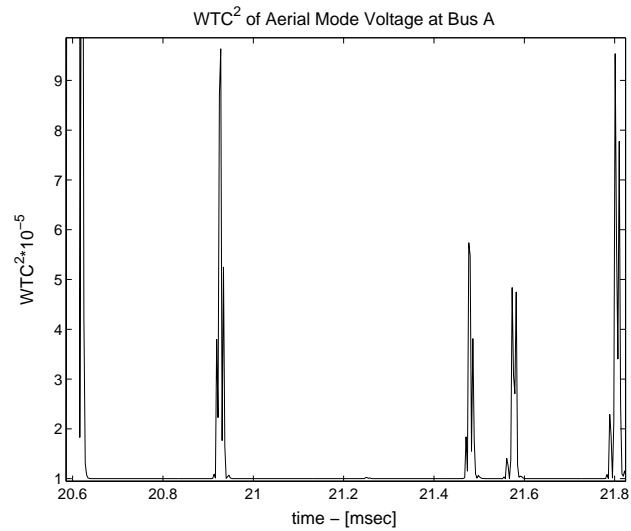
Fig. 19. WTC^2 of the aerial mode voltage at bus A, $X_F = 110$ mi

$$
\begin{aligned}
x &= \frac{\Delta t' \times v}{2} \\
\Delta t' &= \frac{2 \times L}{v} - \Delta t \\
\Delta t &= t_2 - t_1
\end{aligned}
\qquad (4.6)
$$

where L is the total line length. As a result, either one of the equations (4.5) or (4.6) can be used in order to locate the fault. Alternatively, their average value can be used to minimize any estimation errors.
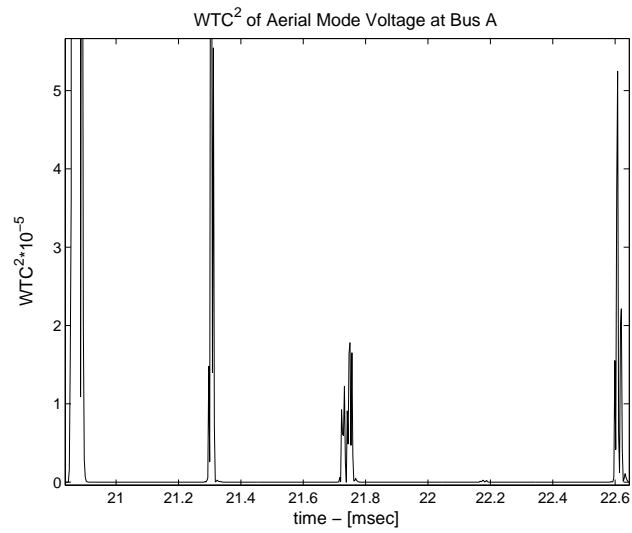
Fig. 20. WTC^2 of the aerial mode voltage at bus A, $X_F = 160$ mi
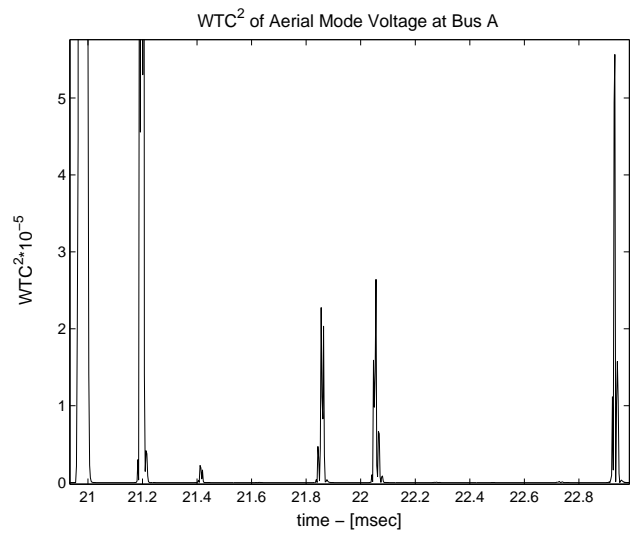
Fig. 21. WTC^2 of the aerial mode voltage at bus A, $X_F = 180$ mi

4. Fault location in a teed circuit using synchronized measurements at three terminals

Now assume that the measurements are synchronized at each bus and voltage transients are recorded at buses A, B and C as shown in Figure 10. After the faulted line segment is identified by comparing the WTC^2s of each bus as described above, the double ended fault location algorithm described in [34] is used to locate the fault. The aerial mode voltage WTC^2s obtained at the sending ends of the faulted line segment and one of the un-faulted line segments are used in this algorithm as follows:

$$x = \frac{L_T - v \cdot \Delta t}{2} \tag{4.7}$$

where Δt is the time difference between the arrival times of the aerial mode WTC^2s of the voltages recorded at the sending ends of the faulted line segment and the chosen un-faulted line segment. L_T is the total line length of the faulted line segment and the chosen un-faulted line segment. Assume that line segment $C - T$ is the faulted line segment and t_a, t_b and t_c are the arrival time instants of the initial peaks of the aerial mode voltage WTC^2s at the buses A,B and C respectively. Then the fault location will be calculated as follows:

$$x = \frac{L_C + L_j - v \cdot (t_j - t_C)}{2} \tag{4.8}$$

where j = A (or B) as the chosen un-faulted line segment.

C. Simulation Results

All simulations are carried out by using ATP/EMTP program and MATLAB with a sampling time interval of 3 μsec. The fault occurrence time is chosen as 0.02 sec. The tower configuration of 220 kV transmission line is given in the Appendix. The

frequency dependent transmission line model is used throughout the simulations. All the line segments are assumed to be fully transposed. The aerial mode propagation velocity is calculated as $1.85882 \ 10^5$ mi/sec in scale-1 corresponding to the frequency interval of 75 kHz - 150 kHz. The studied systems are simulated under various types of faults along different line segments. Line segment lengths are chosen as $L_{AT} = 200$ miles, $L_{BT} = 180$ miles and $L_{CT} = 170$ miles. Simulation results for one phase to ground fault in line segment $A - T$ with a very small fault resistance ($1 \ m\Omega$) are presented.

1. Fault location in a teed circuit

It is assumed that a single line to ground fault occurs at 50 miles away from bus A. After the recorded transient voltages are transformed into modal domain and WTC^2s of the aerial mode is obtained, the faulted line segment is identified by comparing the magnitudes of the WTC^2s of the aerial mode voltages at each bus. The WTC^2s at bus A is shown in Figure 22, while the coefficients at other buses are insignificant indicating that the fault is in line segment $A - T$,

After the faulted line segment is identified as $A - T$, the faulted half of the line is determined by comparing Δt_0 and Δt_m. In this example $\Delta t_0 = 0.0059$ msec where $\Delta t_m = 0.024$ msec indicating that the fault is located at the first half of the line $A - T$. The arrival times of the first and second peaks of the aerial mode WTC^2 at bus A are $t_1 = 20.283$ msec and $t_2 = 20.817$ msec respectively. Equation (4.1) is used to calculate the fault location as follows:

$$x = \frac{1.85882 \cdot 10^5 \times 0.534 \cdot 10^{-3}}{2} = 49.63 \ mi$$
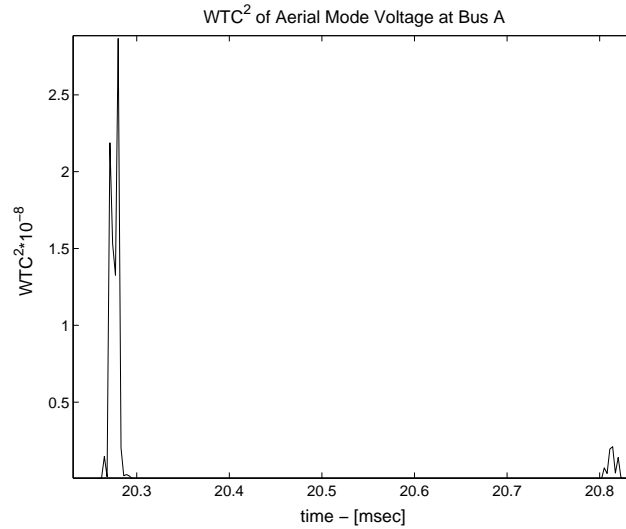
Fig. 22. WTC^2 of the aerial mode voltage at bus A

2.   Fault location in a teed circuit with MOV protected series capacitor

The configuration shown in Figure 12 is simulated. A series compensation rate of 80 % is used for the line $A - T$. The MOV parameters I, q and V_{ref} of Equation (4.4) are chosen as 200 A, 23 and 70 kV respectively. The faulted line segment is identified by comparing the aerial mode WTC^2s recorded at each bus. The faulted section of the line segment for a phase to ground fault located at 50 miles away from bus A is estimated by calculating the difference between the arrival times of the peaks for the aerial and ground mode WTC^2s at bus A. This yields 0.006 msec which is less than the one obtained for a fault at the middle of the line. The arrival times of the first two aerial mode WTC^2 peaks at bus A are $t_1 = 20.283$ msec and $t_2 = 20.817$ msec yielding a time difference of $\Delta t = 0.534$ msec. The fault location can thus be determined by using Equation (4.1) as:

$$x = \frac{1.85882 \cdot 10^5 \times 0.534 \cdot 10^{-3}}{2} = 49.63 \ mi$$

Note that the arrival times of the peaks of aerial mode voltage WTC^2s are same with those obtained in the previous section implying that MOV has no effect on the proposed fault location algorithm.

3.   Fault location in a teed circuit with mutually coupled line section

In this case, the system shown in Figure 17 is studied where the length of the coupled section is 80 miles. It is assumed that the fault occurs within the coupled section $A - T$, 50 miles away from bus A. The fault is declared to be in the region close to the end point M of the coupled section by using the arrival time differences between the initial peaks of aerial and the ground mode WTC^2s. The first peak arrives at bus A at time $t_1 = 20.283$ msec and the third peak arrives at bus A at time $t_3 = 20.829$ msec. The fault location is determined by using Equation (4.3) as:

$$x = \frac{1.85882 \cdot 10^5 \times 0.546 \cdot 10^{-3}}{2} = 50.74 \ mi$$

Next, the fault is assumed to be within the second half of the uncoupled section, 180 miles away from bus A as shown in Figure 18. The first peak of the aerial mode WTC^2s arrives at bus A at $t_1 = 20.985$ msec while the second one arrives at $t_2 = 21.20$ msec. The aerial mode WTC^2 peak which has the largest magnitude after the first two peaks arrive at bus A at $t_{10} = 22.935$ msec as shown in Figure 21. The fault location is determined by using Equation (4.5):

$$\frac{1.85882 \cdot 10^5 \times 1.95 \cdot 10^{-3}}{2} = 181.23 \ mi$$

Alternatively, one can use Equation (4.6), which yields:

$$\frac{2 \cdot 200 - 0.215 \cdot 10^{-3} \times 1.85882 \cdot 10^5}{2} = 180.02 \ mi \qquad (4.9)$$

The differences between the two results are attributed to the sampling errors and are not considered significant.

4. Fault location in a teed circuit using synchronized measurements at three terminals

The same examples in the previous sections are worked out in order to be able to illustrate the simplicity of the algorithm with a fully synchronized measurement system.

Assume that the fault occurs 50 miles away from bus A in the system shown in Figure 12. The arrival times of the initial peaks of the aerial mode WTC^2s at bus A, B and C are $t_A = 20.283$ msec, $t_B = 21.783$ msec and $t_C = 21.74$ msec respectively. The fault location is simply determined by Equation (4.7):

$$x = \frac{(200 + 170) - 1.85882 \cdot 10^5 \times 1.457 \cdot 10^{-3}}{2}$$
$$x = 49.59 \ mi$$

where the recorded transients at the sending terminals of the faulted line segment, namely bus A and bus C are used for the calculations.

Next, the fault is assumed to occur within the coupled section 50 miles away from bus A as shown in Figure 17. The arrival times of the initial peaks of the aerial mode WTC^2s at bus A, B and C are $t_A = 20.283$ msec, $t_B = 21.789$ msec and $t_C = 21.735$ msec respectively. The fault location is then determined by Equation (4.7):

$$x = \frac{(200 + 180) - 1.85882 \cdot 10^5 \times 1.506 \cdot 10^{-3}}{2}$$

$$x = 50.03 \ mi$$

where the recorded transients at the sending terminals of the faulted line segment, i.e. bus A and bus B are used for the calculations.

5. The effect of fault resistance

All the simulations are repeated by replacing the fault resistance by $R_f = 400 \ \Omega$. It is observed that the initial peaks of the square of aerial mode wavelet coefficients are smaller than those obtained by using no fault resistance, however the shape and peak arrival instants of the waveforms remain the same. The fault location results obtained with zero fault resistance, match closely with those obtained by using 400 Ω fault resistance. Based on this limited set of experimental results, it is believed that the algorithm performance will remain insensitive to variations in the fault resistance.

6. The effect of random error

The performance of the fault location algorithm is tested by introducing random error to the simulated voltage signals. A Gaussian noise is generated with zero mean and σ standard deviation which is equal to the 30 % of the quantization error $(0.3 \cdot q)$. The basic formulation of the quantization error introduced by A/D converters is given below [69] :

$$q = 2^{-N} \cdot V \tag{4.10}$$

where $N(=12)$ is the number of the bits of the A/D converter and V is chosen as the rms value of the voltage signal in steady state.

All the simulations are repeated by introducing the random error to the simulated voltage signals. The simulation results of the most complicated case because of the multiple reflections is presented here where a fault occurs in the uncoupled section, 110 miles away from bus A, as shown in Figure 18.
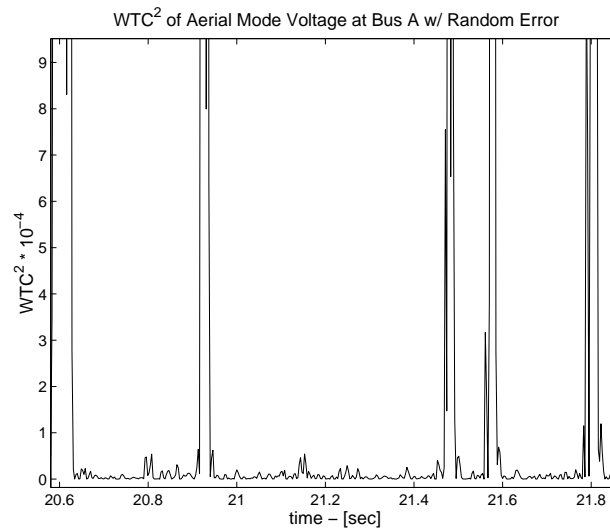
Fig. 23. WTC^2 of the aerial mode voltage at bus A, with random error

It is observed that the random error has no effect on the peak arrival instants of the WTC^2s. Also the magnitudes of the coefficients due to the random errors are insignificant compared to the coefficients which are due to the fault initiated transients as shown in Figure 23. The choice of 12 as the number of bits of the A/D converter is rather conservative. Availability of higher resolution converters will certainly decrease the already insignificant effects of random errors to a minimum.

D. Summary

This chapter presents a fault location procedure for teed circuits. The procedure is based on processing of traveling waves by wavelet transform in order to extract the arrival times of fault-initiated waves reflected from the discontinuities. The fault location algorithm is shown to be insensitive to the existence of series capacitors, fault resistance, fault type and any existing mutual coupling between the lines while the accuracy of the algorithm is proportional to the sampling frequency. Simulation results show good correlation between the actual and estimated fault locations for all the studied cases. In the next chapter a new fault location technique for distribution systems with distributed generation is proposed using a similar procedure presented in this chapter.

CHAPTER V

DWT BASED FAULT LOCATION IN RADIAL DISTRIBUTION NETWORKS
WITH DISTRIBUTED GENERATION

A.   Introduction

Recent trends in proliferation of distributed generation in distribution systems lead
to investigation of protection schemes for such systems. Fault location in distribution
systems presents special challenges due to the lack of fault signal recordings at the
remote end of the feeders. Typically, fault signals are recorded at the substation and
the location of the fault is estimated based on these recordings. Earlier methods
rely heavily on power frequency components, which remain sensitive to fault path
resistance, line loading and source parameters. Existence of distributed generation
causes errors in power frequency based fault location methods, which use apparent
impedance seen from the substation as a criterion to estimate the distance to the
fault point. Such methods also have to deal with the problem of multiple possible
locations for a given set of recorded signals. Furthermore, coordination of relays
and other protective devices becomes unmanageable by these methods due to infeed
currents from distributed generators. Effects of DG on protective device (fuse-fuse,
recloser-fuse, relay-relay) coordination are described in [70], [71] and [72].

Traveling wave methods facilitate the estimation of fault location due to the
insensitivity of the high frequency components to remote infeed currents from the
generator side. As Chapter II explains briefly, traveling wave based techniques make
use of high frequency components of the fault signals and try to capture the arrival
times of fault generated transient waves at the line terminals. In [73] a traveling wave
based method is proposed for distribution systems with tapped loads. A high speed

sampling system is utilized to capture the transients and polarity change is used in order to identify the faulted region. Another protection scheme for fault detection and location in DG systems is proposed in [74] utilizing wavelet associated Artificial Neural Networks for fault detection and fuzzy cluster analysis for fault location.

In this chapter, a traveling wave based fault location method which has been successfully applied to single and double ended fault location problems in transmission systems in [34] and Chapter IV [35], is extended to distribution systems with distributed generation. Illustrative examples simulated by a transients simulation program for various distribution system configurations are presented. It is shown that faults in distribution systems can be accurately located even when there is generator at the remote ends of the feeder.

B.   General Procedure for Fault Location Using Wavelet Transformation

In distribution systems with distributed generation at remote locations, the measurements are only available at the substation. Thus, the fault location procedure described here assumes that voltage measurements are available only at the sending end.

As described in Chapter III the procedure consists of three stages. Once the Clarke's modal transformation is applied to the measured voltage signals DWT is applied to the modal voltages and the squares of the wavelet transform coefficients (WTC^2) are obtained in order to determine the instant when the energy of the signal reaches its maximum value. Following section explains the final stage of the fault location procedure in detail for different possible cases.

C.   Fault Location Procedure

Fault location problem in distribution systems becomes more complicated with the presence of DGs. The impacts of DGs considerably change depending on their location and size. It is known that an increase in generation capacity increases the fault current. Thus, introduction of DGs to the radial distribution systems requires further study on existing protective device coordination and protection configuration. Furthermore, fault location problem in radial distribution systems, where only one-end measurements are available, presents challenges due to the DG involvement in the distribution system. When a fault occurs, the fault current consists of not only the source current but also the DG current. There is an increase in fault current due to the increase in generation capacity, however there is a decrease in source current since the DG is also supplying the fault current. The decrease in source current leads a higher voltage at the measurement location. Since there is an increase in voltage and decrease in current, the impedance seen from the source location will be higher than the value obtained for the same fault conditions on the distribution system without DG. The impedance based fault location methods fail to locate the fault in such cases.

The proposed fault location method first determines the type of the fault by observing the ground mode signal. Provided that the ground mode signal exists for only grounded faults, the proposed technique is developed accordingly. If the fault is ungrounded or balanced, there are no remote end reflections [34]. However for the grounded faults there are reflections of backward and forward traveling waves from all remote ends. Thus, the fault location procedure for grounded and ungrounded faults is described separately. In the following sections the details of the fault location method is described. The investigations based on Bewley diagrams of the various fault conditions are introduced. The distribution system with DG in Figure 24 is

studied. The effect of the DG existence on the proposed fault location technique is also discussed.
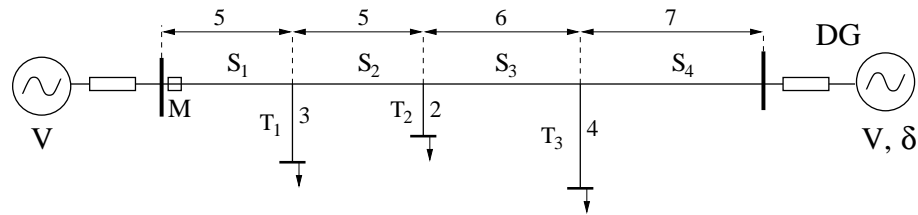
Fig. 24. Studied distribution system with DG. The section lengths are given in miles.

1. Fault location for grounded faults

Due to the multiple and superimposed reflections at the discontinuities, the Bewley diagrams of the grounded faults at different locations give complex traveling wave signatures at the measurement location. The backward and forward traveling waves arriving at the measurement point create different patterns depending on the location of the fault in the distribution system. The faults occurring on the intermediate sections cause more complex traveling wave patterns than those due to the faults occurring on the load branches.

First, the approximate faulted region is determined by comparing the time difference of initial peak arrival times of WTC^2s of aerial and ground mode voltages with those obtained for faults in all sections and load taps. The time difference between the instant peak arrival times of aerial and ground mode WTC^2s increases as the fault location moves far away from the measurement point. Once the approximate distance is predicted, the WTC^2 pattern of the fault is compared with those obtained for the same distance but for different regions such as, one for intermediate section and other for load branch. After the region is identified, the exact fault location is

calculated by using the procedures described in the following sections for intermediate sections and load branches.

a.   Faults on an intermediate section, S_i

Assume a grounded fault located in the first half of the section S_1 as shown in Figure 25. The faulted half is identified by using the comparison of the time difference of initial peak arrivals of aerial and ground mode WTC^2s with the time difference, t_m, obtained for a fault in the middle of the line. If the time difference is smaller than t_m, the faulted region is identified as the first half and Equation (5.1) is used for fault location [34].

$$x = \frac{v \times \Delta t}{2} \qquad (5.1)$$
$$\Delta t = t_2 - t_1$$

where v is the aerial mode velocity, t_1 is the arrival time of the first peak of the aerial mode WTC^2 corresponding to the backward traveling wave and t_2 is the arrival time of the second peak of the aerial mode WTC^2 corresponding to backward traveling wave reflected from fault point.

If the time difference is larger than t_m, the fault is identified to be closer to the remote end as can be seen in Figure 25 and Equation (5.2) is used in order to calculate the distance [34].

$$x = \frac{\Delta t' \times v}{2} \qquad (5.2)$$
$$\Delta t' = \frac{2 \times L}{v} - \Delta t$$
$$\Delta t = t_2 - t_1$$
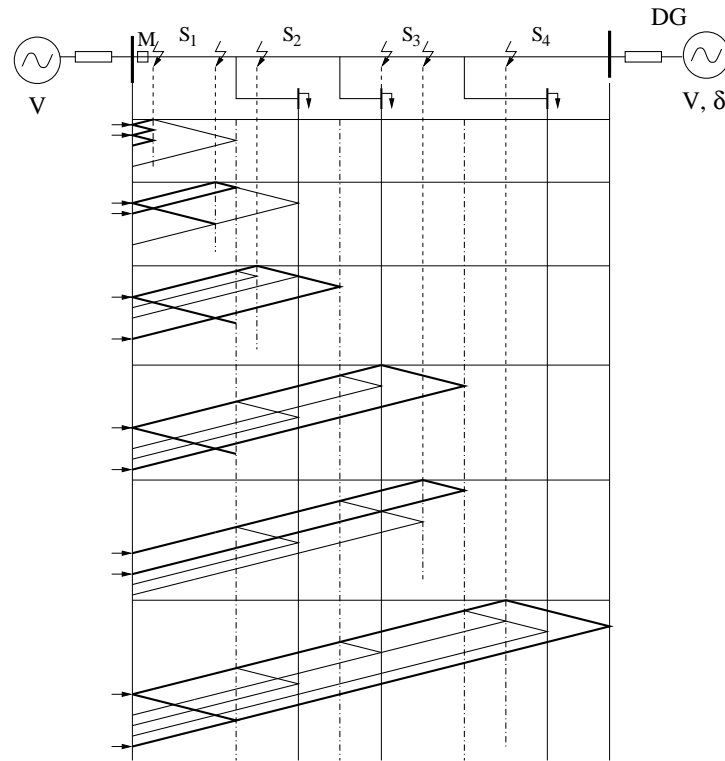
Fig. 25. Bewley diagram for faults located at sections

where v is the aerial mode velocity, t_1 is the arrival time of the first peak of the aerial mode WTC^2, t_2 is the arrival time of the second peak of the aerial mode WTC^2 corresponding to forward traveling wave reflected from the remote end and L is the total line length of S_1.

If the fault is at one of the other intermediate sections (S_2, S_3 or S_4), once the faulted region is identified using the time difference technique, Equation (5.3) is used for exact fault location. The arrival time, t_j, of the WTC^2 peak corresponding to the reflected forward traveling wave increases as the fault location moves closer to the measurement point in the section. Assume a fault in S_3, closer to the measurement location as shown in Figure 25. The forward traveling wave, which is reflected from the remote end of the S_3, arrives at the measurement location as the fourth peak.

However, the forward traveling wave arrives at the measurement location as the second peak for a fault closer to the remote end of S_3. The exact fault location is calculated using Equation (5.3).

$$
\begin{aligned}
x &= \frac{\Delta t' \times v}{2} \\
\Delta t' &= \frac{2 \times L_t}{v} - \Delta t \\
\Delta t &= t_j - t_1
\end{aligned}
\tag{5.3}
$$

where v is the aerial mode velocity, t_1 is the arrival time of the first peak of the aerial mode WTC^2 corresponding to backward traveling wave, t_j is the arrival time of the jth peak of the aerial mode WTC^2 corresponding to forward traveling wave reflected from the remote end and L_t is the total line length from the measurement point to the end of the faulted section. For a fault in S_3, $L_t = L_{S_1} + L_{S_2} + L_{S_3}$.

b. Faults on a load branch, T_i

Depending on the length of the load branches, the arrival time of the forward traveling wave increases as the fault location moves closer to measurement location as shown in Figure 26.

Once the fault is identified in a load branch by using the time difference comparison of initial peak arrivals of aerial and ground WTC^2s, the exact fault location is calculated using Equation (5.3). The procedure is not different than the one for the intermediate sections, however the WTC^2 patterns of faults at load branches are drastically different than those obtained for faults along intermediate sections.
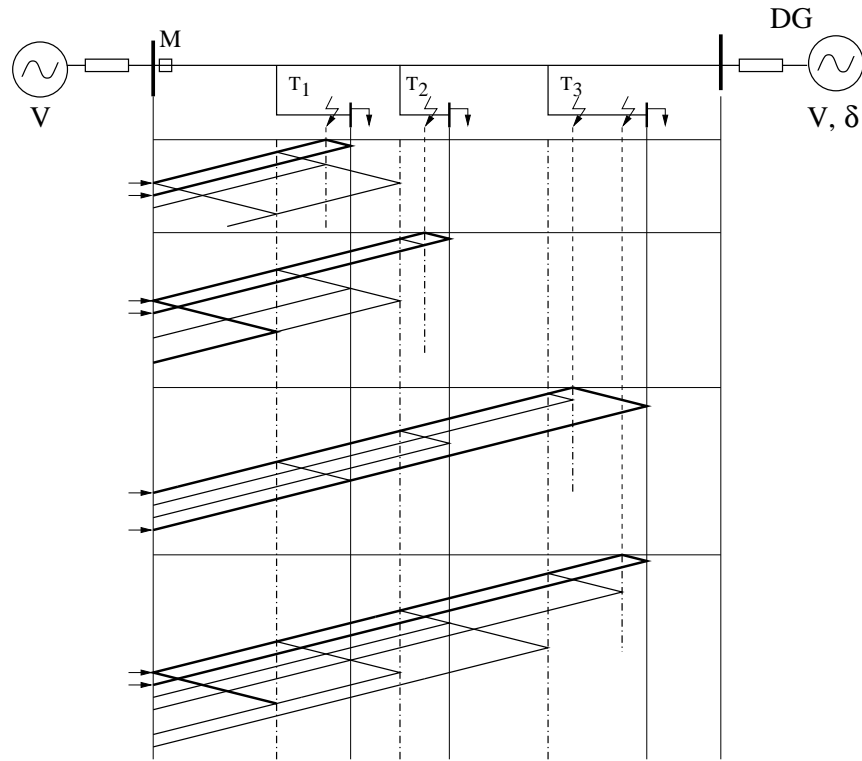
Fig. 26. Bewley diagram for faults located at taps

2.   Fault location for ungrounded/symmetric faults

Provided that there are no remote end reflections for the ungrounded faults, as shown in Figure 27 for an intermediate fault, the approximate region determination is based upon the aerial mode WTC^2 patterns obtained for faults along the sections and along the load branches.

Since there are significant discrepancies between the WTC^2 patterns and magnitudes of intermediate faults and load branch faults, once the approximate region is determined, Equation (5.4) is used for fault location calculations utilizing the Bewley diagram:
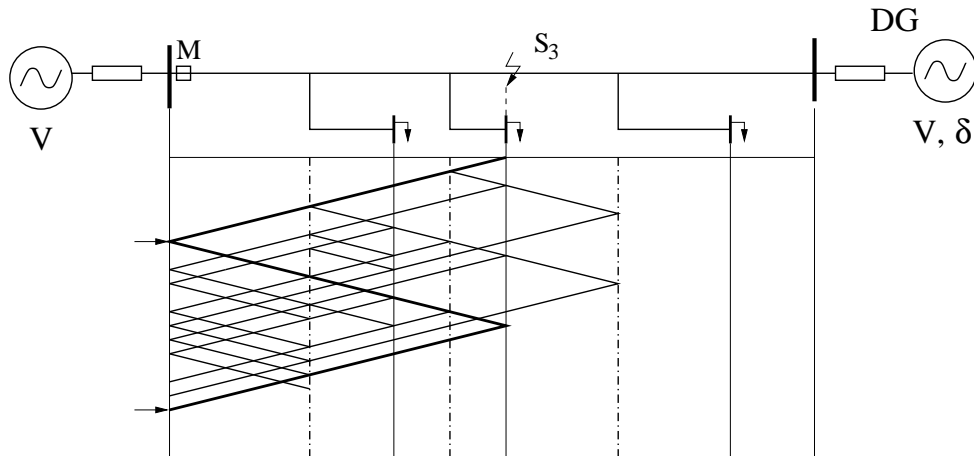
Fig. 27. Bewley diagram for an ungrounded fault

$$x = \frac{v \times \Delta t}{2} \tag{5.4}$$

$$\Delta t = t_j - t_1$$

where v is the aerial mode velocity, t_1 is the arrival time of the first peak of the aerial mode WTC^2 corresponding to the backward traveling wave and t_j is the arrival time of the jth peak of the aerial mode WTC^2 corresponding to backward traveling wave reflected from the fault point.

3.   The effect of DG on fault location procedure

The effect of a fault in distribution system on the main generation decreases due to the existence of DG. Thus, the severeness of the voltage transient recorded at the measurement location, M, is lessened. However, the pattern of the wavelet transform of the voltage signal remains same while the magnitude of the WTC^2s changes as shown in Figure 28 and Figure 29. Nevertheless, the change in magnitude is insignificant and unlike the power frequency based methods, the proposed fault location

procedure is independent of the existence of distributed generation.
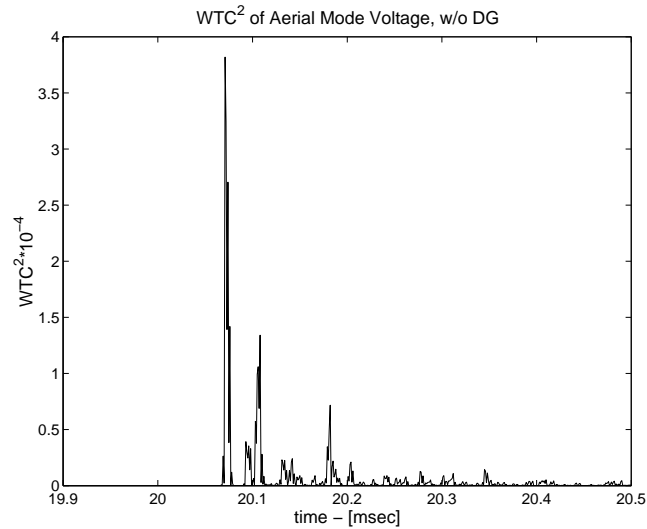
Fig. 28. Aerial mode WTC^2s w/o DG for a fault 13 miles away from M in section S_3

D.   Simulation Results

The transient simulations are carried out by using ATP/EMTP program. The results are processed in MATLAB by using Wavelet Analysis Toolbox. The tower configuration of a 10 kV distribution line is given in Appendix.

Distributed parameter transmission line model is used. The line parameters are evaluated at 5 kHz as well as the aerial mode and ground mode propagation velocities by using ATP LCC line constants routine. Ground mode propagation velocity, v_0, is calculated as 167300 mi/sec while aerial mode propagation velocity, v_1, is calculated as 183837 mi/sec. The sampling frequency is chosen as 1 MHz. All the line segments are assumed to be fully transposed. The fault location procedure is given as:

- Voltage measurements are recorded at one terminal.

- Modal transformation is applied to the measured voltages.
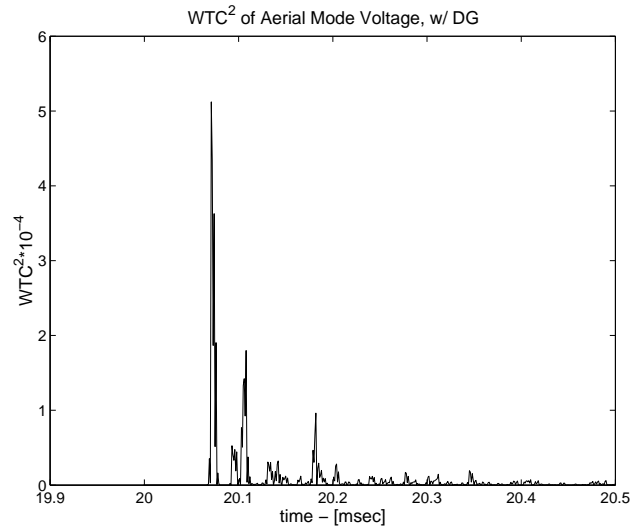
Fig. 29. Aerial mode WTC^2s w/ DG for a fault 13 miles away from M in section S_3

- DWT is applied to the modal and ground mode voltages.

  - If the ground mode is not zero;

    * Calculate the time difference of the arrival peaks of aerial and ground mode WTC^2s, and determine the approximate distance using the pre obtained time differences for various fault locations.

    * Use the pre-obtained WTC^2 patterns to determine the region and
      · use Equation (5.1), if the fault is in first half of the first section
      · use Equation (5.2), if the fault is in second half of the first section
      · use Equation (5.3) otherwise.

  - If the ground mode is zero;

    * Use the pre-obtained WTC^2 patterns to determine the approximate region and use Equation (5.4) for fault location

Figure 30 also presents the fault location algorithm in a more compact way.
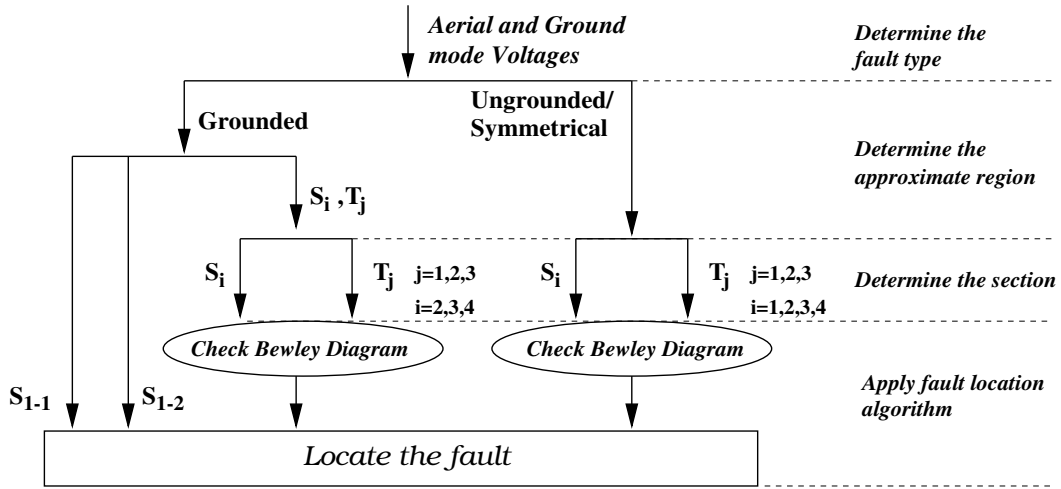
Fig. 30. Fault location algorithm for radial distribution systems w/ distributed generation

Assume a 1-phase-to-ground fault in T_3, 18 miles away from the measurement point. The time difference, Δt, between the initial peak arrivals of aerial and ground mode voltage WTC^2s for various faults in all sections are obtained as:

$$\Delta t = x_f \times (\frac{1}{v_0} - \frac{1}{v_1}) \tag{5.5}$$

where x_f represents fault location, v_0 and v_1 represent ground mode and aerial mode velocities respectively. Table II shows the calculated time difference, Δt for various fault locations. For the simulated fault, this time difference, Δt, is 9 μs as shown in Figure 31. Hence, the faulted region is determined as either S_4 or T_3.

In Figure 32 and in Figure 33 the WTC^2s of the aerial mode voltages are given for two faults located 18 miles away from the measurement point, M in T_3 and in S_4 respectively. The significant difference between the patterns is used to differentiate between faults occurring at the same distance from the substation but on either load branches or line sections.

Table II. Time differences of initial peak arrivals of aerial and ground mode WTC^2s
for various fault locations

x_f - [mi]	Δt - [μsec]	Section
2.5	1.34	S_1
4	2.15	S_1
6	3.22	S_2, T_1
8	4.3	S_2, T_1
12	6.45	S_3, T_2
14	7.52	S_3
18	9.67	S_4, T_3
20	10.75	S_4, T_3
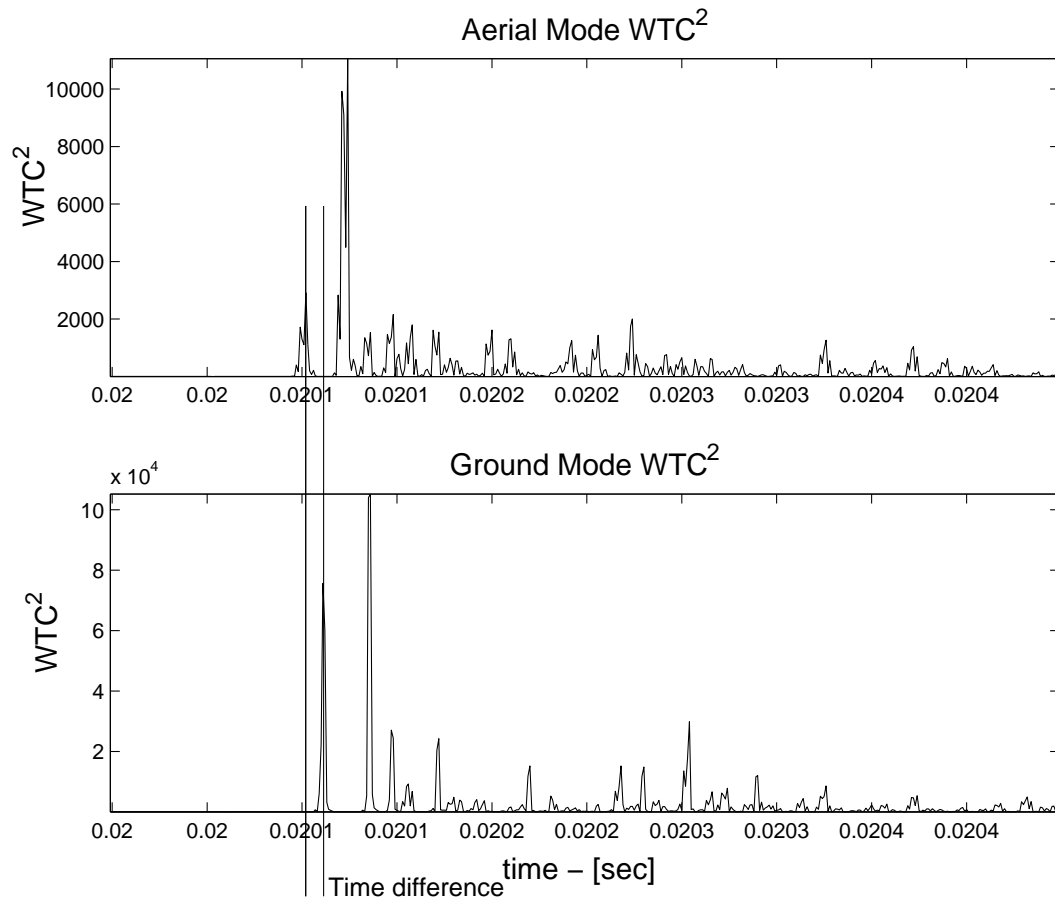
Fig. 31. Aerial and ground mode WTC^2s w/ DG
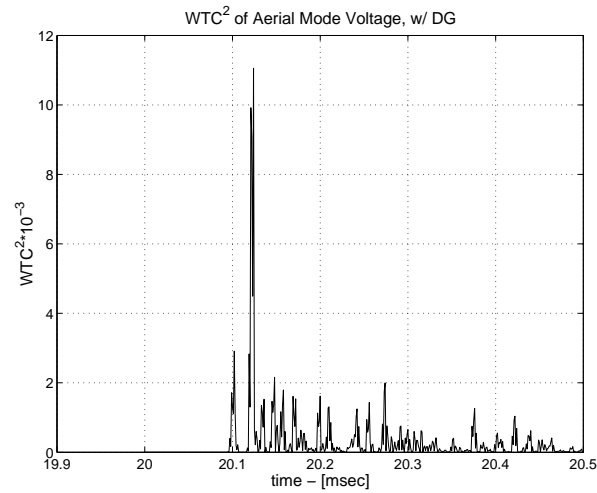
Fig. 32. Aerial mode WTC^2s w/ DG for a fault 18 miles away from M in section T_3
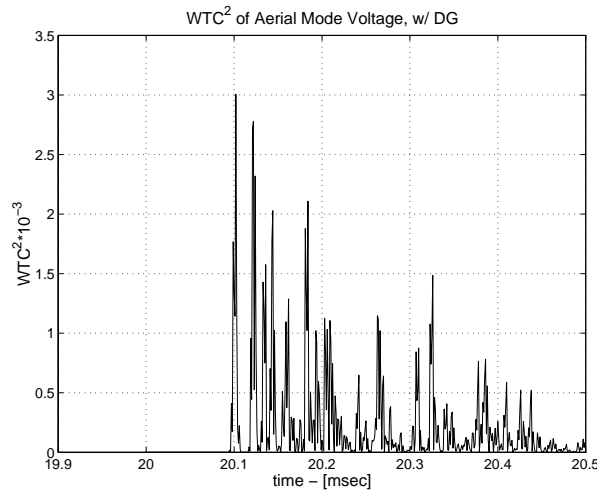
Fig. 33. Aerial mode WTC^2s w/ DG for a fault 18 miles away from M in section S_4

In this example, the observed pattern matches the one corresponding to that of a load branch and hence it is decided that the faulted branch is T_3. Thus, the location of the fault is determined using Equation (5.3) where the forward traveling wave reflected from the remote end of T_3 arrives at M as the second peak and the time difference, $\Delta t_{21} = t_2 - t_1$ between two consecutive peaks of aerial mode WTC^2s as shown in Figure 32 is 22 μsec. Details of the calculations are shown below:

$$
\begin{aligned}
x_f &= \frac{183837}{2} \times \left(\frac{2 \cdot L_T}{183837} - 22 \cdot 10^{-6} \right) = 17.98 \ mi \\
L_T &= S_1 + S_2 + S_3 + T_3 = 20 \ mi
\end{aligned}
$$

where L_T is the total line length from the measurement point, M, to the end of the faulted branch.

E.   Summary

This chapter presents a traveling wave based fault location method to be used in distribution systems with distributed generation. The main advantage of the proposed approach is its insensitivity to naturally occurring infeed from the distributed generators during a fault. Such infeed is typically unpredictable and makes the impedance based conventional fault location methods vulnerable to errors. Furthermore, the proposed approach has the added advantage of requiring fault signals only from the substation end of the distribution feeder. Next chapter proposes a novel method to calculate transmission line voltage profiles.

CHAPTER VI

VOLTAGE PROFILE CALCULATIONS ON POWER TRANSMISSION LINES

A.   Introduction

Power systems experience voltage transients during system faults and switching events. Such transients may produce voltages and currents, which may exceed allowable limits of operation and/or equipment. Protective relaying studies commonly involve simulations of various types of expected transients in order to properly design protection schemes against such events. These studies use the network model, which is made up of buses interconnected by transmission lines, transformers, switches and circuit breakers. Simulation results provide the time domain variation of voltage signals at the buses of interest. There are several versions of Electromagnetic Transients Programs (EMTP) which allow the users to specify these buses of interest and compute the voltage transients at these buses.

While the voltage transients at system buses will yield significant information about potential problems at the substation buses, they will not reveal the voltage transients along individual transmission lines. This information may be useful in particular for long transmission lines where the voltage profile may vary more significantly along the length of the line than those at its two terminal buses. Furthermore, recent advances in computer visualization and animation techniques make it possible to create movies of transients occurring in power systems as a result of faults and switching events. Such movies may be used to aid analysis of recorded events to uncover design problems associated with the existing protection and control practices or they can be utilized as educational tools to learn about the traveling wave propagation within the interconnected power grid. The movies are created by calculating

the voltage profile along each line at each time step.

The concept of transient movies is initially introduced by Woodruff who used transient sculptures [2] in early 1930s in order to create the first transient animations. It can be argued that Bewley diagrams [1] are the first attempts to visualize the behavior of traveling waves along transmission lines. Interest in visualization and animation of transients has been rekindled in the recent years as a result of the developed technologies and tools in computer graphics and animation. Two examples can be found in [75, 76], where new methods for visualization and animation of transients are proposed utilizing the voltage profile information. These studies indicate the need to rapidly calculate and update the voltage profile of a given transmission line at each simulation time step.

In principle, once the terminal bus voltages are known, the voltage profile along a transmission line can be obtained by back-solving the line's traveling wave equations for the desired discrete points along the length of the line. This approach is well documented in [77] where the voltage profile of a line is recovered from the simulated terminal bus voltages in discrete time. Another simple yet computationally taxing alternative is to obtain the voltage information at intermediate points along the line by modeling the transmission line as several cascaded short line sections.

Both of the above approaches require some knowledge of the system and transmission line models, capability to solve wave equations and computation time, which may be significant depending upon the line models used. In this chapter, an alternative approach that is initially proposed in [78] will be presented . The proposed method utilizes time series analysis and does not require any knowledge of the line model or wave equations. The main idea is to develop time series models for voltages at intermediate points along the line as a function of the terminal bus voltages whose discrete time simulations are typically available from a standard electromag-

netic transients program. Once these models are developed, they will remain valid for all transient events irrespective of their location and type. Hence, animation programs can utilize these models to rapidly generate voltage profile screen shots, which can then produce a transients' movie.

First the procedure of obtaining time series models for calculating intermediate point voltages is described. Then, various different transient cases are studied in order to illustrate the performance of the time series models in predicting the correct voltage profile along transmission lines.

B.   Methodology

Electromagnetic transient simulation programs commonly solve for nodal voltages in discrete time. It can therefore be assumed that given a transmission line of interest, its terminal bus voltages can be obtained by using a simulator at discrete time instants for any desired observation period. The objective of this chapter is to utilize this information in order to determine the voltage values at intermediate points along a transmission line. This can be accomplished by creating a fictitious bus at an intermediate point along the line and writing the wave equations for the line section connecting the fictitious bus to the terminal buses. Since the voltage at the terminal bus is known, the fictitious bus voltage can be solved based on the line parameters and wave equations. Multi-phase lines require this calculation to be carried out in the modal domain.

This approach is taken in [77] where calculation of the voltage profile of a line in modal domain using traveling wave equations is described in detail. Aerial voltage at an intermediate point is calculated as shown in (6.1) in terms of backward and forward traveling waves. In compact form, this voltage can be expressed by:

$$V_k(t) = \frac{b_k(t) + f_k(t)}{2} \tag{6.1}$$

where k is an intermediate point along a transmission line, f_k and b_k are forward and backward traveling waves at that intermediate point respectively, each of which can be written as follows:

$$f_{j\Delta k}(t) = \sum_{x=1}^{m} c_k f_{j\Delta k,x}(t - \Delta t) +$$
$$+ d_k f_{(j-1)\Delta k,x}(t - \tau) + e_k f_{(j-1)\Delta k,x}(t - \Delta t - \tau)$$
$$b_{j\Delta k}(t) = \sum_{x=1}^{m} c_k b_{j\Delta k,x}(t - \Delta t) +$$
$$+ d_k b_{(j+1)\Delta k,x}(t - \tau) + e_k b_{(j+1)\Delta k,x}(t - \Delta t - \tau)$$

where $j\Delta k$ is an intermediate point along a transmission line, m is the number of sections along the transmission line, Δt is simulation step size, τ is travel time of the fastest frequency component which propagates along the line, c_k, d_k and e_k are constants, $(j-1)\Delta k$ and $(j+1)\Delta k$ are one section before and after that intermediate point respectively. Further details can be found in [77].

Based on the fact that an intermediate point voltage is calculated from the summation of backward and forward traveling waves in (6.1), the expression can be further expanded to yield:

$$V_k(t) = \sum_{x=1}^{m} c_k(f_{k,x}(t - \Delta t) + b_{k,x}(t - \Delta t)) +$$
$$+ d_k(f_{(k-1),x}(t - \tau) + b_{(k+1),x}(t - \tau)) +$$
$$+ e_k(f_{(k-1),x}(t - \Delta t - \tau) + b_{(k+1),x}(t - \Delta t - \tau)) \tag{6.2}$$

where the first term in the summation is equal to $2V_k(t - \Delta t)$ by definition. It can be

observed from (6.2) that the voltage at any intermediate point, k, at time instant t is a function of its values and of the voltages at neighboring intermediate points one section before, $k-1$, and one section after, $k+1$, at several previous time steps.

The above observation constitutes the main motivation behind this work. It suggests that the voltage profile of a transmission line during a system fault can be obtained by a time series model whose parameters can be identified and estimated only once as long as the line geometry and conductor type remain the same, which is typically the case for power systems. A time series model should be developed for each intermediate point that will be used in the spatial approximation of the voltage profile.

Given the multi-phase structure of the line, the model will be built in the modal domain. Hence, a time series model is proposed as shown below in (6.3) for the aerial mode voltage at an intermediate point along a transmission line which is modelled simply by using two sections only:

$$
\begin{aligned}
V_k(t) = a V_k(t - \Delta t) + \\
+ b_1 V_{k-1}(t - \Delta t) + b_2 V_{k-1}(t - 2\Delta t) + \cdots + \\
+ b_N V_{k-1}(t - N\Delta t) + \\
+ c_1 V_{k+1}(t - \Delta t) + c_2 V_{k+1}(t - 2\Delta t) + \cdots + \\
+ c_N V_{k+1}(t - N\Delta t) \quad\quad (6.3)
\end{aligned}
$$

where N is the model order that corresponds to the number of history terms of sending and receiving end voltages, M is the model length that corresponds to the number of discrete time steps of the simulation which are used to create the model.

Thus, there is only one intermediate point along the line and nodes $k-1$ and

$k + 1$ correspond to the sending and receiving end respectively.

Figure 34 illustrates the model identification, parameter estimation and model validation stages. The observation interval includes the pre-fault and post-fault period. The data simulated for this period are used to build the time series model, estimate its parameters. The prediction interval includes post-fault simulation results and these are used to validate the model against the simulation results.
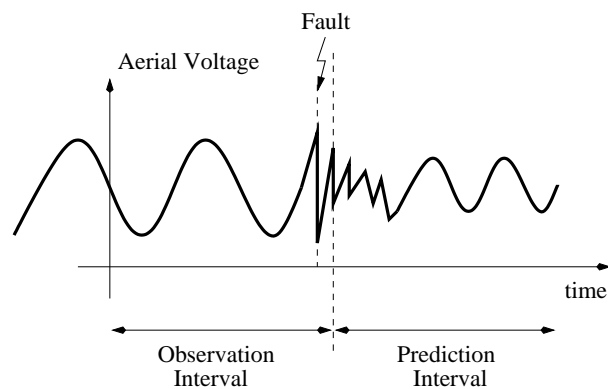
Fig. 34. Observation and prediction intervals

Simulation results are obtained first for a period of M discrete time steps. These include not only the terminal bus voltages but also all intermediate point voltages. The next step is to identify time series models for each of these intermediate point voltages. The model order, N, is chosen in such a way that the model will duplicate the voltage samples with minimal errors. This is done based on the expression given by (6.2), where it is obvious that the model order will have to be at least as large as $(\Delta t + \tau)$ or larger. The most appropriate model order is chosen in order to minimize the computational burden and maximize the goodness of fit. This is done by gradually increasing the model order and calculating the maximum normalized residuals. When no further improvement is observed as a result of an increase in model order, most

recently used order is chosen as the optimal.

Writing the expressions for the intermediate point voltage for all M time steps, since N is much smaller than M, the following set of over-determined system of equations will be obtained:

$$V_k(t) = aV_k(t - \Delta t) +$$
$$+ b_1 V_{k-1}(t - \Delta t) + b_2 V_{k-1}(t - 2\Delta t) +$$
$$+ \cdots + b_N V_{k-1}(t - N\Delta t) +$$
$$+ c_1 V_{k+1}(t - \Delta t) + c_2 V_{k+1}(t - 2\Delta t) +$$
$$+ \cdots + c_N V_{k+1}(t - N\Delta t)$$
$$V_k(t + 1) = aV_k(t + 1 - \Delta t) +$$
$$+ b_1 V_{k-1}(t + 1 - \Delta t) + b_2 V_{k-1}(t + 1 - 2\Delta t) +$$
$$+ \cdots + b_N V_{k-1}(t + 1 - N\Delta t) +$$
$$+ c_1 V_{k+1}(t + 1 - \Delta t) + c_2 V_{k+1}(t + 1 - 2\Delta t) +$$
$$+ \cdots + c_N V_{k+1}(t + 1 - N\Delta t)$$
$$\vdots$$
$$V_k(t + M) = aV_k(t + M - \Delta t) +$$
$$+ b_1 V_{k-1}(t + M - \Delta t) + b_2 V_{k-1}(t + M - 2\Delta t) +$$
$$+ \cdots + b_N V_{k-1}(t + M - N\Delta t) +$$
$$+ c_1 V_{k+1}(t + M - \Delta t) + c_2 V_{k+1}(t + M - 2\Delta t) +$$
$$+ \cdots + c_N V_{k+1}(t + M - N\Delta t) \qquad (6.4)$$

Equation (6.4) can be written in matrix form as follows:

$$
\begin{bmatrix}
V_k(t) \\
V_k(t+1) \\
\cdot \\
\cdot \\
\cdot \\
\cdot \\
V_k(t+M)
\end{bmatrix}
=
$$

$$
\begin{bmatrix}
V_k(t-\Delta t) & V_{k-1}(t-\Delta t) & \ldots & V_{k-1}(t-N\Delta t) & V_{k+1}(t-\Delta t) & \ldots & V_{k+1}(t-N\Delta t) \\
V_k(t+1-\Delta t) & V_{k-1}(t+1-\Delta t) & \ldots & V_{k-1}(t+1-N\Delta t) & V_{k+1}(t+1-\Delta t) & \ldots & V_{k+1}(t+1-N\Delta t) \\
\cdot & \cdot & \cdot & \cdot & \cdot & \cdot & \cdot \\
\cdot & \cdot & \cdot & \cdot & \cdot & \cdot & \cdot \\
\cdot & \cdot & \cdot & \cdot & \cdot & \cdot & \cdot \\
\cdot & \cdot & \cdot & \cdot & \cdot & \cdot & \cdot \\
V_k(t+M-\Delta t) & V_{k-1}(t+M-\Delta t) & \ldots & V_{k-1}(t+M-N\Delta t) & V_{k+1}(t+M-\Delta t) & \ldots & V_{k+1}(t+M-N\Delta t)
\end{bmatrix}
\cdot
\begin{bmatrix}
a \\
b_1 \\
\vdots \\
b_N \\
c_1 \\
\vdots \\
c_N
\end{bmatrix}
$$

$$(6.5)$$

Note that Equation (6.5) is an approximation since the true model order is not finite. In order to reflect this in the set of equations an error term will be added and the above equation can be written in compact form as below:

$$[V_k]|_t^{t+M} = [V_{k,k-1,k+1}] \cdot [\delta] + [e] \tag{6.6}$$

$$[\delta] = \begin{bmatrix} a & b_1 & \cdots & b_N & c_1 & \cdots & c_N \end{bmatrix}^T$$

where the dimension of V_k, the vector of aerial voltage at intermediate point k, is M, the dimension of the $V_{k,k-1,k+1}$, the matrix of the past values, is $M \times (2N+1)$ and the dimension of δ, the model coefficients vector is $(2N+1)$. [e] represents the model error vector.

A solution to the over-determined set of linear equations can be found in the least squares sense and the goodness of fit for the estimated model can be tested based on the normalized residuals as shown below:

$$\hat{\delta} = ([V_{k,k-1,k+1}]^T [V_{k,k-1,k+1}])^{-1} [V_{k,k-1,k+1}]^T [V_k]|_t^{t+M}$$

$$\hat{V}_k = [V_{k,k-1,k+1}] \cdot [\hat{\delta}]$$

$$r = \frac{V_k - \hat{V}_k}{|V_k|} \tag{6.7}$$

The procedure is repeated for all other intermediate points and the voltage profile is estimated using the predicted aerial mode voltages along the transmission line.

C.   Simulations

A 3 bus system made up of two transmission lines shown in Figure 35 is used for all simulations. Transient simulations are carried out by the ATP/EMTP program. Frequency dependent transmission line models are used to represent the transmission lines. Simulation time step, Δt, is chosen to be 50 μsec. Identical tower configurations

shown in the Appendix are used for both of the transmission lines in the system. Simulations are run for 0.04 sec (801 time steps) and the fault is applied at 0.02 sec (401th time step). Voltage transients at the terminals and at different intermediate points along the transmission line AB are simulated by creating a fictitious bus along the line once at a time for each intermediate point.
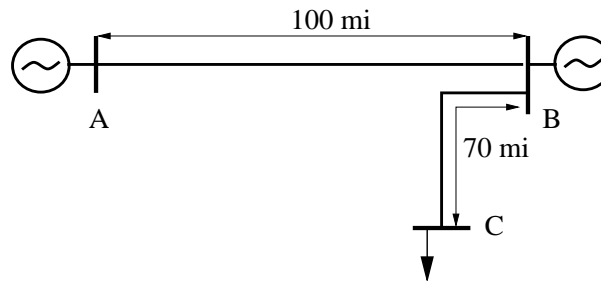
Fig. 35. Studied 3-bus system

Time series model development, identification and estimation of model parameters, and model validation against ATP simulations, are all carried out in MATLAB environment. Clarke transformation is used for modal decomposition of the phase voltages. The traveling time, τ, of the transmission line AB in aerial mode is calculated as τ = L / v = 538 μsec where L=100 mi is the total length of the line AB and $v = 1.85618e^5$ mi/sec is the aerial mode velocity evaluated at 20 kHz. Travelling time, τ, corresponds approximately to 11 discrete time steps, since $\tau_{\Delta t} = \tau/\Delta t \simeq 10.77$.

The following indices are calculated to quantify the goodness of fit and prediction errors for the identified model.

- $r_{max-ident}$: Maximum normalized residual for the observation interval which is used to identify and estimate model parameters. This index is a measure of goodness of fit for the estimated parameters of the identified model.

- $r_{max-est}$: Maximum normalized residual for the prediction interval where voltages are predicted using the developed time series model. This index is a measure of prediction performance of the proposed model.

- $r_{max-pred}$: Maximum normalized residual for the voltage transients due to a different type of fault at a different location.

Determining the model order: Different model orders are chosen and corresponding models are built. Performances of these models are tested in terms of goodness of fit and computational burden. Table III provides the maximum normalized residuals, $r_{max-ident}$, for the models formed for the aerial mode voltage at mid-point of line AB. A single-phase to ground fault at bus C is used to simulate the voltage transients for this test. Chosen model orders ranged from τ to 10τ.

Table III. Maximum normalized residuals versus model order

Model Order	$r_{max-ident}$
τ	0.67
2τ	0.0575e-3
3τ	0.8996e-3
4τ	0.1285e-3
5τ	0.0649e-3
6τ	0.0192e-3
7τ	0.0081e-3
8τ	0.0057e-3
9τ	0.0391e-3
10τ	0.1395e-3

The optimal model order for this case is chosen as 2τ, which corresponds to 22 time steps. Using τ as the model order or increasing the model order beyond 2τ yields larger errors as evident from Table III. Errors are reduced for model orders larger than 5τ, but the trade-off between increased cpu time versus error reduction favors keeping 2τ as the chosen order.

The following sections present the simulation results of the models for different intermediate points along the line AB in Figure 35. In all sections, a single-phase to ground fault at load bus C, is used to simulate transients based on which the time series models are developed. All models are developed by using the first 450 time steps, i.e. until 2.5 msec (50 time steps) after the fault occurrence, as the observation period.

Initially, the time series model for the voltage at the intermediate point of line AB is identified and its parameters are estimated using the simulation data for the observation period. Then, the same model is used to predict the voltage transient at that same intermediate point for the remaining part of the post-fault period, i.e. from 451th time step to the end of the simulation time. Furthermore, the same model is then used to also predict the voltage transients at the same intermediate point of line AB for different types of faults at different locations along the neighboring transmission line, CB. The predicted voltage transients are validated by comparing with the simulated results and a normalized residual analysis is done to quantify the closeness of their match.

1. Model for the midpoint voltage

This section describes the details of the time series model developed for the middle point of line AB. Identified and estimated model coefficients are plotted in Figure 36. It is worthwhile to note that coefficients of sending end history terms corresponding

to $[b_1 \cdots b_{22}]$ appear to be dominant in the model.
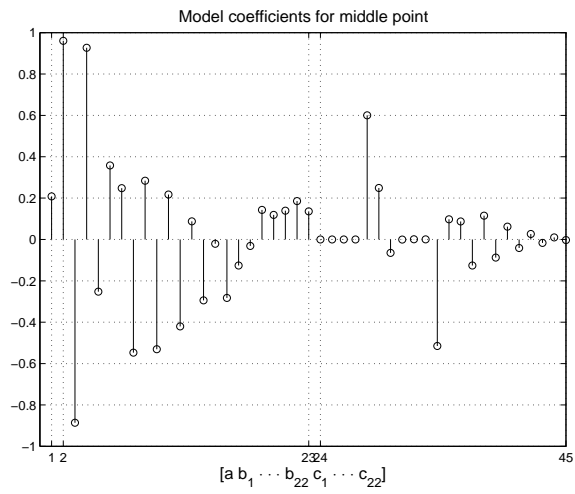
Fig. 36. Model coefficients for the middle point aerial voltage

Fig. 37. Model identification: estimated and simulated aerial mode voltages at the midpoint of line AB for the first 450 time steps
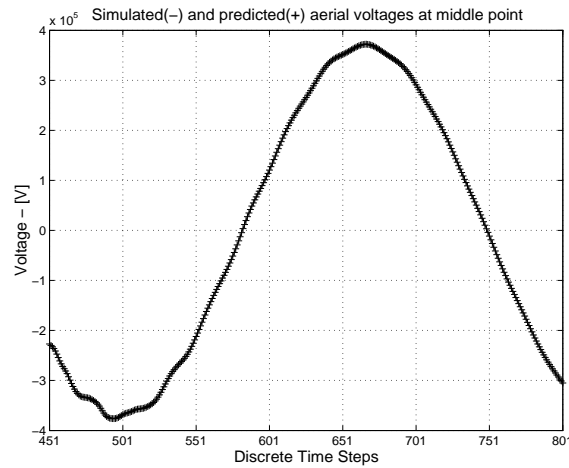
Fig. 38. Model validation: predicted and simulated aerial voltages at the midpoint of line AB from 451th to 801th time step

Goodness of fit for the identified model is quantified by computing the normalized residuals for the voltage samples in the observation period. The analysis of the aerial mode voltages which are shown in Figure 37 yields a maximum normalized residual, $r_{max-ident}$ of $1.54e^{-5}$. Then, using the same model, the remaining part of the post-fault transients is predicted for the same aerial mode voltage. The results are plotted in Figure 38 where the maximum normalized residual, $r_{max-est}$ is found to be $5.03e^{-5}$.

The same model is then tested by varying the type and location of the fault. A three-phase to ground fault is assumed to occur at 20 miles away from bus C. The same model is then used to predict the voltage transients for this fault. The maximum normalized residual, $r_{max-pred}$ of the aerial mode voltages as shown in Figure 39 is found to be $9.76e^{-5}$ in this case.

2. Model for an intermediate point voltage - 25 miles away from bus A

This case illustrates another model, this time for the voltage at a point 25 miles away from bus A. In determining the voltage profile along a given line, several such models
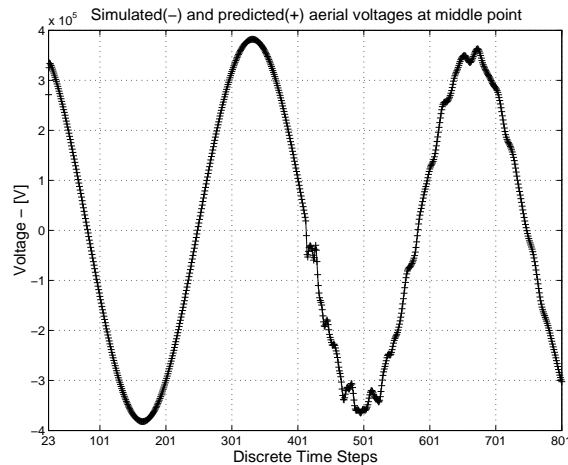
Fig. 39. Model validation: predicted and simulated aerial voltages at the midpoint of line AB during a three-phase to ground fault at 20 miles away from load bus, C

will be needed. The number of models will depend on the desired spatial resolution for the profile calculation. Hence, this illustrated case can simply be repeated by only changing the location, in order to obtain similar models with similar performances for as many point as needed along the line.

The time series model is identified and its coefficients are estimated as described above. The coefficients that are estimated for the aerial mode voltage model are shown in Figure 40.

Normalized residual analysis is observed for model verification. The estimation of the aerial voltage in Figure 41 has a maximum normalized residual, $r_{max-ident}$ of $1.66e^{-5}$. A maximum normalized residual, $r_{max-est}$ of $5.2e^{-3}$ is obtained from the prediction of the aerial voltage in Figure 42.

The model is used to predict the aerial mode voltage at 25 miles away from bus A for a different fault, three-phase to ground, at a different location, bus B. The maximum normalized residual, $r_{max-pred}$ of the aerial voltage prediction as shown in Figure 43 is $2.5e^{-2}$.
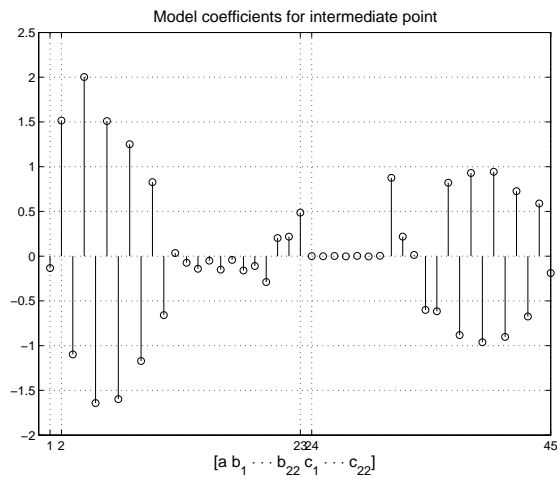
Fig. 40. Model coefficients for aerial mode voltage at the intermediate point 25 miles away from bus A
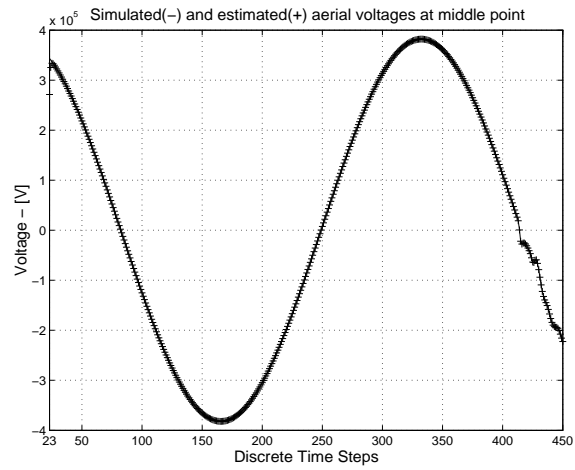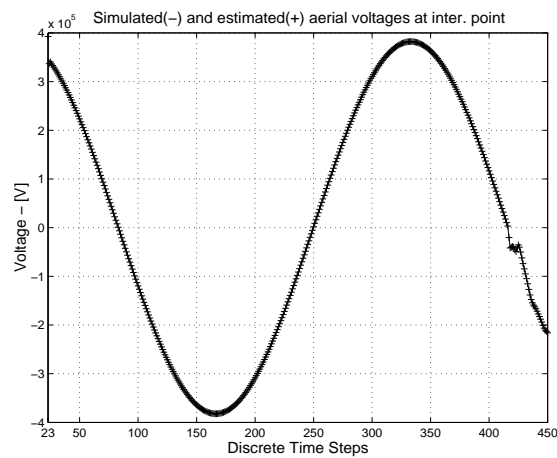

Fig. 41. Model identification: estimated and simulated aerial voltages at 25 miles away from bus A for the first 450 time steps
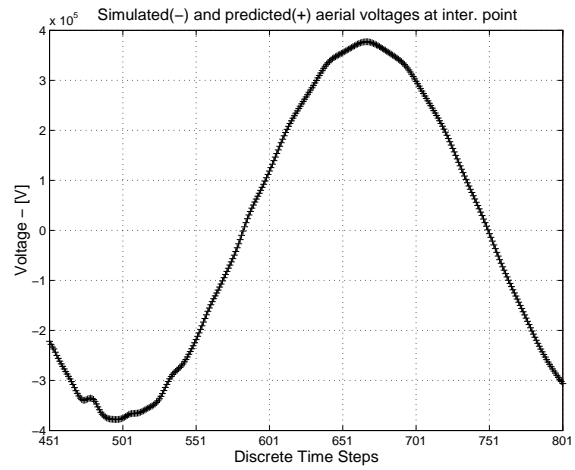
Fig. 42. Model validation: predicted and simulated aerial mode voltages at 25 miles away from bus A from 451th to 801th time step

Fig. 43. Model validation: predicted and simulated aerial mode voltages at 25 miles away from bus A during a three-phase to ground fault at bus B

3.   Model for an intermediate point voltage - 75 miles away from bus A

This case is similar to the above, except for the location of the intermediate point selected. This time, the model is created for another intermediate point, 75 miles away from bus A, along transmission line AB. Figure 44 presents the model coefficients for aerial mode voltages.
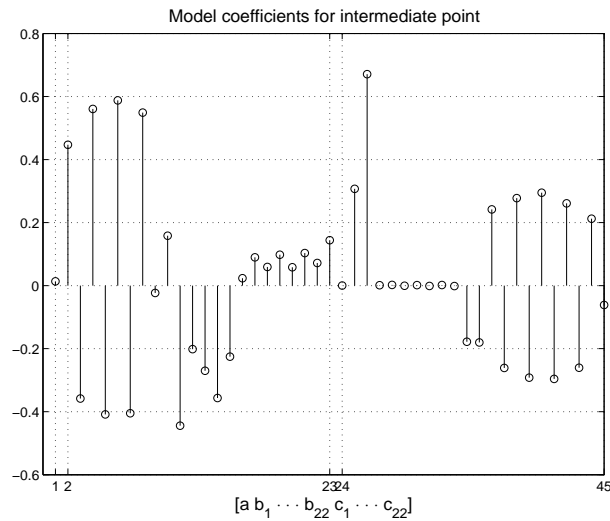
Fig. 44. Model coefficients for aerial mode voltage at the intermediate point 75 miles away from bus A

The normalized residuals calculated for the observation period are plotted in Figure 45. The maximum normalized residual, $r_{max-ident}$ in this case is $0.46e^{-5}$. When the model is used for prediction of the aerial mode voltages in the prediction period, the results look like those in Figure 46 where the maximum normalized residual, $r_{max-est}$ is now $1.91e^{-3}$.
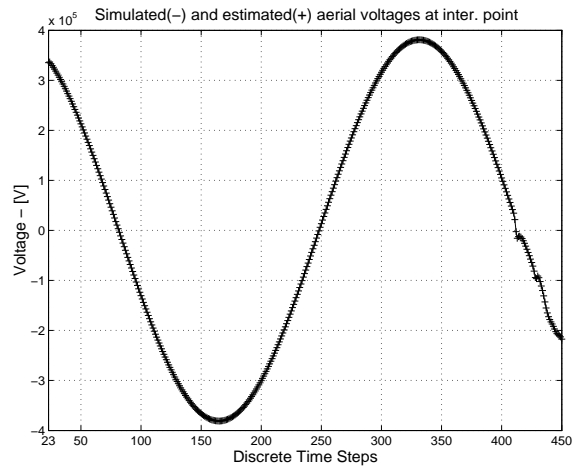
Fig. 45. Model identification: estimated and simulated aerial voltages at 75 miles away from bus A for the first 450 time steps
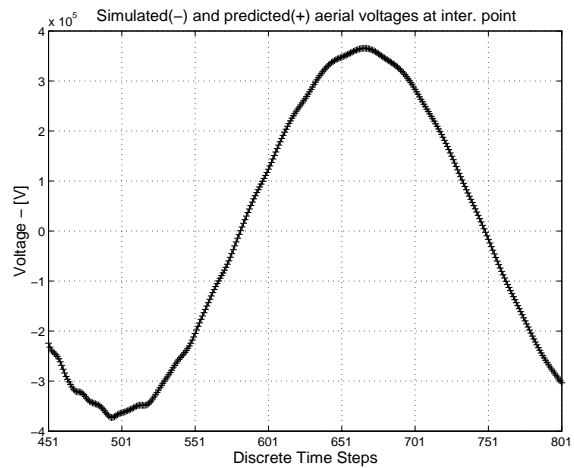
Fig. 46. Model validation: predicted and simulated aerial voltages at 75 miles away from bus A from 451th to 801th time step

The same model is also tested to predict the aerial voltage at 75 miles away from bus A for a different type of fault at a different location. A three-phase to ground fault as in the previous section is assumed to occur at bus B. The maximum normalized residual, $r_{max-pred}$ of the aerial mode voltage prediction in Figure 47 is found to be $9.23e^{-3}$.

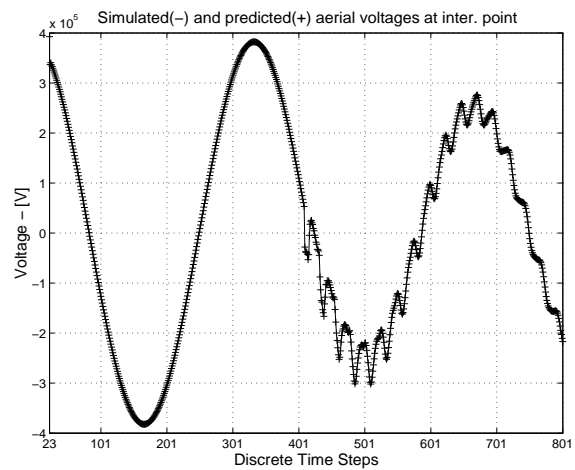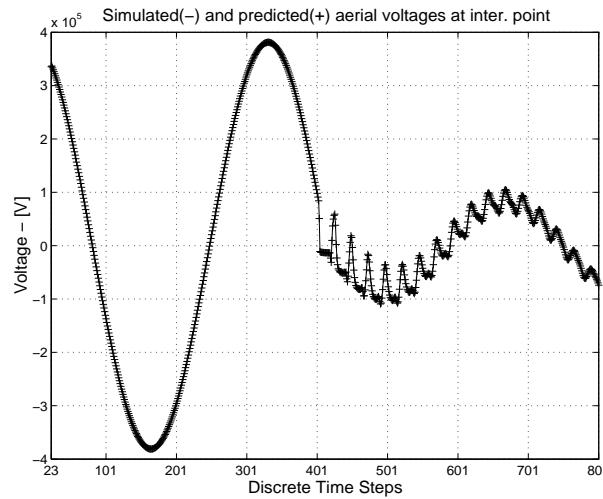Fig. 47. Model validation: predicted and simulated aerial voltages at 75 miles away from bus A during a three-phase to ground fault at bus B

In summary, the above results strongly imply that by applying the presented procedure for enough number of intermediate points, a good spatial approximation for the voltage profile of a transmission line can be obtained for each time step of the entire simulation. One such example will be shown in the next section.

4. Voltage profile calculation

This case illustrates results of a seven point voltage profile approximation using the proposed time series model. This is accomplished by identifying time series models for every intermediate point along the line and estimating their parameters using simulated voltage transients for a single-phase to ground fault at bus C.

In order to validate the model for faults of different type and location, simulations are carried out for a balanced three-phase to ground fault at 20 miles from bus C. Previously developed model is used to predict the transient voltage profile for this fault. In Table IV the maximum normalized residuals are presented for each intermediate point followed by Figure 48 showing the voltage profile along the transmission

line for 7 intermediate points at 501th time step.

Table IV. The maximum normalized residuals for each intermediate point at 501th time step

	Distance from bus A - [mi]	$r_{max-ident}$	$r_{max-est}$	$r_{max-pred}$
1	0.0 - bus A	-	-	-
2	12.5	$2.41e^{-6}$	$1.93e^{-4}$	$3.89e^{-4}$
3	25.0	$1.66e^{-5}$	$5.20e^{-3}$	$1.32e^{-2}$
4	37.5	$2.06e^{-5}$	$2.11e^{-2}$	$3.90e^{-2}$
5	50.0	$1.54e^{-5}$	$5.03e^{-5}$	$9.76e^{-5}$
6	62.5	$1.22e^{-5}$	$1.04e^{-2}$	$2.00e^{-2}$
7	75.0	$4.66e^{-6}$	$1.91e^{-3}$	$4.93e^{-3}$
8	87.5	$7.72e^{-5}$	$1.52e^{-5}$	$7.73e^{-5}$
9	100.0 - bus B	-	-	-
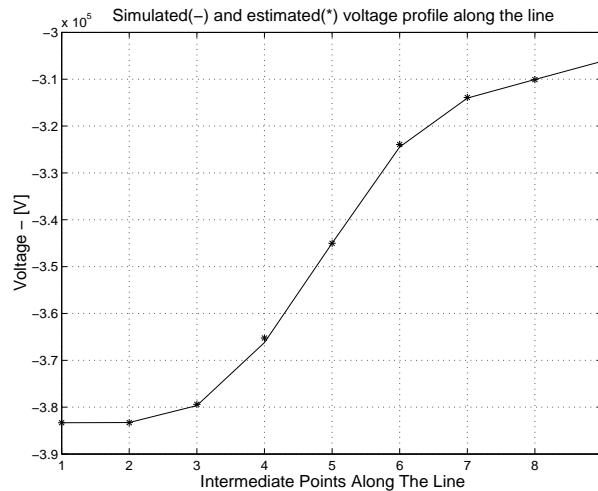
Fig. 48. The voltage profile along the transmission line AB at the 501th time step

5. Computational benefits

It is difficult to properly compare the computational times of using the proposed time series approximation versus the use of wave equations, since they are implemented

in different environments, namely EMTP and MATLAB. The following results are expected to improve in favor of the proposed approach if it is implemented in the same environment as EMTP.

Assuming that a time series model is already formed, the computation time required to predict the voltage at an intermediate point for one time step in MATLAB 6.1 environment is recorded as approximately 15 msec. Thus, a 7 point approximation for the entire voltage profile of the transmission line AB can be predicted in approximately $7 \cdot 15e^{-3} \cdot 801 = 0.84$ sec for the total simulation duration (801 time steps). The same 7 point approximation is then obtained by using the ATP/EMTP program and the total simulation time is recorded as 2.1 sec. This implies a 2.5 times reduction in the cpu time for this simulation case. All the simulations are run in a notebook with Intel Celeron 2.4 GHz microprocessor and a 448 MB memory configuration.

D. Summary

This chapter presents a simple yet effective approach to accurately and rapidly obtain the voltage profile along a transmission line during fault transients. The objective of the presented method is to eliminate the need to use wave equations and line parameters provided that an EMTP type transients simulator is available for generating bus voltage transients for a given fault. This is accomplished by developing a time series model to estimate the voltage at an intermediate point along the transmission line. The model is formed for each intermediate point separately. Once the model is obtained it can be used to predict the transient voltage at that point along the line during any fault in the system. The approach can potentially be useful as a post processor to a transient simulator and can be used by developers of transient animations and movies for illustrating fault-initiated propagation of traveling waves in power

systems. In Chapter VII new methods for visualization and animation techniques for power system electromagnetic transients are presented.

CHAPTER VII

VISUALIZATION AND ANIMATION OF TRANSIENTS

A.   Introduction

The behavior of the fault or switching initiated power system transients is extremely important not only for power system protection, control and power quality analysis but also for educational purposes. Significant contributions exist in the area of simulation tools, which provide numerical solutions. The commonly used simulation tool for transient simulations in time domain is the electromagnetic transients program [79].

Electromagnetic transients simulators provide numerical solutions for the voltages at buses in the power system. The details of voltage transients are revealed by plotting these solutions over a time interval. However, the variation of the voltage along the transmission line, referred as the voltage profile, is usually not calculated. Once the terminal voltages are known as a function of time, the voltage profile along the transmission line can be obtained by using traveling wave equations or by using the proposed scheme in Chapter VI. Calculating this profile at each time step allows the user to observe the time variation of the traveling waves along the transmission line. As mentioned in the previous chapter this procedure constitutes the basis of a traveling wave *movie* which is useful not only as an educational aid, but also for observing the propagation of transients into the system. The Bewley diagrams [1] are the first attempts to capture the traveling wave behavior on paper.

Previous studies on visualization of power systems mainly focus on steady state operation [80], [81]. Animation is used for displaying direction and changes in the amount of power flows, limit violations for transmission lines and bus voltages, etc.

but visualization of fast voltage transients have not received the same level of attention.

Travelling wave concepts can be better understood by using advanced visualization techniques. Animation is one of the visualization methods, which can help to explain the complex time-space behavior of traveling waves during faults or other disturbances. Time domain simulation programs calculate the voltage signals only at line terminals. However, animation of transients provides the variation of the voltage profile of a transmission line. Understanding the behavior of traveling waves is also important for fault location techniques, which utilize traveling wave concepts. Recently, flexible Java tools are used to develop web exercises demonstrating the basic behavior of traveling waves on lossless transmission lines [82]. A similar animation program showing the traveling waves on interconnects in VLSI circuits and providing voltage-distance figures for specific RLC circuits is described in [83]. Another Java tool illustrating the wavelet transforms of traveling waves along a single transmission line, is explained in [84].

Woodruff introduced transient sculptures [2] in early 1930s that were ingeniously created with very limited resources. The preliminary work of our study which is motivated by [2] is introduced in [75] and [76]. These results are extended in this chapter and a comprehensive review of the developed methods is presented.

B.   Animation of Travelling Waves

In this section three methods for traveling wave visualization are presented: (1) *Animated Lines* (2) *Virtual Transient Sculptures* and (3) *Animated Pipes*. A new software tool is presented in order to implement the first method. Second method is an extension of [2] using Computer Graphics techniques. This is referred to as *virtual*

transient sculptures. First two methods focus on single-phase power system transients animation problem while the last method concentrates on transients animation along three-phase transmission lines.

All proposed methods require the voltage profile information along the transmission line for all time steps of the simulation. A simple way to obtain the voltage information at intermediate points along the line is to represent the transmission line as several cascaded line sections of small lengths. The voltage signals at terminal buses of these sections are calculated by a simulation program such as ATP/EMTP. Nevertheless, once the voltages at both ends are calculated via ATP/EMTP, they can be utilized to determine the intermediate voltages along the line using traveling wave equations as done in [77] or utilizing the proposed scheme in the previous chapter.

In this study, transmission lines with distributed parameters are studied by using ATP/EMTP. The lines are represented by n number of sections and the voltage signal at each intermediate point is obtained by ATP/EMTP.

The details of the visualization methods are described in the following sections.

1.   Animated lines

In this method the main idea is printing out the simulated single phase voltages at each point along the line at the same time for every time step during the simulation. The logic behind the cartoon movies constitutes the logic of the animation. Updating the voltage signal at each intermediate point along the transmission line at every time step creates the traveling wave motion. A software program is written in order to implement this method. It is presented in the implementation section.

2. Virtual transient sculptures

In power systems, the voltage signals reach their maximum values during a switching or a fault usually at the sending or receiving ends of a transmission line. However, there are such cases where the voltage transients are much higher along the transmission line than those at both ends. The *virtual transient sculptures* technique is very helpful for revealing the hidden voltage information along the transmission line.

In order to create *virtual transient sculptures*, the simulation results are processed in MATLAB in a way to form a special *object* file which is read by Maya, a 3D visualization and animation program. This procedure composes a three dimensional time-line distance-voltage profile picture of the transmission line which is named as *virtual transient sculpture*. By using proper lighting different views are rendered from different angles. An interesting by-product of this rendering approach shows up when the "sculpture" is observed from top. The top view actually provides the well-known Bewley diagram of the transients. Bewley diagrams are used for understanding the complex traveling wave behavior and they are also used for fault location purposes. The details of such traveling wave based fault location methods can be found in [34], [35] and [36]. In the three-dimensional perspective view x, y and z coordinates correspond to time, line distance and voltage respectively. In the two-dimensional top view x and y coordinates correspond to time and line distance. Implementation section illustrates this by examples.

3. Animated pipes

The main idea in this method is representing the voltage profile of a three-phase transmission line as a *pipe*. The logic is the same logic used in *Animated Lines* method, however since the cross-sections of the pipes are changed according to the

three phase voltage information, the resulting motion is named as *animated pipes.*
Two types of cross-sections for pipes are proposed: (1) Triangular for three-phase
voltages (2) Circular for modal voltages. The following transformation is used to
convert the voltage information:

$$f : \Re^3 \longrightarrow \Re^{+n} \tag{7.1}$$

where $\Re^+$ represents radius (a positive real number) of the pipe in a given angle,
$n = 3$ is used for triangle case and $n = 2$ for circle case. The examples of triangular
and circular cross-sections are shown in Figures 49 and 50 respectively.
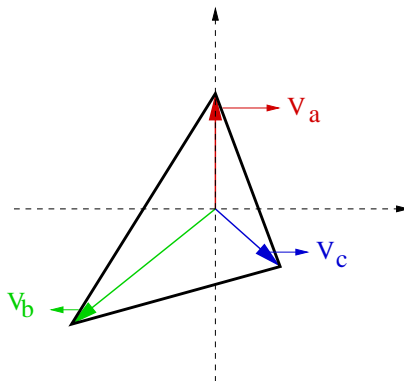

Fig. 49. Triangular representation of 3-phase voltages for one section of the transmission line

The *movie* is obtained when the voltage information at each section is updated at
the same time at every time step. The examples can be found in the implementation
section.
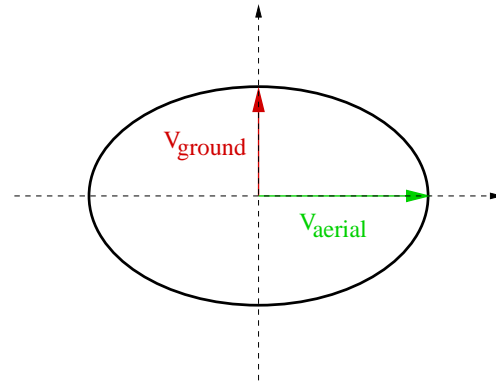
Fig. 50. Circular representation of modal voltages for one section of the transmission line

C. Coloring Based Visualization of Three-Phase Power System Transients - Use of RGB Coloring

A scheme is required in digital environment in order to store and display color information. There are various color systems, however the most common one is RGB (Red,Green and Blue) color system, where the basic idea is to produce a particular color by superimposing three lights colored by red, green and blue colors. The level or intensity of each of the three lights determines the color. All colored graphics in digital display devices even in televisions are based on **RGB Coloring** and its color space is given in Figure 51.

In this work the three colors are assigned to the three-phase voltages along a transmission line. When applied to a faulted transmission line voltage transients, a color pattern describing the variations of the voltage profile along the transmission line will emerge. This pattern can then be used in determining the type and the location of the fault. As will be illustrated in the following sections it is sufficient to apply RGB coloring to the voltage transients recorded at the line terminals only in order to determine the fault location. However, applying it to the entire voltage profile
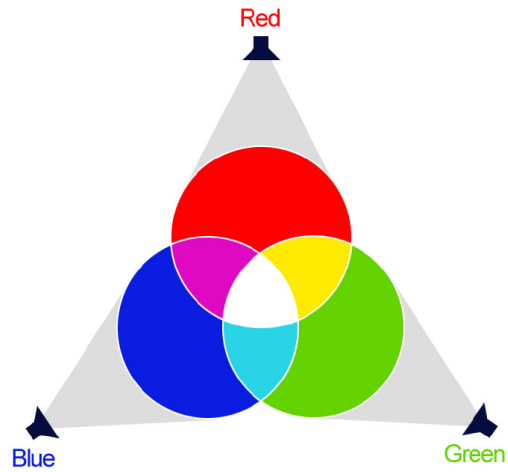
Fig. 51. Red-Green-Blue (RGB) Color Space

along the faulted line reveals the link to traveling waves and hence will also be done. This will necessitate the calculation of the voltage profile variation along the entire line length. One simple way to obtain the voltage profile of a transmission line is to represent it as several cascaded line sections of much smaller length. Terminal buses of these small sections will serve as discrete points along the line length where voltage solution will be available by some simulation program such as the ATP-EMTP.

An image is created by converting 3 phase transient voltage information at each section for each time step by using a transformation function:

$$f : \Re^3 \longrightarrow [0, 255]^3 \qquad (7.2)$$

An RGB image file consists of pixels on the 2D space while one pixel is made up of 3 colors; red, green and blue (RGB). In this study, the 2D coordinates of one pixel is composed by treating *x-axis* as *time* and *y-axis* as *line sections* as shown in an example in Figure 52. As seen in this example, the voltage profile color pattern is obtained by transforming the voltage signals at each section for each time step to RGB values where each color value varies in the range of 0 to 255. Different transformation

functions will be used for the phase and modal voltages.
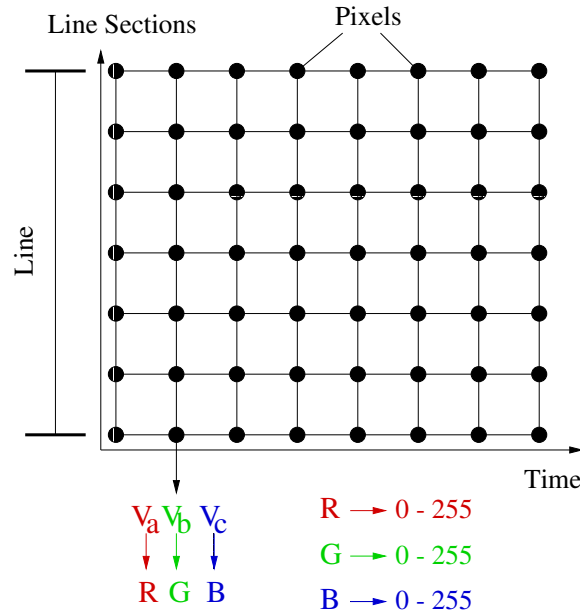
Fig. 52. An example of transformation function that converts voltage profile to an image.

D. Implementation

Since the proposed two methods, *Animated Lines* and *Virtual Transient Sculptures* are developed for single-phase power systems, the implementation of these methods are presented together in one section followed by the implementation of *Animated Pipes* and *RGB Coloring*.

1. Animated lines and virtual transient sculptures

Results of three cases are given in this section. These cases involve DC energization of a transmission line with open end line terminations, a ground fault occurring along a single-phase transmission line and a ground fault occurring in a single-phase three-bus

power system. All necessary simulated waveforms are obtained by using ATP/EMTP package. The transmission lines are studied using distributed parameter model and the lines are represented by 25 sections. The simulation time interval is chosen as 50 μsec, which is smaller than the traveling time of one section. The simulation time is chosen to be 0.1 sec which is enough for dissipation of the transients. Once the voltage signals at intermediate points are obtained by using ATP/EMTP, they are processed in MATLAB to create the data file for the animation software to implement the *animated lines*.

The animation software is written in C/C++ and it is implemented under Microsoft Visual Studio environment. Three dimensional graphical user interface is created by using OpenGL and FLTK libraries. The sending and receiving end buses are represented by conic towers. The voltage profile of a transmission line is represented by a red line connecting the two towers (buses) where the tips of the towers correspond to 0 V level.

Open and capacitive end terminations of a transmission line are studied for DC energization. In addition, the animations of a ground fault on a single-phase transmission line and in a three-bus system are presented. The perspective views of 3D transient sculptures are shown. In the faulted line example the closer side corresponds to the bus B.

a.   DC energization of an open-end line

An open-end transmission line which is modelled using the distributed parameter line model, is energized by 1 V DC source. The receiving end voltage is simulated as shown in Figure 53. A perspective view of the 3D time-distance-voltage profile is shown in Figure 54. As expected, it is observed that the voltage along the transmission line suddenly becomes almost twice the supply voltage at the beginning and it gradually
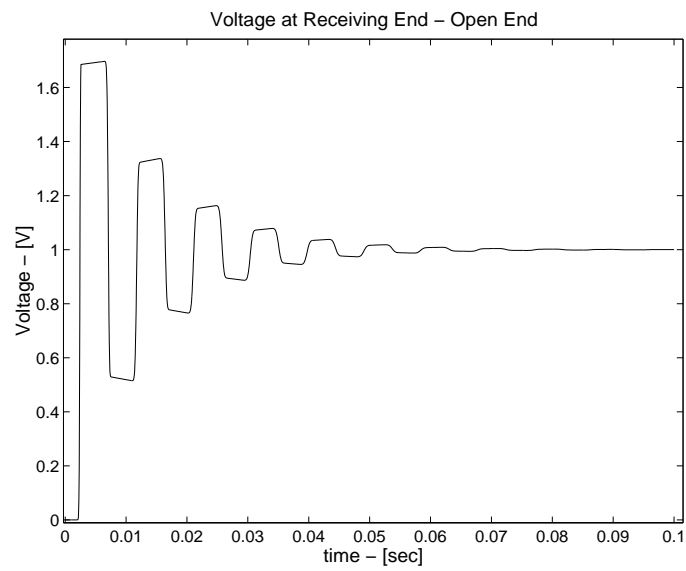
settles down around 1 V.

Fig. 53. Voltage at the receiving end of the open-end transmission line
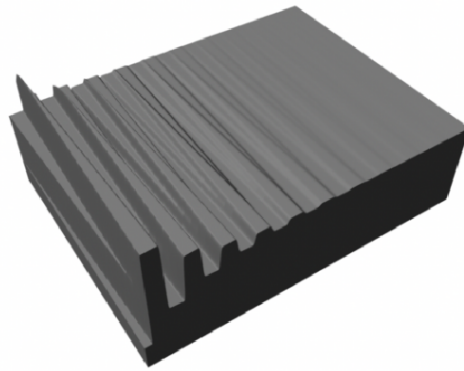
Fig. 54. Perspective view of open-end transmission line 3D voltage profile
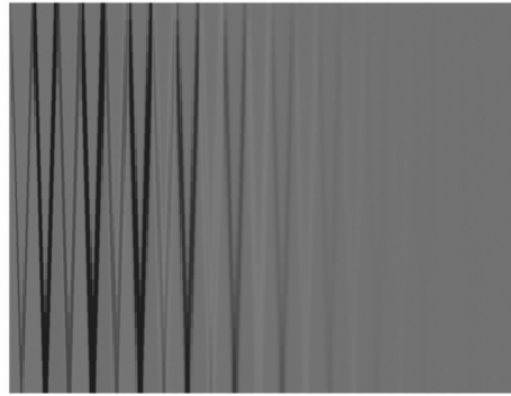
Fig. 55. Top view for open-end transmission line 3D voltage profile
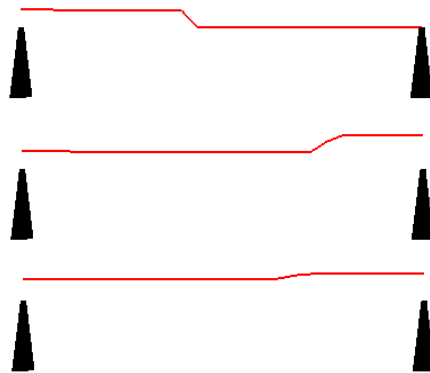
Fig. 56. Screen shots from the animation of open end energization

The Bewley diagram of the energization can be obtained by rendering the top view of the virtual transient sculpture (three dimensional time-distance-voltage profile) of the transmission line in Figure 55. The upper x-axis corresponds to sending end of the transmission line. Note that after a couple of reflections the traveling wave dies out as can be easily observed in the top view. Three screen shots from the animation is presented in Figure 56. The tower on the left side represents the sending end bus. The very top shot corresponds to switching instant and the lower shots show the attenuation of the traveling wave as time progresses.

b. DC energization of a line with capacitive termination

The same transmission line used in the previous section is now terminated by a capacitor and energized by 1 V DC source. The receiving end voltage is given in Figure 57.

Fig. 57. Voltage at receiving end of the capacitive ended transmission line
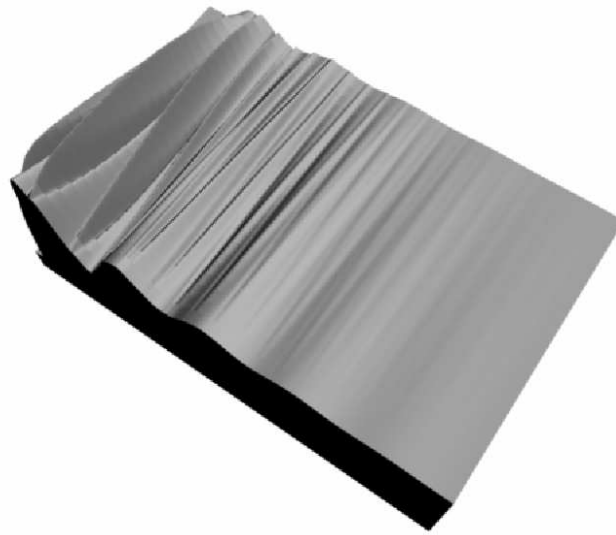
Fig. 58. Perspective view of capacitive ended transmission line 3D voltage profile
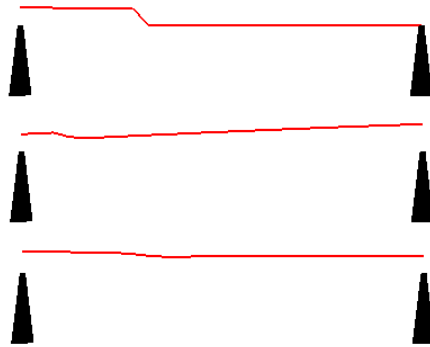
Fig. 59. Screen shots from the animation of the capacitive end energization

The variance of the voltage along the transmission line is shown in Figure 58. As expected, the receiving end voltage increases to almost twice the sending end voltage and then gradually settles down to 1 V. Three screen shots from the animation is presented in Figure 59.

Note that in Figure 58 the amplitude of the transient voltage signal at the beginning of the simulation right at the middle of the transmission line is much higher than those at both ends.

c.   Ground fault on a single-phase line

Single phase, two bus system as shown in Figure 60 is studied. AC sources with 60 Hz frequency and 1 V magnitude are used. A phase to ground fault occurs on the transmission line closer to bus B. The simulated voltage signal at bus B is given in Figure 61.
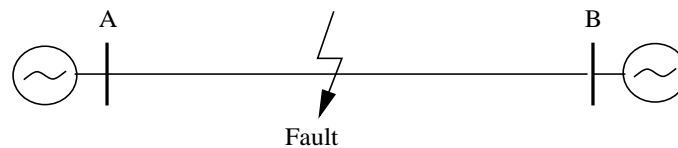
Fig. 60. Phase to ground fault on a double-ended transmission line

Virtual transient sculpture is given in Figure 62. The Bewley diagram can be seen in Figure 63 which is obtained by rendering the top view of the sculpture. The bottom x-axis in the top view corresponds bus B. As expected, the arrival time of the forward traveling wave (towards B) at bus B is smaller than the arrival time of the backward traveling wave (towards A) at bus A. Since the simulation time is not long enough for the traveling waves to settle in a stationary state, the reflections at both ends are still observable. Three screen shots from this animation are shown in Figure 64. Note that the tower on the left side represents bus A.
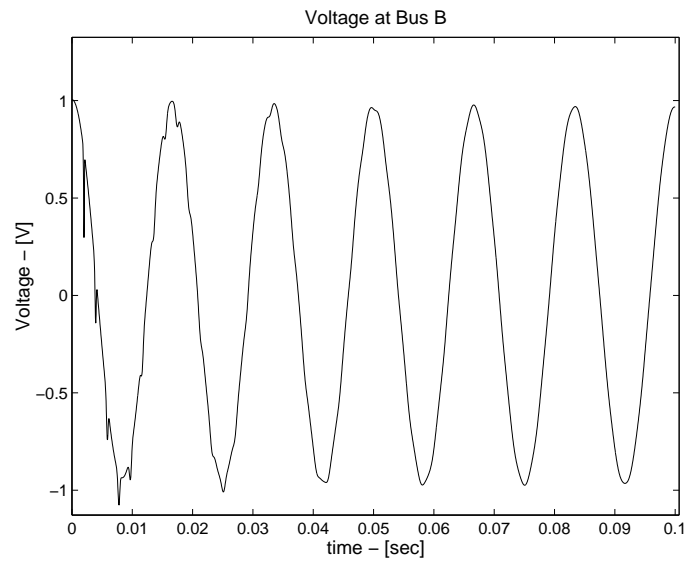
Fig. 61. Voltage at bus B during the fault
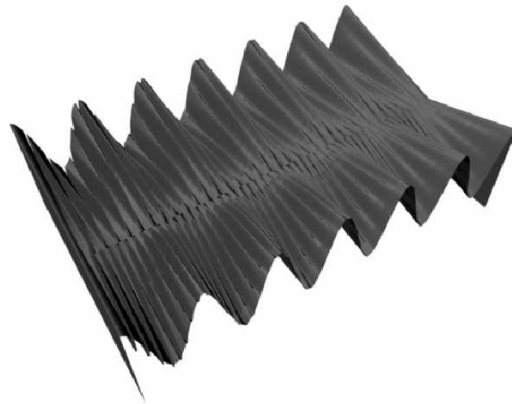
Fig. 62. Perspective view of the transmission line 3D voltage profile during a fault

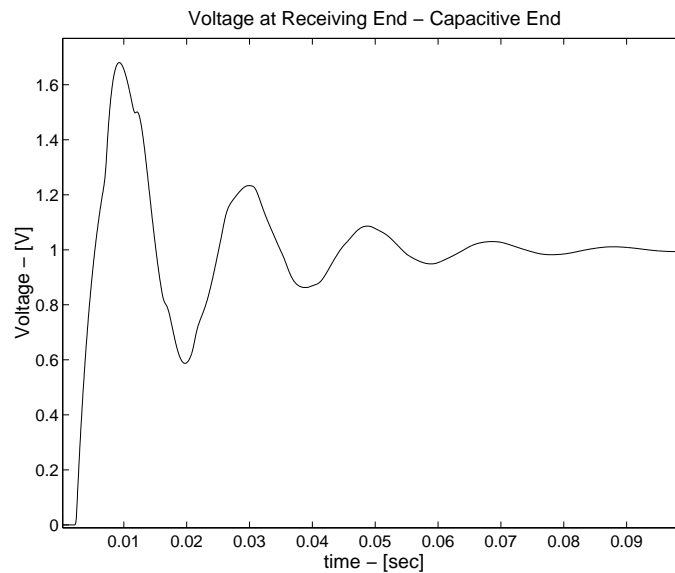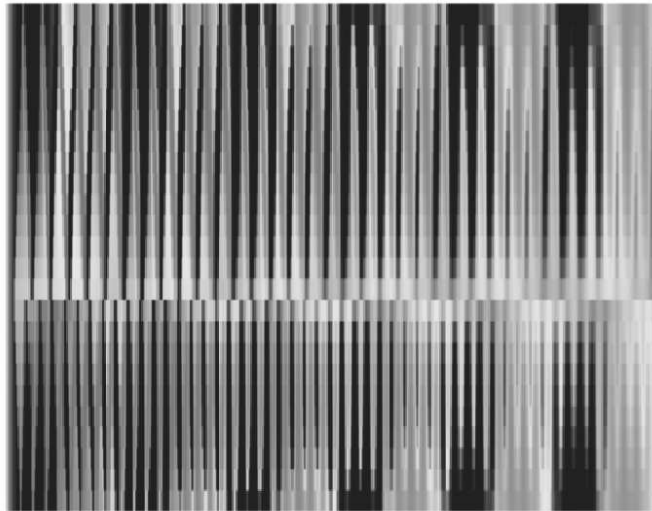Fig. 63. Top view of the transmission line 3D voltage profile during a fault
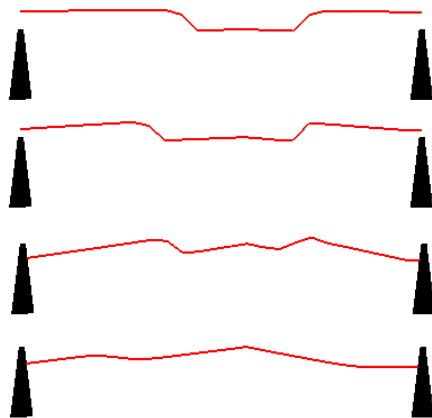
Fig. 64. Screen shots from the animation of the faulted transmission line

d.   Ground fault in a three-bus system

A single-phase three bus power system is studied with identical transmission lines as shown in Figure 65. A ground fault next to bus A, between bus A and bus B is animated and the screen shots from the animation are given in Figure 66 and 67.
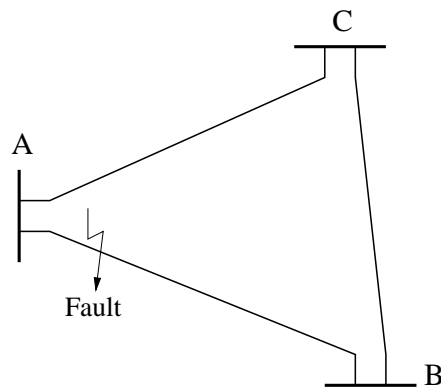
Fig. 65. Three bus power system
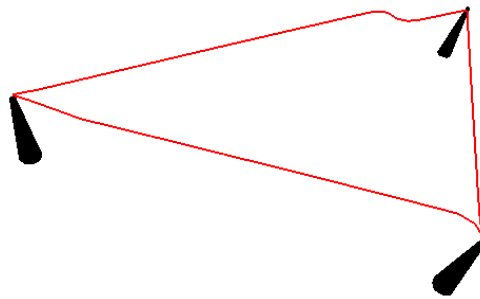
Fig. 66. Animation of a fault in 3-bus power system, screen shot-1

2.   Animated pipes

The animation technique for 3-phase power system transients are presented for two different ways:
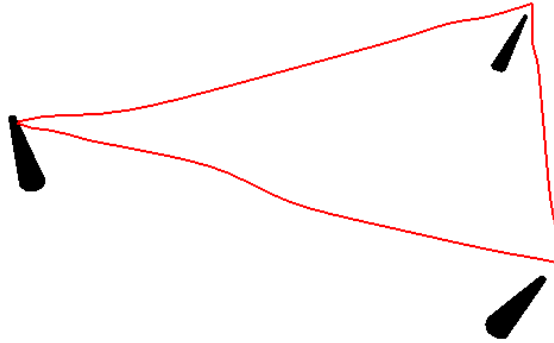
Fig. 67. Animation of a fault in 3-bus power system, screen shot-2

- Triangular representation using 3-phase voltage signals

- Circular representation using aerial and ground mode voltages

Following sections will provide the implementation along with the illustrative examples.

a.   Triangular pipes

The 3-phase instantaneous voltage values are directly used to obtain the triangular representation. For each line section at each time step the voltage value of each phase is first normalized and then it is treated as a vector with a magnitude of the instantaneous value of the corresponding phase and with 0, 120 and −120 degrees angle for phase A, B and C respectively. Once the three vectors representing the 3-phase instantaneous voltages are drawn, the triangular shape is created by connecting the head of the three vectors as shown in Figure 49. These operations define the transformation function in Equation (7.1)

The triangles representing the 3-phase instantaneous voltage values of the line sections are placed one after another in the 3D space and the triangular representation of the voltage profile is obtained.

The transient animation is created by using MATLAB Visualization Toolbox. Screen shots of perspective and front views are shown in Figure 68, Figure 69 and Figure 70, Figure 71 respectively.
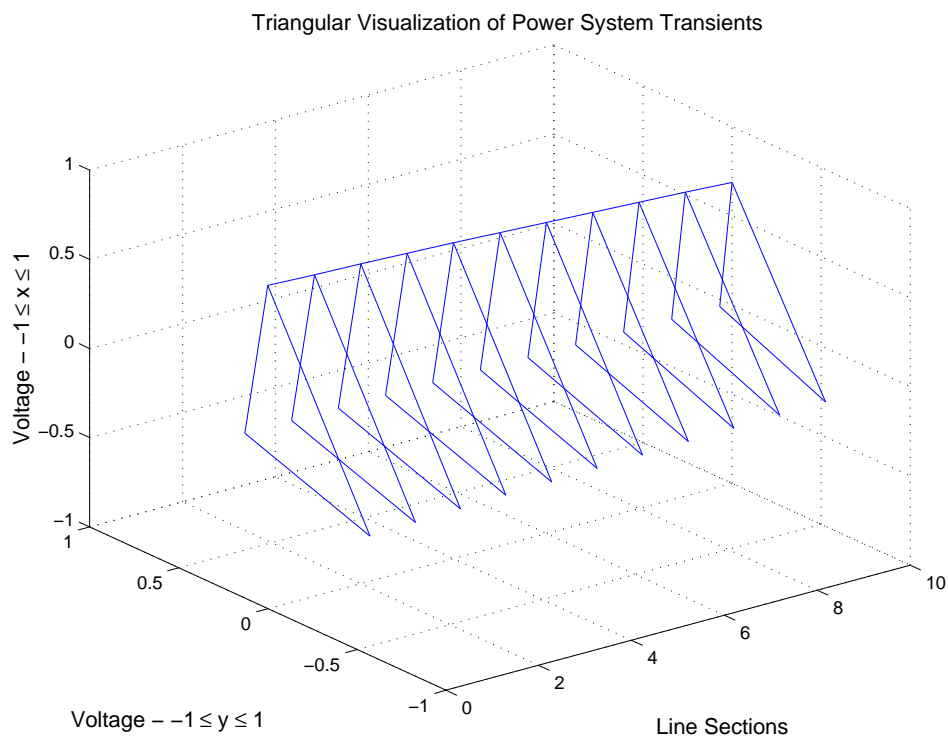
Fig. 68. Perspective view screen shot-1 of triangular animation of voltage profile before a three-phase to ground fault
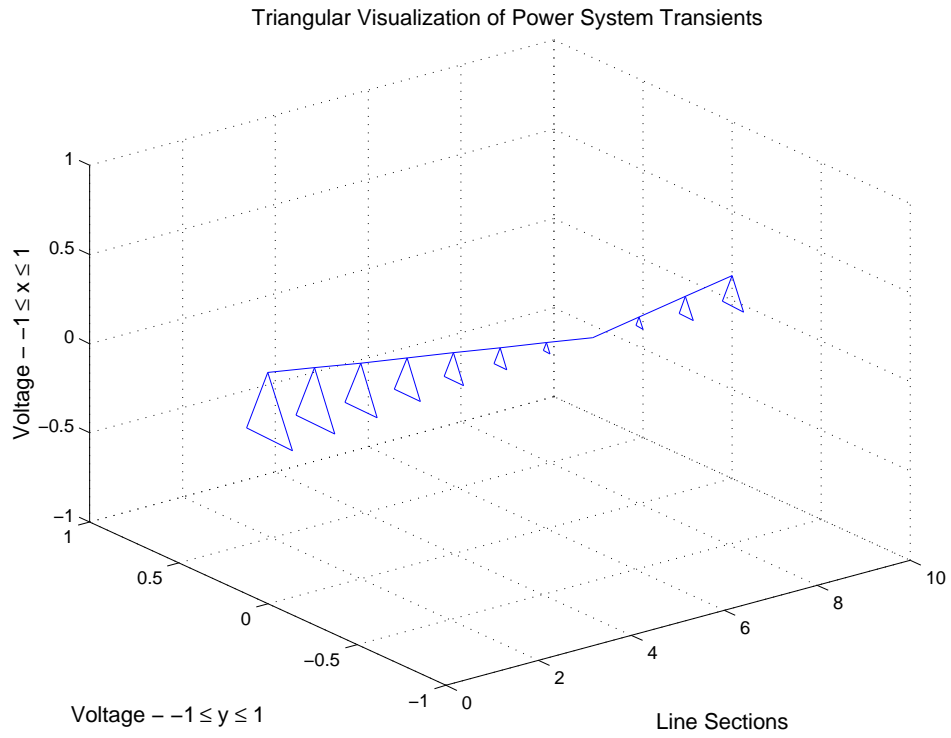
Fig. 69. Perspective view screen shot-2 of triangular animation of voltage profile during a three-phase to ground fault
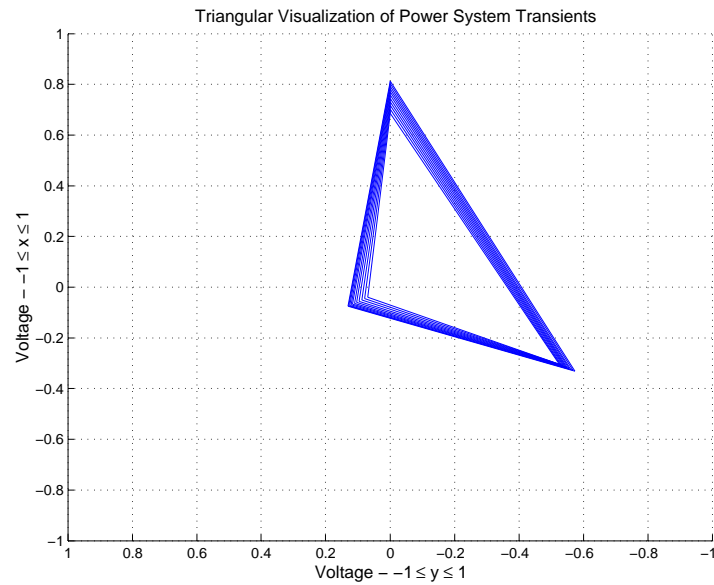
Fig. 70. Front view screen shot-1 of triangular animation of voltage profile before a three-phase to ground fault
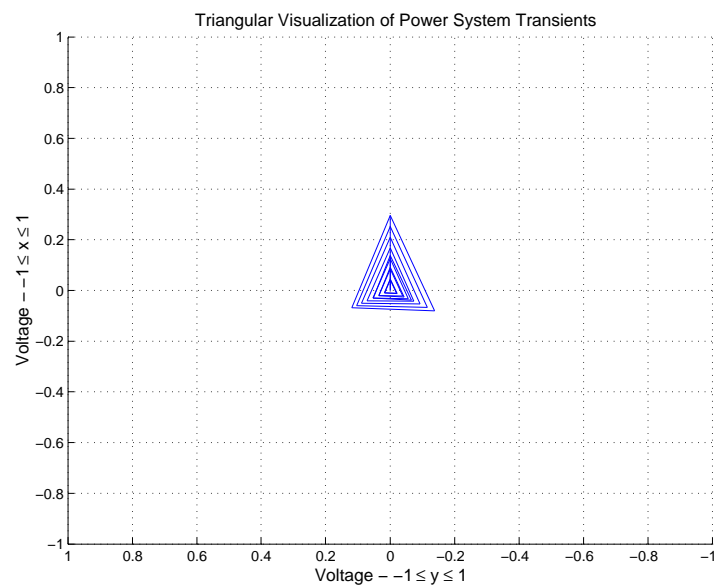
Fig. 71. Front view screen shot-2 of triangular animation of voltage profile during a three-phase to ground fault

b. Circular pipes

After simulating 3-phase voltages, they are transformed into aerial and ground modes via the Clarke transformation for every line section at each time step. The instantaneous voltage values of the two modal components are used to create an ellipse as illustrated in Figure 50.

The ellipse of each line section is placed one after another in 3D space and the circular representation of the voltage profile is obtained.
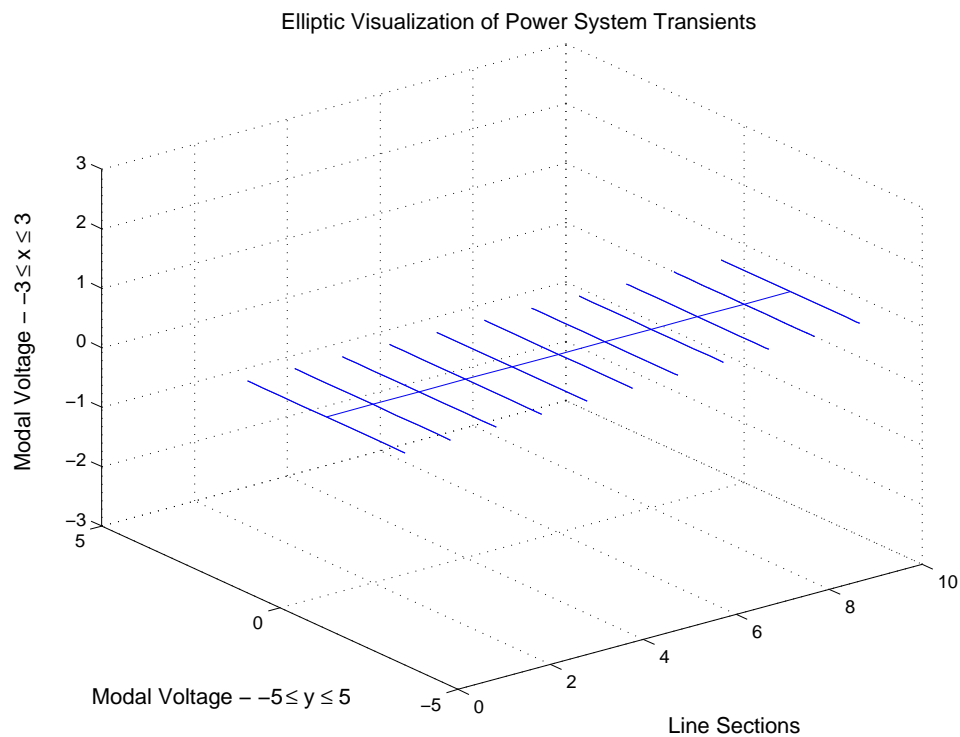
Fig. 72. Perspective view screen shot-1 of circular animation of voltage profile before a single-phase to ground fault

Figure 72, which shows the pre-fault conditions, where the ground mode is 0,

results in a single line instead of an ellipse representing the sinusoidal change in aerial mode. Once the fault occurs, both modal voltages will be present and will create the elliptic shapes at each line section as shown in Figure 73. Two screen shots of front view of the animation are given in Figure 74 and Figure 75.
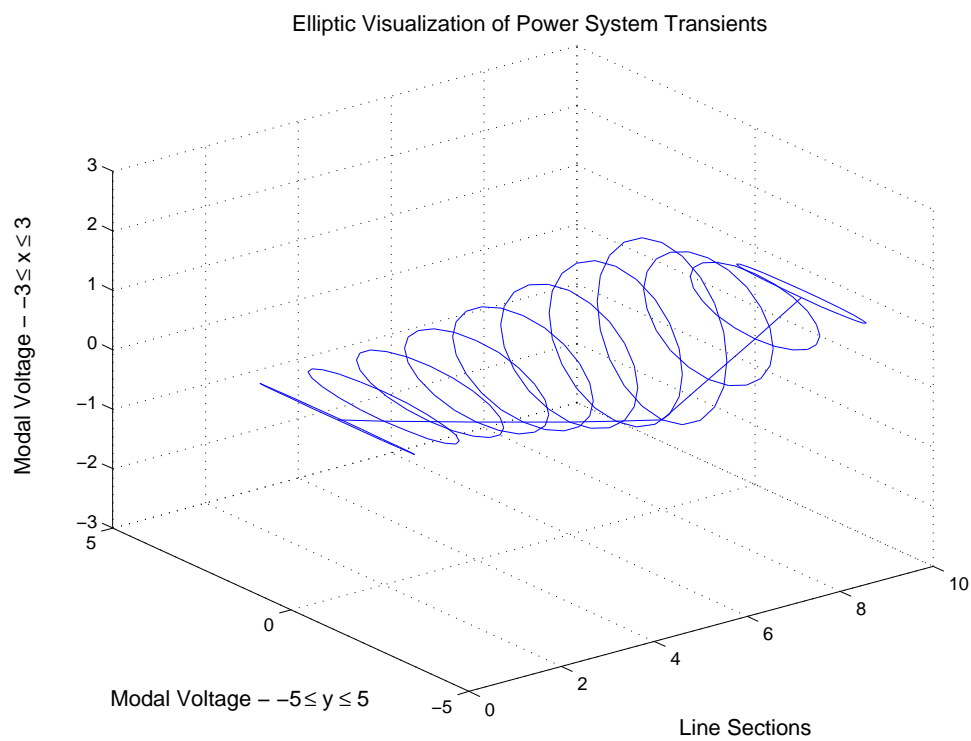
Fig. 73. Perspective view screen shot-2 of circular animation of voltage profile during a single-phase to ground fault
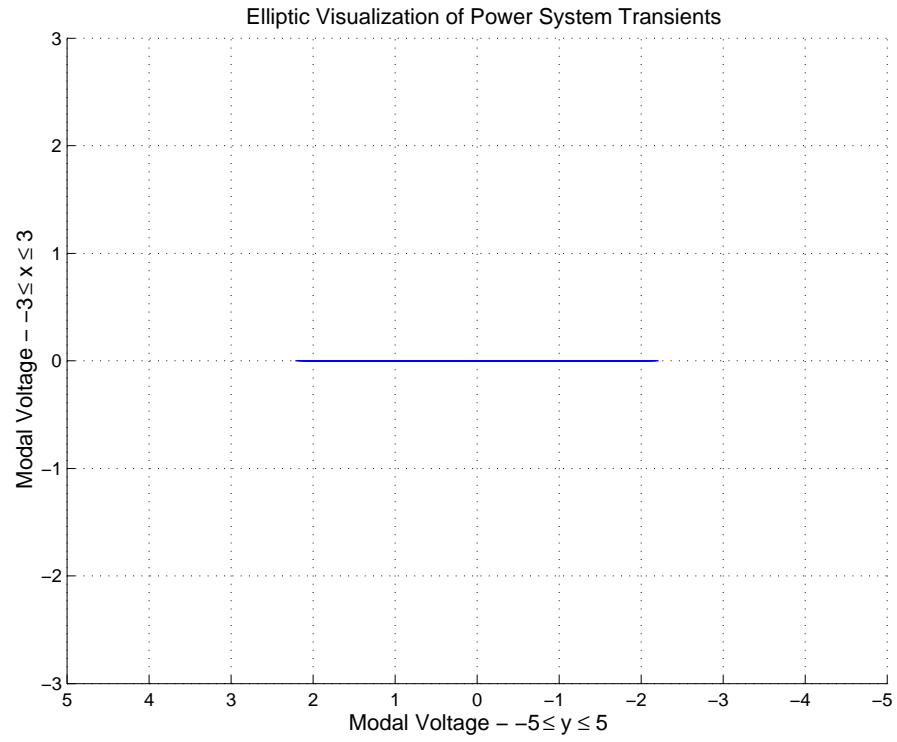
Fig. 74. Front view screen shot-1 of circular animation of voltage profile before a single-phase to ground fault
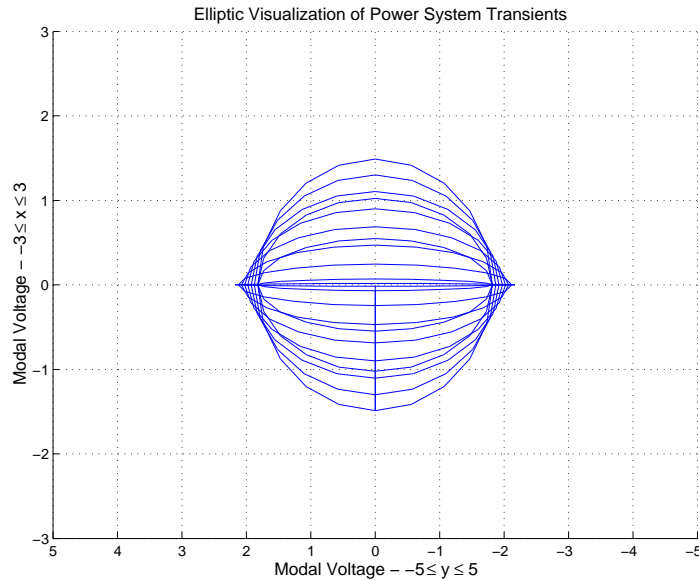
Fig. 75. Front view screen shot-2 of circular animation of voltage profile during a single-phase to ground fault

As evident from the above examples, animated pipes allow the user to easily observe various characteristics and phenomena associated with traveling waves. These are the traveling wave propagation, the type and the location of the fault, the effects of the traveling waves on each phase or modal component.

3. RGB Coloring

In order to illustrate the application of RGB coloring, a fault is simulated along a 100-mile high-voltage transmission line by using ATP-EMTP program. The line is represented by a distributed parameter model with *10* line sections and transient voltages are simulated for each section. The fault is assumed to occur at the 8th line section. The RGB image file of the voltage profile color pattern is created in MATLAB and then processed in Adobe Photoshop. The resulting images will be referred to as *Painted Transients*.

RGB coloring method is applied not only to the three-phase transient voltages, but also to the two modal components of these voltages, namely the aerial and the ground mode voltage transients. The results of these simulations reveal an interesting property of the RGB coloring method. In order to illustrate this, the simulation results for both cases will first be presented below.

a. Use of phase voltages

The transformation function shown in Equation (7.2) involves a two step procedure. First, the voltage values are normalized and shifted in the positive y direction to make them bounded between 0 and 1. Each discrete point on the sampled signal is then multiplied by 255.
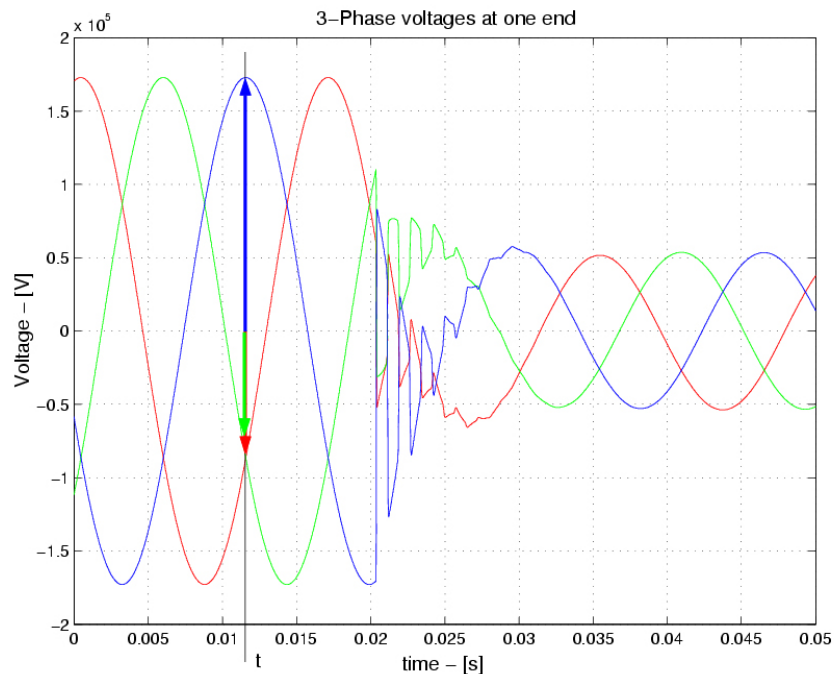
Fig. 76. Transient voltages at one end of the transmission line for a symmetric fault

A three-phase symmetric fault is simulated and the three-phase voltage waveforms recorded at one end of the line are shown in Figure 76. In creating this image, three-phase instantaneous voltage values are used at each line section and for each time step.

Voltage profile color pattern is shown in Figure 77 when there is no fault. The pattern is created for almost one cycle.
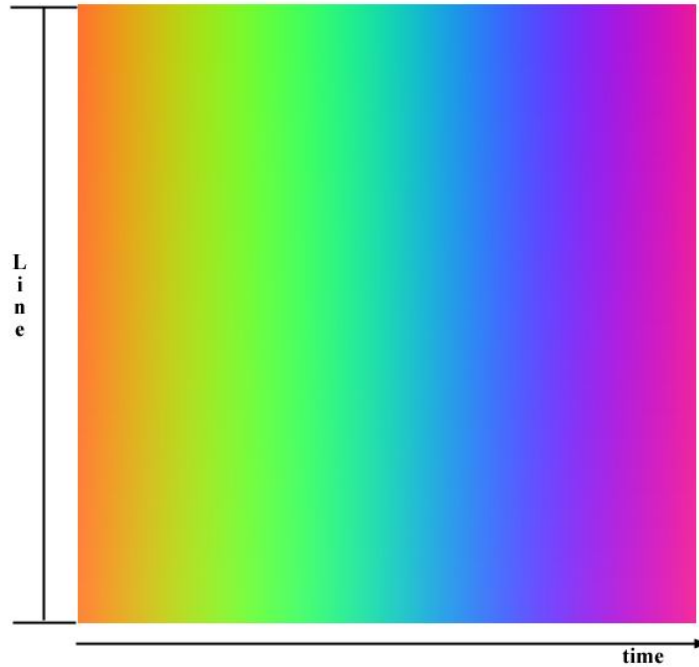
Fig. 77. Voltage profile color pattern w/o fault using phase voltage magnitudes

In Figure 78 and Figure 79, color patterns for single-phase to ground and 3 phase to ground faults are presented. It is noted that the color patterns produced by this particular coloring approach reproduce the well known traveling wave lattice (Bewley) diagrams [1] for the simulated cases. This allows easy tracing of the time-

space variation of the traveling waves initiated by the faults. The type and location of the faults can therefore be easily decoded from the resulting images.
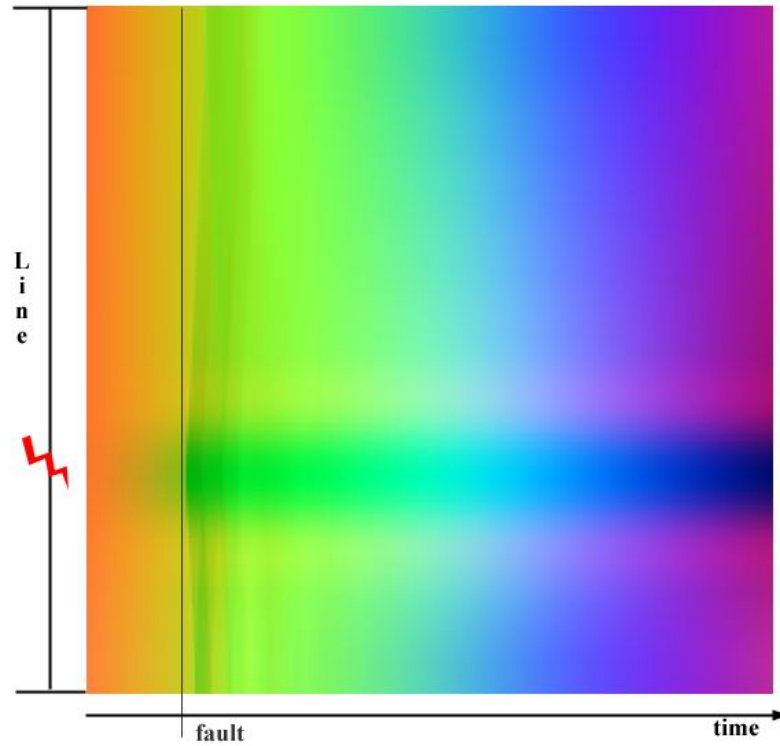
Fig. 78. Voltage profile color pattern for a single-phase to ground fault using phase voltages
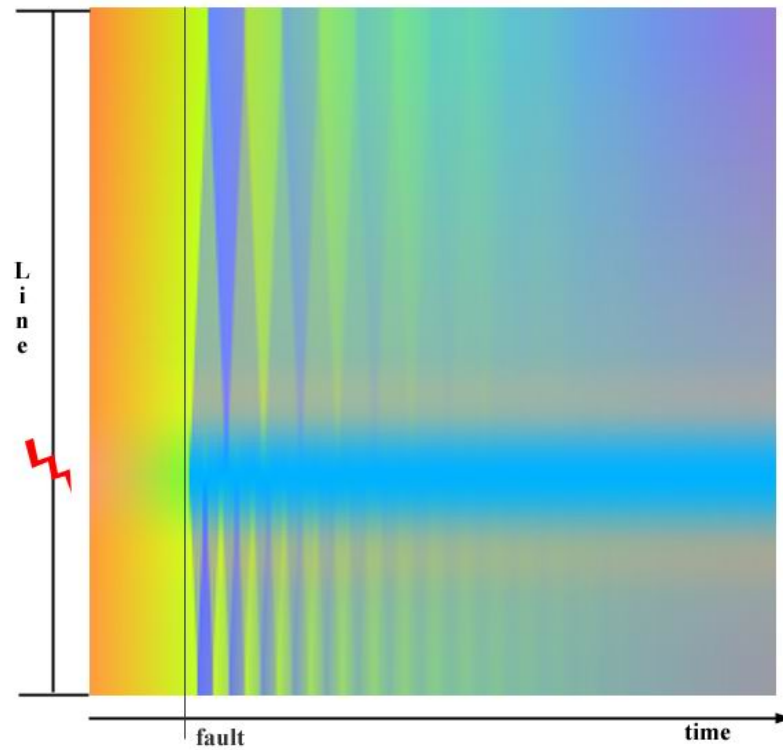
Fig. 79. Voltage profile color pattern for a three-phase to ground fault using phase voltages

b.   Use of modal voltages

Once the simulated waveforms at each line section are obtained, their modal compo-
nents are calculated using the Clarke's transformation [13]. Similar to the above case
of phase voltages, calculated waveforms are normalized and shifted in the positive y
direction so that they are bounded between 0 and 1. After the aerial and ground
mode voltages are processed, they are used to create the color patterns.

Modal voltages are painted by choosing only one of the three RGB colors, which
make up a pixel. The remaining two colors are assigned null voltages.
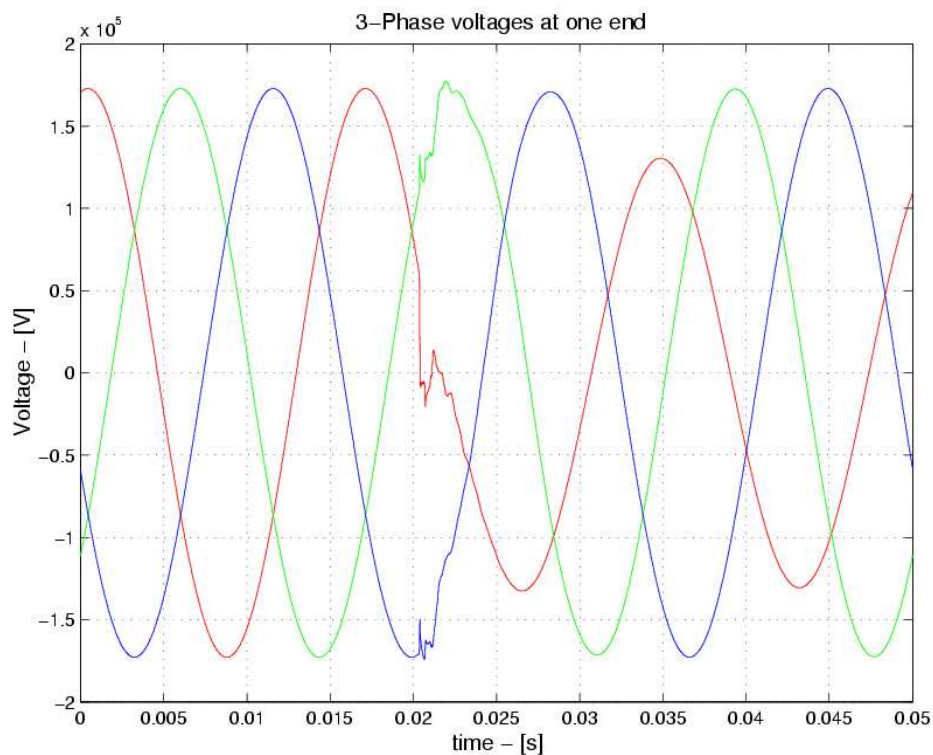
Fig. 80. Phase voltages at one end of the transmission line for a single-phase to ground
       fault

A single-phase to ground fault is simulated and only one-end voltage signals are obtained as shown in Figure 80. The aerial and ground mode voltages as shown in Figure 81 are normalized, shifted in the positive y direction and finally multiplied by 255. They are then used to create the color patterns.
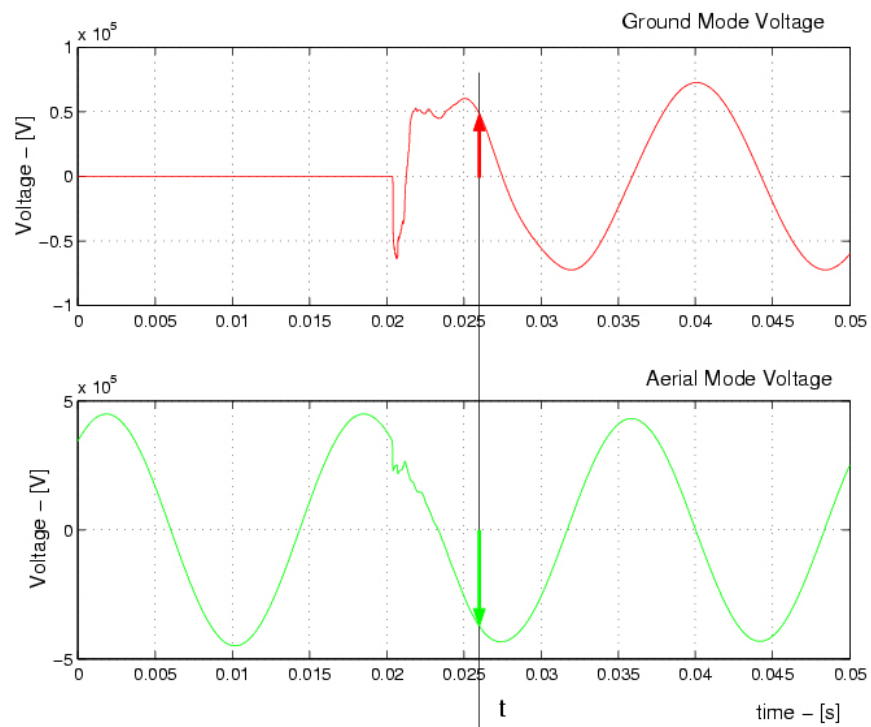
Fig. 81. Modal voltages at one end of the transmission line for a single-phase to ground fault

Voltage profile color patterns for the modal components (ground or aerial) are generated using only one of the RGB colors. Red channel is assigned to the ground mode voltage, while assigning the remaining green and blue channels null voltages. Similarly, green channel is assigned to the aerial mode voltage, while the red and blue channels are assigned null voltages. Figures 82 and 83 show the aerial and ground mode color patterns respectively, for a single-phase to ground fault. In case of a symmetric fault, no ground mode will be present and only the aerial mode voltage will be displayed. Figure 84 shows such a case.
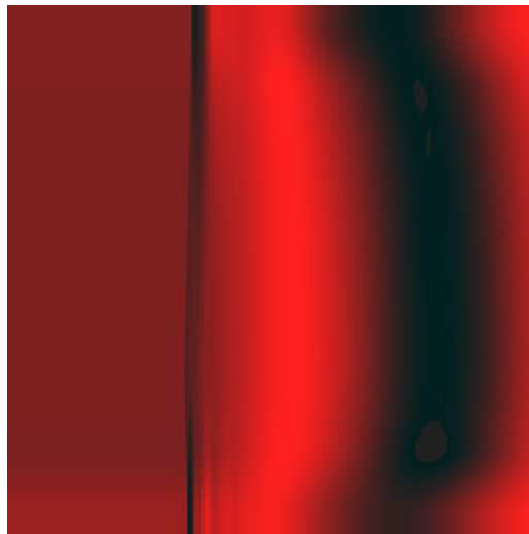
Fig. 82. Voltage profile color pattern for a single-phase to ground fault using ground mode voltage

Note that the color patterns obtained by using phase voltages in Figures 78 and 79 are identical with those obtained by aerial mode voltage in Figures 83 and 84. The arrival times of backward and forward traveling waves match almost exactly with each other. This interesting observation will be used to develop a new fault location method as described in the following chapter.
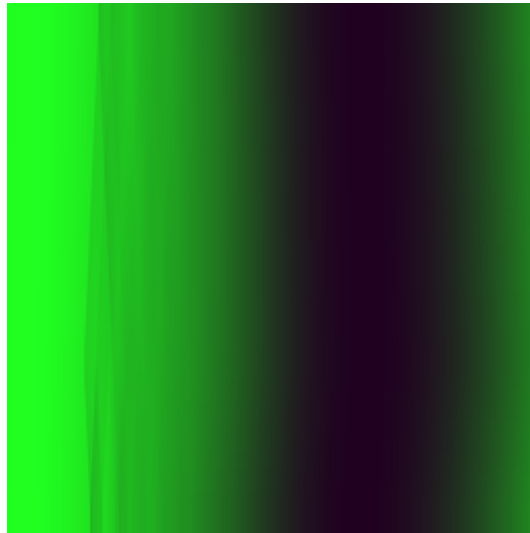
Fig. 83. Voltage profile color pattern for a single-phase to ground fault using aerial mode voltage
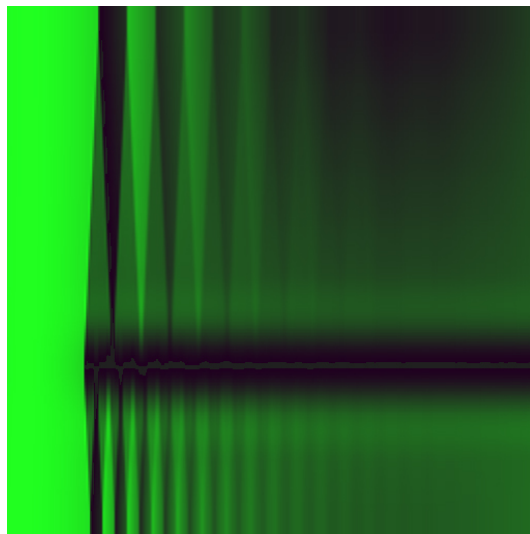
Fig. 84. Voltage profile color pattern for a three-phase to ground fault using aerial mode voltage

E. Summary

In this chapter three new methods for animating the power system transients are presented. *Animated Lines* is proposed to animate the single-phase power system transients. A new software tool, which allows user to observe the traveling wave motion in power systems during a fault, is introduced to implement the proposed method. The three-dimensional graphical user interface facilitates the understanding of the mechanism of propagation of traveling waves in the entire system. *Virtual Transient Sculptures* is presented as an extension of three dimensional voltage-line distance-time graphics in [2] using advanced computer graphics techniques. These two techniques strictly focus on single-phase transients animation while a third method called *Animated Pipes*, allows the animation of three phase power system transients, using either phase or modal voltages.

In addition to the new techniques for animating the traveling waves, a new visualization method for transients is also proposed by using *RGB Coloring* technique. RGB Coloring method produces color images created from recorded three-phase voltage transients. The color patterns of these images reveal traveling wave information. Chapter VIII suggests the use of RGB coloring method for fault location in power transmission lines.

CHAPTER VIII

VISUALIZATION BASED FAULT LOCATION FOR TRANSMISSION LINES

Locating faults occurring in high-voltage transmission systems using voltage and current transients recorded at one end of the transmission lines has long been a challenge for the power industry. A general review of fault location techniques is given in Chapter II.

Recent developments in signal processing techniques provide motivation for some novel applications in power systems. One example is the use of the discrete wavelet transform for extracting travel times of fault initiated voltage waveforms between the fault and the line terminals, which is first proposed in [34] as briefly reviewed in Chapter III. The method uses the discrete wavelet transform of the aerial and ground mode components of the fault signals in order to determine the arrival times of the backward and forward traveling waves created by the fault. The expected traveling wave patterns are determined based on the well-known Bewley diagrams. This method is later extended for three-terminal circuits [35] and distribution systems with distributed generation [36] as described in Chapters IV and V respectively.

Travelling waves carry important information about the fault that initiates them. However, they are typically difficult to visualize especially if they occur in a large power system. Advances in computer graphics and visualization techniques offer novel avenues for exploring the electromagnetic transients and the corresponding traveling waves. Use of visualization methods to extract relevant properties of traveling waves is not new. One of the first clever applications is the famous Bewley diagram [1] which illustrates the complex space-time evolution of transient signals in a two dimensional figure. Pioneering work of Woodruff [2] introduces animation via transient sculptures as a first example of visualization of transients in the literature. An extension of this

approach using recent computer graphics techniques is presented in Chapter VII.

This chapter will present a new application of visualization to the analysis of power system faults, specifically to the problem of fault location. The proposed application is based on the visualization method known as RGB Coloring. RGB Coloring method is introduced in Chapter VII and it basically produces color images created from recorded three-phase voltage transients. The color patterns of these images reveal traveling wave information as will be shown in the following sections. This approach eliminates the need to use modal transformations and/or wavelet transform on the recorded signals. Preliminary work reported in [76] is further developed and results of applying this method to fault location for different types of faults are provided in this chapter.

A.   Travelling Wave Based Fault Location

The essential idea behind the traveling wave based fault location methods is to extract the time of arrival of these waves at the line terminal where the transient signals are recorded. A method which makes use of the wavelet transform for extracting this information is presented in [34] and briefly explained in Chapter III. It will be shown that this approach can be simplified by eliminating the need to use modal transformation as well as the wavelet transform, by using a visualization technique known as RGB coloring. However, in order to validate the results obtained by this new approach, they will be compared with those given by the method of [34]. In the following section the proposed RGB coloring based fault location method is described in detail.

1. Proposed fault location using RGB Coloring

As noted above, applying RGB coloring to the three-phase transient voltage samples at *one end* of the transmission line, yields color patterns that closely match those obtained for the aerial mode voltage. The arrival times of the backward and forward traveling waves can therefore be easily extracted and used for fault location since the color pattern of the phase voltages matches the color pattern of the aerial mode voltage. This observation suggests a shortcut in determining arrival instants of fault initiated traveling waves by avoiding the modal transformation and the wavelet transform required by [34]. The forward and backward traveling wave arrival instants at one end of the line can be easily observed by using the phase voltage samples directly to create the color pattern at that line end. Hence, the fault location method proposed in [34] must be accordingly modified to derive the proposed RGB coloring based fault location procedure.
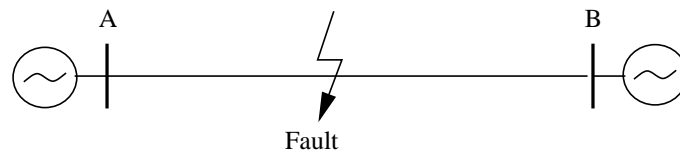
Fig. 85. 200-mile high-voltage power system transmission line

The faulted half of the transmission line in Figure 85 is detected by comparing the color pattern with the one obtained for a fault at the middle of the transmission line. If the fault is located at the first half of the transmission, Equation (8.1) will be used [34],

$$
\begin{aligned}
x &= \frac{v \times \Delta t}{2} \\
\Delta t &= t_2 - t_1
\end{aligned}
\tag{8.1}
$$

where t_1 is the arrival time of the backward traveling wave at bus A, t_2 is the arrival time of the reflected backward traveling wave at bus A, v is the aerial mode propagation velocity. The painted transients obtained by using the phase voltages closely match those obtained by using the squared wavelet coefficients (WTC^2) of the aerial mode voltage for scale-1, which corresponds to the frequency interval $[f_s/4 - f_s/2]$. The velocity of the painted transients can therefore be approximated by the propagation velocity of the aerial mode voltage in scale-1. The average frequency corresponding to scale-1 can be calculated as:

$$\frac{3f_s}{8} = \frac{1}{2}(\frac{f_s}{4} + \frac{f_s}{2})$$

where f_s is the sampling frequency. Hence, the propagation velocity for the aerial mode signal can be approximately calculated at $3f_s/8$.

Equation (8.2) is used for a fault occurring in the second half of the transmission line [34].

$$
\begin{aligned}
x &= \frac{\Delta t' \times v}{2} \\
\Delta t' &= \frac{2 \times L}{v} - \Delta t \\
\Delta t &= t_2 - t_1
\end{aligned}
\tag{8.2}
$$

where L is the total length of the transmission line, v is the aerial mode propagation velocity, t_1 and t_2 are the arrival times of the backward and forward traveling waves at bus A respectively.

Since there will be no remote end reflections for ungrounded or symmetrical faults [34], Equation (8.1) will be used for locating such faults.

B.   Simulation Results

All simulations are carried out by using the ATP-EMTP package. A 200-mile transmission line, which is modelled as a frequency dependent parameter line, is used throughout the simulations. The corresponding tower configuration for this line can be found in [35]. The sampling frequency, f_s, is chosen to be 200 kHz. The aerial mode velocity is calculated as 185847 mi/sec at $3f_s/8 = 75$ kHz. A single-phase to ground fault is simulated first at 20 miles away from bus A as seen in Figure 85. Then, a three-phase to ground fault is created at 180 miles away from bus A. This case is also used to illustrate the change in the color pattern which enables the identification of the faulted half of the line. Fault resistance is chosen as ($R = 0.0001\ \Omega$) for both cases.

1.   Single-phase to ground fault

Consider a single-phase to ground fault occurs at 20 miles away from bus A in Figure 85. Once the phase voltages at bus A are obtained for almost one cycle, they are processed in MATLAB in order to create RGB images. Resulting image, *Painted Transients*, is imported into Adobe Photoshop. Figure 86 demonstrates the RGB image for bus A phase voltages for almost one cycle. The height of the image is artificially increased from 1 to 512 pixels for better viewing while the width of the image remains same which is *3200* pixels corresponding to the time duration. (The simulation results start from 0 and ends at 5000 time steps, however, an excerpt of the x-axis is chosen for space considerations consisting of the time steps between 1800 and 5000.) Since, the sampling frequency is 200 kHz corresponding to a time interval, $\Delta t = 5\ \mu$sec, 3200 pixels correspond to $3200 \cdot \Delta t = 0.016$ sec which is less than one cycle (0.01667 sec).

Fig. 86. Voltage profile color pattern for a single-phase to ground fault 20 miles away from bus A.

An image filtering technique, which improves the contrast, called Emboss in Adobe Photoshop program is applied to the image in order to extract the arrival times of the traveling waves easier. Figure 87 shows the resulting image.

Fig. 87. Voltage profile color pattern for a single-phase to ground fault 20 miles away from bus A - Emboss filter is applied.

Once the faulted half of the transmission line is identified by comparing the color pattern with that of the mid-line fault, arrival time of the backward traveling wave (the first traveling wave to arrive at bus A) is extracted from the Figure 87 as the 220th pixel corresponding to $1800 + 220 = 2020$th pixel that is 0.010100 sec. Arrival time of the reflected backward traveling wave (the second traveling wave to arrive at bus A) is extracted as 2064th pixel corresponding to 0.010320 sec. Then, Equation (8.1) can be used to estimate the distance to the fault location as:

$$x = \frac{185847 \times (10.320 - 10.100) \cdot 10^{-3}}{2} = 20.44 \ mi$$

The above results are compared with those which will be obtained by the method of [34]. Figure 88 shows the wavelet transform coefficients of aerial mode voltages at

bus A in scale-1 for the same fault for 0.016 sec. Daubechies-4 mother wavelet is used for wavelet transformation in MATLAB and Clarke transformation is applied to the phase voltages in order to obtain modal voltages at bus A.
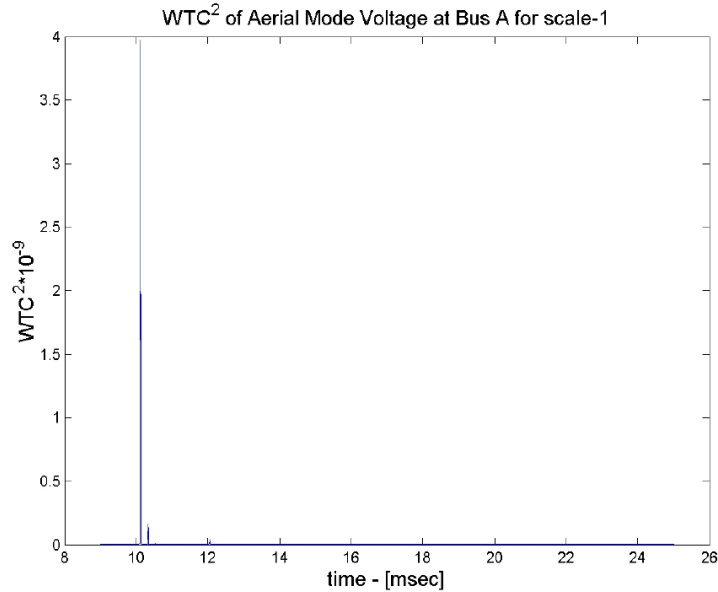
Fig. 88. WTC^2 of aerial mode voltage at bus A for scale-1

As indicated in [34], the arrival times of the traveling waves correspond to the peak values of the squared wavelet transform coefficients. The first peak occurs at 0.010115 sec corresponding to backward traveling wave and the second peak occurs at 0.010340 sec corresponding to reflected backward traveling wave. Using Equation (8.1) the distance to the fault location will be given as [34]:

$$x = \frac{185847 \times (10.340 - 10.115) \cdot 10^{-3}}{2} = 20.90 \ mi$$

A magnified view of Figure 88 is provided in Figure 89 in order to better observe

the traveling wave arrivals, which are also observable in Figures 86 and 87.
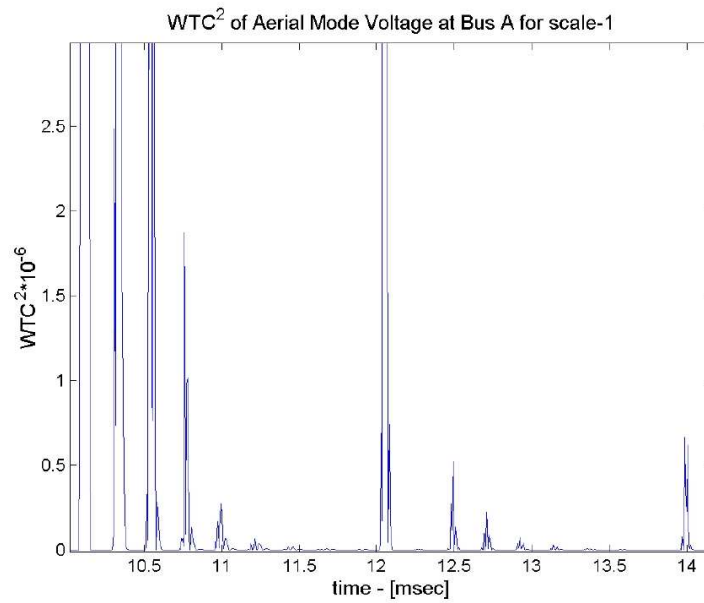
Fig. 89. WTC^2 of aerial mode voltage at bus A for scale-1 - zoomed version

2. Three-phase to ground fault

Next, a three-phase to ground fault is assumed to occur at 180 miles away from bus A. The resulting *Painted Transients* are given in Figure 90, and the filtered version in Figure 91 after Emboss filter is applied.

Fig. 90. Voltage profile color pattern for a three-phase to ground fault 180 miles away from bus A.
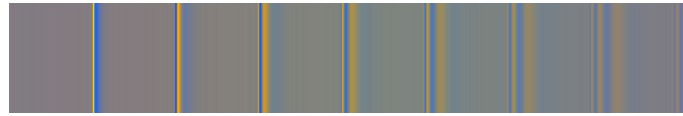
Fig. 91. Voltage profile color pattern for a three-phase to ground fault 180 miles away from bus A - Emboss filter is applied.

Arrival time of the backward traveling wave as the first traveling wave at bus A is extracted from the Figure 91 as the 2193rd pixel corresponding to 0.010965 sec. Arrival time of the reflected backward traveling wave as the second traveling wave at bus A is extracted as 2580th pixel corresponding to 0.012900 sec. Equation (8.1) yields the distance to the fault location as:

$$x = \frac{185847 \times (12.895 - 10.960) \cdot 10^{-3}}{2} = 179.8 \ mi$$

C.   Summary

This chapter uses the traveling wave theory and a visualization method known as RGB coloring to derive a new fault location method. The proposed method is simple to implement, requiring sampled voltage transients at one end of the faulted transmission line only. The relation between the proposed method and a previously presented wavelet transform based fault location method is also illustrated and comparative simulation results are given for validation.

The main contribution of this chapter is the use of a common visualization method to extract traveling wave arrival time information from recorded three-phase voltages at one end of a line. This information is then used to estimate the distance to the fault location. This chapter also shows how the well-known Bewley diagrams will be obtained when the transient voltages along the line length are painted via

the presented coloring method. Simulation results obtained by the proposed method show good agreement between the actual and estimated fault locations for the studied cases.

CHAPTER IX

CONCLUSIONS

The contributions of this dissertation are categorized under three main topics; *fault location*, *voltage profile calculation* and *visualization and animation of transients*.

New fault location methods are developed for complex topologies such as three-terminal transmission lines with MOV protected series capacitors or mutually coupled line sections and for distribution systems with distributed generations in order to satisfy the needs emerging with the deregulated power systems. Both proposed fault location techniques are traveling wave based and they utilize wavelet transformation theory.

A new voltage profile calculation method is proposed in modal domain in order to provide the voltage variation along the transmission lines. The proposed technique uses terminal voltage of a transmission line as well as the intermediate point voltages prior to develop a method based on time series analysis.

Finally, to help understanding the complex behavior of power systems during transient operation new visualization and animation methods are developed. Implementations of these methods are also given.

A.   Fault Location Using Wavelets

Technological developments in system monitoring devices present great opportunities to the researchers. Previously not available information is now provided by intelligent electronic devices (IED). The costs of these devices are decreasing every day while the maintenance expenses are being cut off in the new deregulation environment. In this dissertation two fault location techniques are presented for complex power system topologies. Both procedures are based on processing of traveling waves by

wavelet transform in order to extract the arrival times of fault-initiated waves reflected from the discontinuities. The voltage recordings are assumed to be available by measurement devices with very high-frequency cut-offs.

First, a new fault location procedure for teed circuits is presented. The fault location algorithm is shown to be insensitive to the existence of series capacitors, fault resistance, fault type and any existing mutual coupling between the lines. Simulation results show good correlation between the actual and estimated fault locations for all the studied cases.

Then, a novel fault location technique is proposed to be used in distribution systems with distributed generation. The main advantage of the proposed approach is its insensitivity to naturally occurring infeed from the distributed generators during a fault. Such infeed is typically unpredictable and makes the impedance based conventional fault location methods vulnerable to errors. Furthermore, the proposed approach has the added advantage of requiring fault signals only from the substation end of the distribution feeder.

B.   Voltage Profile Calculation

A new method to predict the voltage profile of a transmission line is proposed in modal domain. Unlike the existing techniques, the new method utilizes a time series model to predict the voltage at an intermediate point along the transmission line. The model is formed for each intermediate point separately. Terminal voltages and one intermediate point voltage at a time are assumed to be known so that a model for the intermediate point of interest can be developed. Once the model is obtained through least squares fitting, it is used to predict the intermediate point voltage during a fault at a neighboring transmission line. The procedure is carried out in modal domain.

The estimation results show good correlation with the simulation results.

C.   Visualization and Animation of Transients

First, three new methods for animating the power system transients are presented in this part of the dissertation: *Animated Lines* is proposed to animate the single-phase power system transients. A new software tool, which allows user to observe the traveling wave motion in power systems during a fault, is introduced to implement the proposed method. Three-dimensional graphical user interface facilitates the understanding of the mechanism of propagation of traveling waves in the entire system. *Virtual Transient Sculptures* is presented as an extension of three-dimensional voltage-line distance-time graphics in [2] using advanced computer graphics techniques. These two techniques strictly focus on single-phase transients animation while a third method called *Animated Pipes*, allows the animation of three-phase power system transients, using either phase or modal voltages.

In addition to the new techniques for animating the traveling waves, a new visualization method for transients is also proposed by using *RGB Coloring* technique. RGB coloring method produces color images created from recorded three-phase voltage transients. The color patterns of these images reveal traveling wave information. The use of this technique for fault location purposes along transmission lines is also suggested.

REFERENCES

[1] L.V. Bewley, *Travelling Waves on Transmission Systems.* New York: John Wiley & Sons, 1951.

[2] L.F. Woodruff, "Transmission line transients in motion movies," *AIEE Transactions*, vol. 57, pp. 391-400, Jul. 1938.

[3] Hewlett Packard, *Travelling Wave Fault Location in Power Transmission Sytem.* Application Note 1285, Palo Alto, CA.

[4] F. H. Magnago, *Advanced Techniques for Meter Placement and Fault Location in Power Systems*, Ph.D. Dissertation, Texas A&M University, College Station, Texas, 2000.

[5] J. R. Carson, J.R., "Wave propagation in overhead wires with ground return," *Bell System Technical Journal*, vol. 5, pp 539-554, 1926.

[6] H. W. Dommel, *EMTP Theory Book, Second Edition.* Vancouver, BC: Microtran Power System Analysis Corporation, 1992.

[7] J. R. Marti, L. Marti and H. W. Dommel, "Transmission line models for steady-state and transients analysis," in *Proc. Power Tech Conference*, Sep. 1993.

[8] H. W. Dommel, "Digital computer solution of electromagnetic transients in single- and multi-phase networks," *IEEE Transactions on Power Apparatus and Systems*, vol. PAS-88, pp. 388-399, Apr. 1969.

[9] A. Greenwood, *Electrical Transients in Power Systems.* New York: John Wiley & Sons, 1991.

[10] J. D. Glover and M. Sarma, *Power System Analysis and Design.* Boston, MA: PWS Publishing Company, 1994.

[11] J. R. Marti, "Accurate modelling of frequency dependent transmission lines in electromagnetic transient simulations," *IEEE Transactions on Power Apparatus and Systems*, vol. PAS-101, pp. 147-155, Jan. 1982.

[12] L. M. Wedepohl, "Application of matrix methods to the solutions of travelling-wave phenomena in polyphase systems," *Proceedings of IEE*, vol. 110(12), pp. 2200-2212, Dec. 1963.

[13] E. Clarke, *Circuit Analysis of AC Power Systems, Symmetrical and Related Components.* New York: John Wiley & Sons, 1943.

[14] W. Lewis, "Fundamental basis for distance relaying on a 3-phase system," *AIEE Transactions*, vol. 66, pp. 694-708, 1947.

[15] E. O. Schweitzer, "A review of impedance-based fault locating experience," *Fourteenth Annual Iowa-Nebraska System Protection Seminar*, Omaha, NE, Oct. 1990.

[16] IEEE Standard PC37.114, *Draft Guide for Determining Fault Location on AC Transmission and Distribution Lines.* New York City, NY, 2004.

[17] M. M. Saha, K. Wikstrom, J. Izykoski and W. Rosolowski, *Fault Location Techniques.* http://citeseer.ist.psu.edu/393844.html, July 2006.

[18] V. Cook, "Fundamental aspects of fault location algorithms used in distance protection," *Proceedings of IEE-Part C*, vol. 133, pp. 359-368, Sep. 1986.

[19] M. S. Sachdev, R. Agarwal, "A technique for estimating transmission line fault locations from digital impedance relay measurements," *IEEE Transactions on Power Delivery*, vol. 3, no. 1, Jan. 1988

[20] T. Takagi, Y. Yamakoshi, M. Yamaura, R. Kondou, and T. Matsushima, "Development of a new type fault locator using the one-terminal voltage and current data," *IEEE Transactions on Power Apparatus and Systems*, vol. PAS-101, no. 8, pp. 2892-2898, Aug. 1982.

[21] K. Zimmerman and D. Costello, *Impedance Based Fault Location Experience*. Pullman, WA: Schweitzer Engineering Laboratories, Inc, 2004.

[22] R. Poncelet, "The use of digital computers for network protection," *24th Session CIGRE*, Paper no. 32-08, Paris, France, 1972.

[23] A. Ranjbar and B. Cory, "An improved method for the digital protection of high voltage transmission lines," *IEEE Transactions on Power Apparatus and Systems*, vol. PAS-94, pp. 544-550, 1975.

[24] A.O. Ibe and B.J. Cory, "A travelling wave-based fault locator for two and three terminal networks," *IEEE Transactions on Power Systems*, vol. PWRD-1, no. 2, pp. 283-288, Apr. 1986.

[25] A. Ranjbar, A. Shirani and A. Fathi, "A new approach for fault location problem on power lines," *IEEE Transaction on Power Delivery*, vol. 7, pp.146-151, 1992.

[26] A. Gopalakrishnan, M. Kezunovic, S. M. McKenna, and D. M. Hamai, "Fault location using the distributed parameter transmission line model," *IEEE Transactions on Power Delivery*, vol. 15, no. 4, pp. 1169-1174 , Oct. 2000.

[27] H. W. Dommel and J.M. Michels, "High speed relaying using traveling wave transient analysis," in *Proc. IEEE PES Winter Meeting*, Jan. 1978.

[28] M. Vitinis, "A correlation method for transmission line protection," *IEEE Transactions on Power Apparatus and Systems*, vol. PAS-97, no. 5, pp. 1607-1617, Sep. 1978.

[29] P. Crossley and P. McLaren, "Distance protection based on travelling waves," *IEEE Transactions on Power Apparatus and Systems*, vol. PAS-102, no. 9, pp. 2971-2983, Sep. 1983.

[30] E. Shehab-Eldin and P. McLaren, "Travelling wave distance protection - problem areas and solutions," *IEEE Transaction on Power Delivery*, vol. 3, no. 3, pp. 894-902, Jul. 1988.

[31] G. B. Ancell and N. C. Pahalawaththa, "Maximum likelihood estimation of fault lcoation on transmission lines using travelling waves," *IEEE Transactions on Power Delivery*, vol. 9, no. 2, Apr. 1994.

[32] G.B. Ancell, N.C. Pahalawaththa, "Effects of frequency dependence and line parameters on single ended travelling wave based fault location schemes," *IEE Proceedings on Generation, Transmission and Distribution*, vol. 139, no. 4, pp. 332-342, Jul. 1992.

[33] B. Lian and M. Salama, "An overview of digital fault location algorithms for power transmission lines using transient waveforms," *Electric Power System Research*, vol. 29, pp.17-25, 1994.

[34] F.H. Magnago and A. Abur, "Fault location using wavelets," *IEEE Transactions on Power Delivery*, vol. 13, no. 4, pp. 1475-1480, Oct. 1998.

[35] C.Y. Evrenosoglu and A. Abur, "Travelling wave based fault location for teed circuits," *IEEE Transactions on Power Delivery*, vol. 20, no. 2, pp. 1115-1121, Apr. 2005.

[36] C.Y. Evrenosoglu and A. Abur, "Fault location in distribution systems with distributed generation," in *Proc. Power Systems Computation Conference*, Aug. 2005.

[37] S. Bickerton, *An Introductory Guide to Wavelets*, Lecture Notes, 2001, Private Collection, C. Y. Evrenosoğlu.

[38] C. Valens, *A Really Friendly Guide to Wavelets*, http://perso.orange.fr/polyvalens/clemens/wavelets/wavelets.html, 1999.

[39] A. Grapps, "An Introduction to Wavelets," *IEEE Computational Science and Engineering*, vol. 2, no. 2, Summer 1995.

[40] R. Polikar, *The Engineer's Ultimate Guide to Wavelet Analysis*, http://users.rowan.edu/∼polikar/WAVELETS/WTtutorial.html, July 2006.

[41] G. Strang, "Wavelets," *American Scientist*, vol. 82, pp. 250-255, Apr. 1994

[42] I. Daubechies, *Ten Lectures on Wavelets*. Philadelphia, PA: SIAM, 1992.

[43] G. Kaiser, *A Friendy Guide to Wavelets*. Boston, MA: Birkhäuser, 1994.

[44] S. Mallat, *A Wavelet Tour of Signal Processing, Second Edition (Wavelet Analysis & Its Applications)*. San Diego, CA: Academic Press, 1999.

[45] G. Strang, *Signal Processing for Everyone*, http://www-math.mit.edu/∼gs/papers/papers.html, 2000.

[46] D. C. Robertson, O. I. Camps, J. S. Mayer and W. B. Gish, "Wavelets and electromagnetic power system transients," *IEEE Transactions on Power Delivery*, vol. 11, no. 2, pp. 1050-1057, Apr. 1996.

[47] W. A. Wilkinson and M. D. Cox, "Discrete wavelet analysis of power system transients," *IEEE Transacations on Power Systems*, vol. 11, no. 4, pp. 2038-2043, Nov. 1996.

[48] P. Pillay and A. Bhattacharjee, "Application of wavelets to model short-term power system disturbances," *IEEE Transactions on Power Systems*, vol. 11, no. 4, pp. 2031-2037, Nov. 1996.

[49] S. Santoso and P. Hoffmann, "Power quality assessment via wavelet transform analysis," *IEEE Transactions on Power Delivery*, vol. 11, no. 2, pp. 924-930, Apr. 1996.

[50] A. P. S. Meliopoulos and C. Lee, "Power disturbance analysis via wavelet domain equivalents," in *Proc. 8th International Conference on Harmonics and Quality of Power*, vol. 1, pp. 388-394, Oct. 1998.

[51] S. Huang, C. Hsieh and C. Huang, "Application of morlet wavelets to supervise power system disturbances," *IEEE Transactions on Power Delivery*, vol. 14, no. 1, pp. 235-243, Jan. 1999.

[52] T. Zheng, E. B. Makram and A. A. Girgis, "Power system transient and harmonic studies using wavelet transform," *IEEE Transactions on Power Delivery*, vol. 14, no. 4, pp. 1461-1468, Oct. 1999.

[53] T. Nagasawa, M. Abe, N. Otsuzuki, T. Emura, Y. Jikihira and M. Takeuchi, "Development of a new fault location algorithm for multi-terminal two parallel

pransmission lines," *IEEE Transactions on Power Delivery*, vol. 7, no. 3, pp. 1516-1532, Jul. 1992.

[54] A.A. Girgis, D.G. Hart and W.L. Peterson, "A new fault location technique for two and three terminal lines," *IEEE Transactions on Power Delivery*, vol. 7, no. 1, pp. 98-107, Jan. 1992.

[55] Q. Gong, Y. Chen, C. Zhang and Z. Wang, "A Study of the accurate fault location system for transmission line using multi-terminal signals," in *Proc. IEEE PES Winter Meeting*, vol. 4, pp. 2533-2538, Jan. 2000.

[56] D.A. Tziouvaras, J.B. Roberts and G. Benmouyal, "New multi-ended fault location design for two or three terminal lines," *IEE Developments in Power System Protection*, no. 479, pp. 395-398, 2001.

[57] Y. Lin, C. Liu, C. Yu, "A new fault locator for three terminal transmission lines - using two terminal synchronized voltage and current phasors," *IEEE Transactions on Power Delivery*, vol. 17, no. 2, pp. 452-459, Apr. 2002.

[58] S. Rajendra and P.G. McLaren, "Traveling wave techniques applied to the protection of teed circuits: multi- phase/multi-circuit system," *IEEE Transactions on Power Apparatus and Systems*, vol. PAS-104, no. 12, pp. 3351-3557, Dec. 1985.

[59] Z. Qingchao, Z. Yao, S. Wennan, Y. Yixin and W. Zhigang, "Fault location of two-parallel transmission line for non-earth fault using one-terminal data," *IEEE Transactions on Power Delivery*, vol. 14, no. 3, pp.863-867, July 1999.

[60] Z. Qingchao and D.W.P. Thomas, "Accurate fault location algortihms for two-parallel transmission line using one-end data," in *Proc. IEEE/PES Transmission*

and Distribution Conference and Exposition, vol. 1, pp. 527-530, 2001.

[61] J. Izykowski and R. Kawecki, "Location of faults in partially parallel transmission networks," in *Proc. Power Tech Conference*, vol. 3, pp. 6, Sep. 2001.

[62] C. Chen, C. Liu and J. Jiang, "A new adaptive PMU based protection scheme for transposed/untransposed parallel transmission lines," *IEEE Transactions on Power Delivery*, vol. 17, no. 2, pp. 395-404, Apr. 2002.

[63] S. Kang, S. Lee, Y. Kwon, Y. Kang, "A fault location algorithm for parallel transmission line with a teed circuit," in *Proc. IEEE PES Summer Meeting*, vol. 2, pp. 921-926, 2001.

[64] B. Bachmann, D. Novosel, D. Hart, Y. Hu and M.M. Saha, "Application of artificial neural networks for series compensated line protection," *Intelligent Systems Applications to Power Systems*, pp. 68-73, 1996.

[65] M.M. Saha, J. Izykowski, E. Rosolowski and B. Kasztenny, "A new accurate fault locationg algorithm for series compensated lines," *IEEE Transactions on Power Delivery*, vol. 14, no. 3, pp.789-797, Jul. 1999.

[66] J. Sadeh, N. Hadjsaid, A.M. Ranjbar and R. Feuillet, "Accurate fault location algorithm for series compensated transmission lines," *IEEE Transactions on Power Delivery*, vol. 15, no. 3, pp.1027-1033, Jul. 2000.

[67] C.Y. Evrenosoglu and A. Abur, "Fault location for three terminal lines using traveling waves," in *Proc. North American Power Symposium*, Oct. 2002.

[68] C.Y. Evrenosoglu and A. Abur, "Fault location for teed circuits with mutually coupled lines and series capacitors," in *Proc. Power Tech Conference*, Jun. 2003.

[69] A.G. Phadke, J.S. Thorp, *Computer Relaying for Power Systems*. New York: John Wiley & Sons, 1988.

[70] A. Girgis and S. Brahma, "Effect of distributed generation on protective device coordination in distribution system," in *Proc. Large Engineering Systems Conference on Power Engineering*, pp. 115-119, Jul. 2001.

[71] C.W. So and K.K. Li, "Protection relay coordination on ring-fed distribution network with distributed generations," in *Proc. IEEE Region 10 Conference on Computers, Communications, Control and Power Engineering*, vol.3, pp. 1885-1888, Oct. 2002.

[72] M.T. Doyle, "Reviewing the impacts of distributed generation on distribution system protection," in *Proc. IEEE PES Summer Meeting*, vol. 1, pp. 103-105, Jul. 2002.

[73] Z.Q. Bo, G. Weller and M.A. Redfern, "Accurate fault location technique for distribution system using fault-generated high-frequency transient voltage signals," *IEE Proceedings on Generation, Transmission and Distribution*, vol. 146, no. 1, pp. 73-79, Jan. 1999.

[74] Z. Xiangjun, K.K. Li, W.L. Chan, S. Sheng, "Multi-agents based protection for distributed generation systems," in *Proc. IEEE International Conference on Electric Utility Deregulation, Restructuring and Power Technologies*, vol. 1, pp. 393-397, Apr. 2004.

[75] C.Y. Evrenosoglu, A. Abur and E. Akleman, "Visualization of electromagnetic transients along transmission lines," in *Proc. IEEE Power Systems Conference and Exposition*, Oct. 2004.

[76] C.Y. Evrenosoglu, E. Akleman, O. O. Ozener and A. Abur, "Two methods for travelling wave visualization in multi-phase power systems: painted transients and animated pipes," in *Proc. International Conference on Power Systems Transients*, Jun. 2005.

[77] L. Marti and H.W. Dommel, "Calculation of voltage profiles along transmission lines," *IEEE Transactions on Power Delivery*, vol. 12, no. 2, pp. 993-998, Apr. 1997.

[78] C.Y. Evrenosoglu and A. Abur, "Estimation of voltage profiles along power transmission lines," in *Proc. IEEE Power Systems Conference and Exposition*, Oct. 2006

[79] H. W. Dommel, *Electromagnetic Transients Program*. Portland, OR:Bonneville Power Administration, 1986.

[80] J.D. Weber and T.J. Overbye, "Voltage contours for power system visualization," *IEEE Transactions on Power Systems*, vol. 15, no.1, pp.404-409, Feb. 2000.

[81] B. Xu, C.Y. Evrenosoglu, A. Abur and E. Akleman, "Interactive evaluation of ATC using a graphical interface," in *Proc. IEEE PES General Meeting*, Jun. 2004.

[82] F.H. Magnago and A. Abur, *Java Exercises for Power Education*, http://www.ece.neu.edu/∼abur/java _ exer.html, July 2006.

[83] C.W. Trueman, "Animating transmission-line transients with BOUNCE," *IEEE Transactions on Education*, vol. 46, no. 1, pp. 115-123, Feb. 2003.

[84] K.P. Wong and K. Lee, "Visualizing wavelet transformed travelling waves on

power transmission line using JAVA," *Advances in Power System Control, Operation and Management*, Oct. 2000.

APPENDIX A

ATP CONDUCTOR AND TOWER CONFIGURATION DATA

Table A-I. Data for a 220 kV transmission line

Ph.	Skin	R [Ω/mi]	IX	X	D [in]	Hor. [ft]	Vtower [ft]
0	0.5	6.74	4	0	0.36	45	114
0	0.5	6.74	4	0	0.36	75	114
1	0.5	0.0984	4	0	1.196	60	101
2	0.5	0.0984	4	0	1.196	45	80
3	0.5	0.0984	4	0	1.196	75	80

Ph.	Vmid [ft]	Separ. [in]	α [deg]	NB
0	114	0	0	0
0	114	0	0	0
1	101	18	0	2
2	80	18	0	2
3	80	18	0	2

Table A-II. Data for a 10 kV distribution line

Ph.	Skin	R [Ω/mi]	IX	X	D [in]	Hor. [ft]	Vtower [ft]	Vmid [ft]
0	0.5	2.26	4	0	0.621	0	33	33
1	0.5	0.2797	4	0	0.741	-3.66	28.5	28.5
2	0.5	0.2797	4	0	0.741	0	28.5	28.5
3	0.5	0.2797	4	0	0.741	3.66	28.5	28.5

VITA

Cansın Yaman Evrenosoğlu received his B.S. and M.S. degrees from the Department of Electrical Engineering, majoring in power systems at İstanbul Teknik Üniversitesi (ITU-Istanbul Technical University), İstanbul, Türkiye (Turcia, Turkia, a.k.a. Turkey in English) in 1998 and 2001 respectively. He was a teaching and research assistant at ITU from 1998 to 2001 during his M.S. studies under the supervision of Dr. Hasan Dağ. He started his Ph.D. degree with Dr. Ali Abur in 2002. He was a research assistant between January 2002 and May 2006 and became the teaching assistant of ELEN 460 and 459 in Fall 2004 and in Spring 2005 respectively. He defended his dissertation in March 2006 and received his Ph.D. in Electrical Engineering from Texas A&M University, College Station, Texas in Fall 2006. He can be contacted at cyevrenosoglu@ieee.org.

Permanent address of Mr. Evrenosoğlu is as follows:
Kayasultan Sok. Belediye Sit. P Blok D:29
Kozyatağı, İstanbul, Türkiye, 81090

This dissertation was typed in LaTeX by Cansın Yaman Evrenosoğlu